Bernhard Müller, BSc

Luminescent pH-sensitive Nanoparticles for the Application in Microfluidic Systems

MASTER'S THESIS

to achieve the university degree of

Master of Science
Master's degree programme: Chemistry

submitted to

Graz University of Technology

Supervisor
Assoc.Prof. Dipl.-Chem. Dr.rer.nat. Torsten Mayr

Institute of Analytical Chemistry and Food Chemistry
Graz University of Technology

Graz, April 2015

AFFIDAVIT

I declare that I have authored this thesis independently, that I have not used other than the declared sources/resources, and that I have explicitly indicated all material which has been quoted either literally or by content from the sources used. The text document uploaded to TUGRAZonline is identical to the present master‘s thesis dissertation.

Date	Signature

Abstract

The goal of this thesis it the development of pH sensitive nanobeads for the application in microfluidic systems. Three different aza-BODIPY dyes served as pH indicators and enabled the coverage of a broad pH range (pH 3.5 to pH 9). One of the used indicators (ClOHbutoxy-complex) was successfully synthesized via a condensation of nitromethane adducts of chalcones with ammonium acetate. The pH sensitive dyes where physically entrapped in three matrix materials (PSPVP, RL100 and PAcM) which exhibit different properties concerning the shift of the apparent pKa value, their brightness, their particle size, their cross-sensitivity to the salinity and their stability as colloid. The synthesized particles were characterized regarding these properties and their apparent pKa values were determined with fluorescence spectra taken at various pH values.

The measurement inside microfluidic chips was done via dual lifetime referencing (DLR) with $PtTPTBPF_4$ as a reference dye. The lifetime of this dye is sensitive to oxygen (decreases with rising O_2 levels) and therefore an oxygen impermeable matrix (PViCl-PAN) was used for the reference particles. A measurement set-up was realized where the read-out of the phase shift of the DLR signal was done fiber-optically. With this set-up the calibration curves of the nine different pH sensitive DLR systems, containing 0.25 % of indicator dye, were recorded in a 300 µm deep microfluidic glass chip. The measurements with this set-up showed excellent reproducibility. However, when the particles where applied for long time in a microfluidic system a drift was observed. This drift is due to aggregation and sedimentation of reference particles and therefore closer studies of the colloid stabilities are needed to enable measurement over a longer time period.

Additionally to the DLR system, a referenced NIR imaging system, based on the OHbutoxy-complex and Lumogen® Red entrapped in PSPVP particles, has been realized. Although just very few experiments have been done, their outcome looks quite promising.

Kurzfassung

Das Ziel dieser Masterarbeit ist die Entwicklung pH sensitiver Nanopartikel für die Anwendung in mikrofluidischen Systemen. Es wurden drei verschiedene aza-BODIPY Farbstoffe als Indikator eingesetzt, um einen möglichst großen pH-Bereich abzudecken (pH 3,5 bis pH 9). Einer der dazu verwendeten Farbstoffe (ClOHbutoxy-Komplex) wurde erfolgreich durch die Kondensation von Nitromethan-Addukten von Chalkonen mit Ammoniumacetat hergestellt. Die Indikatorfarbstoffe wurden in drei verschiedenen Matrixmaterialien (PSPVP, RL100, PAcM) eingebracht. Diese unterscheiden sich aufgrund ihres Einflusses auf den scheinbaren pKs Wert, ihrer Helligkeit, ihrer Partikelgröße, ihrer Querempfindlichkeit bezüglich Salinität und ihrer Stabilität als Kolloid. Die hergestellten Partikel wurden hinsichtlich dieser Eigenschaften charakterisiert und ihr scheinbarer pKs Wert wurde durch die Aufnahme mehrerer Fluoreszenzspeckten bei unterschiedlichen pH Werten ermittelt.
Die Messung in mikrofluidischen Systemen erfolgte mittels „dual lifetime referencing“ (DLR), wobei $PtTPTBPF_4$ als Referenzfarbstoff diente. Die Lebenszeit dieses Farbstoffes ist abhängig von der Sauerstoffkonzentration (sie sinkt mit steigendem O_2-Gehalt), weswegen das sauerstoffimpermeable Co-polymere PViCl-PAN als Matrix für die Referenzpartikel verwendet wurde. Im entwickelten Messaufbau erfolgte die Messung der Phasenverschiebung des DLR Signals faser-optisch. Die Kalibrationskurven der neun realisierten pH sensitiven DLR-Systeme, mit einer Indikatorkonzentration von je 0,25 %, wurden in einem 300 µm tiefen Mikrofluidikchip aufgenommen. Die Messungen mit diesem Set-Up zeigten eine exzellente Reproduzierbarkeit. Wenn jedoch die Partikel für längere Zeit in einem mikrofluidischen System eingesetzt wurden, konnte ein driften der Signale festgestellt werden. Dieser Drift ist durch Aggregation und Sedimentation der Referenzpartikel zu erklären weswegen weitere Untersuchungen hinsichtlich der Kolloidstabilität notwendig sind um Messungen über einen längeren Zeitraum möglich zu machen.
Zusätzlich zum DLR System wurde ein referenziertes NIR-Imaging System, basierend auf mit ClOHbutoxy-Komplex und Macrolex® Red gefärbten PSPVP Partikeln, realisiert. Mit diesem System wurden zwar nur wenige Versuche durchgeführt, die Resultate daraus sehen aber sehr vielversprechend aus.

Acknowledgment

An erster Stelle möchte ich mich bei Prof. Torsten Mayr bedanken, der diese Arbeit erst möglich gemacht hat. Danke, dass du steht's ein offenes Ohr für mich hattest, mir wertvollen Input gabst und mich mit deinem Enthusiasmus auch in mühsamen Zeiten motiviert hast.

Großer Dank gebührt auch Birgit Ungerböck, Martin Strobl und Josef Ehgartner. Danke, dass ihr mir zu jedem Zeitpunkt eine so große Hilfe wart, mir immer mit Rat und Tat zur Seite gestanden seid und mir mit euren Erfahrungen und Tipps die Arbeit sehr erleichtert habt.
Weiters möchte ich mich bei der gesamten Arbeitsgruppe bedanken. Das freundschaftliche und kollegiale Klima das hier herrscht, spornt unheimlich an und ermöglicht nicht nur fachlich äußerst produktive Diskussionen sondern lässt auch Raum für soziale Interaktionen. Das gemeinsame Mittagessen, die unterhaltsamen Kaffeepausen und diverse Aktivitäten abseits der Arbeit möchte ich nicht missen! Ihr seid für mich die Definition eines perfekten Arbeitsumfeldes.

Danke an alle meine Studienkollegen für die gemeinsame Studienzeit. Sie wird mir unvergesslich bleiben und ich werde die unzähligen Lernsessions oder das gelegentliche Feierabendbier sehr vermissen.
Außerdem möchte ich mich bei all jenen bedanken, die abseits des Studiums immer für mich da waren und sind. Vielen Danke für erkenntnisreiche Diskussionen, Abenteuer in den Bergen und eine lustige, abwechslungsreiche Zeit.

Zu guter Letzt möchte ich mich bei meiner Familie bedanken. Ein riesen Dank gehört dabei meiner Schwester Eva. Danke, dass du immer für mich da bist und ich mich auf dich verlassen kann. (Und natürlich für den ganzen Rest.)
Danke Mama und Papa, dass ihr mir das Studium ermöglicht habt, mir Rückhalt bietet, mich unterstützt, mir Sicherheit gebt und immer für mich da seid.

Bernhard Müller Graz, April 2015

Contents

1 Introduction

The pH value is one of the most important parameters in industrial, environmental and biomedical applications. It has a big impact in a lot of processes and is of great interest in life sciences, food and beverage processing, soil examination, and in marine and pharmaceutical research. There is a need for sensors which are capable to measure and monitor pH in real world applications and can tackle the challenges which comes with it.[1]

Microfluidic systems have experienced a step rise in academia in the last two decades due their unique properties. Their origin lies in miniaturized analytical systems like a gas chromatograph, which was developed at Stanford University [2], or systems for total analysis.[3] Microfluidic systems are defined by small processed volumes (usually µl to fl) which leads to large surface to volume ratios. Because of the miniaturization this technology offers a lot of advantages like minimized reagent and sample consumption, high reproducibility and controllability, the possibility for increased automatization and high cost efficiency due to mass-production from inexpensive polymers. Research fields such as industrial and environmental monitoring, diagnostics, point-of-care testing, analytics and microreachtion technology have great interest in microfluidics and are pinning their hopes on it.
One of the biggest challenges for this technology is the measurement and monitoring of certain parameters. The most promising tool therefore are optical sensors.

Hence the aim of this thesis is the development of an optical pH sensors for microfluidic applications. With respect to the trend of using droplet microfluidic systems it was decided to focus on nanobeads as a platform since it is possible to incorporate them into almost every microfluidc system. Because of the superior sensing properties of light in the near infrared, an indicator dye which absorbs and emits in this region of the electromagnetic spectrum is used. Since this is true for aza-BODIPY dyes and due to their excellent photostability, their expected pKa around pH 7 (when entrapped into a matrix) and their acceptable quantum yield they where chosen as indicator dyes. In order to enable a referenced measurement, $PtTPTBPF_4$ was used as a reference dye for establishing a DLR system.
The reached goals and the certain limitations of this attempt to designing a pH sensitive optical sensor system based on nanoparticles is covered in this thesis.

2 Theoretical Background

2.1 Fundamentals of Luminescence [4]

Luminescence is the emission of photons from an electronically excited species. A particular case of luminescence is photoluminescence which can be differentiated into fluorescence, phosphorescence and delayed fluorescence. It is defined by absorption of light being the mode of the excitation.
In this chapter various aspects of photoluminescence and the possibility to be used for sensing purposes will be discussed.

2.1.1 Transition Processes between Electronic States [4]

The best way to visualize transition processes between electronic states is with the so called Perrin-Jablonski diagram (shown in fig. 2.1). In this diagram S_X describes the electronic singlet states with S_0 being the fundamental electronic state ($\widehat{=}$ ground state). T_X on the other hand describes the electronic triplet state. Each of this electronic states possesses several different vibrational levels.
The transitions between this energy level happen at different time scales shown in table 2.1.

Table 2.1: Characteristic times.

process	time
absorption	10^{-15} s
vibrational relaxation	10^{-13} - 10^{-10} s
lifetime of the excited state S_1	10^{-10} - 10^{-7} s $\rightarrow$ fluorescence
intersystem crossing	10^{-10} - 10^{-8} s
internal conversion	10^{-11} - 10^{-9} s
lifetime of the excited state T_1	10^{-6} - 1 s $\rightarrow$ phosphorescence

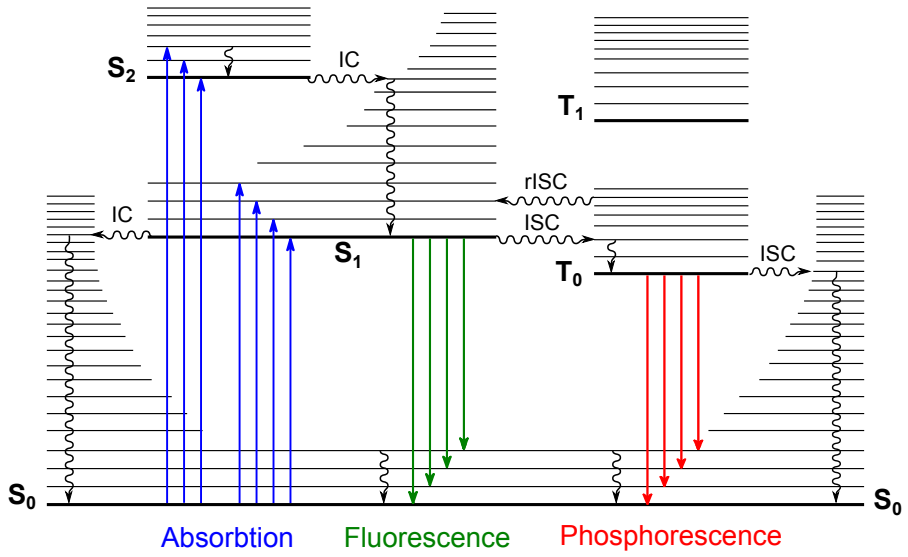

Figure 2.1: Perrin-Jablonski diagram.

Absorption

Through absorption of a photon an electron of the HOMO (Highest Occupied Molecular Orbital) of a molecule is promoted to its LUMO (Lowest Unoccupied Molecular Orbital). The energy difference between those two orbitals defines the wavelength ($\widehat{=}$ energy) of the absorbed photon. This energy difference depends amongst others on the type of orbitals between which the transition is happening. In the case of n $\longrightarrow \pi^*$ or $\pi \longrightarrow \pi^*$ transitions the needed energy corresponds to photons of the visible light. $\sigma \longrightarrow \sigma^*$ or n $\longrightarrow \sigma^*$ transitions take place at higher energies and therefore the wavelength of the absorbed photons is lower (absorption in the far UV-region).
The energy difference between the orbitals for $\pi \longrightarrow \pi^*$ transitions is mainly depending on the size of conjugated π-system. The larger the system, the smaller the energy difference. Usually several conjugated bonds are needed to enable absorption in the VIS-region.

The probability for a transition to happen is an intrinsic property of a molecule and can be described with the Beer-Lambert law (eq. 2.1). In this law A_λ is the absorbance at wavelength λ of a sample and describes the amount of absorbed photons. I_0 is the intensity of the irradiated light whereas I_1 is the intensity of the transmitted light. c is the molar concentration of the absorbing molecule, d is the pathlength of the light through a sample (normally given in cm) and ϵ_λ represents the (decadic) molar extinction coefficient at the wavelength λ given in $l \cdot mol^{-1} \cdot cm^{-1}$.

$$A_\lambda = \log\left(\frac{I_0}{I_1}\right) = \epsilon_\lambda \cdot c \cdot d \tag{2.1}$$

In general the spin multiplicity of the molecule is not change during excitation. The ground state exhibits in most cases a spin quantum number of zero (S= Σs_i, with $s_i = +\frac{1}{2}$ or $-\frac{1}{2}$) and since this remains unchanged, both the ground and the excited state have spin multiplicities equal to 1 ($M = 2S + 1$). They are therefore called singlet states and the absorption is a singlet-singlet transition process.

As stated in table 2.1 absorption is a very fast process (10^{-15} s). According to the Born-Oppenheimer approximation the movement of the electrons is therefore much faster than the motions of heavy nuclei ($10^{-10} - 10^{-12}$ s) and they can be considered as stationary during the excitation. Due to the fact that the positions of atoms in the ground state will not be equal of to the positions in the excited state, the "vertical transition" from the vibrationally lowest state will most likely populate a vibrationally excited state. This is called the Frank-Condon principle.

Internal Conversion

If an electron is excited in a higher singlet state than the S_1 internal conversion (IC) to a isoenergetic state of a lower singlet state is possible. In solutions this process is typically combined with vibrational relaxation which causes the electron to drop energywise to lowest vibrational level of the occupied electronic state. This whole cascade reaches the lowest vibrational level of S_1 within a timescale of 10^{-13} to 10^{-10} s. This much faster than all other possible transitions.
The internal conversion form S_1 to the electronic ground state S_1 is much slower though and has to compete with emission of photons (fluorescence) and intersystem crossing to the triplet state from which phosphoresce is possible. This is due to the larger energy gap between S_1 and S_0 than between the other singlet states which makes the internal conversion less efficient and therefore slower.

Fluorescence

Fluorescence is the emission of photons accompanied with the $S_1 \longrightarrow S_0$ relaxation. This emission happens almost always from the lowest vibrational level of S_1 because of vibrational relaxation. Therefore the emission wavelength is independent of the excitation wavelength.
Moreover this vibrational relaxation and possible internal conversion beforehand leads to a certain energy loss. This is the reason why the emitted light has always a longer wavelength (lower energy) than the absorbed light. This difference in is called the Stokes shift. Since the emission of light energy follows the same rule as the absorption of light, the Frank-Condon principle also applies. Therefore mainly excited vibartional levels of the ground state are

populated. Since the energy difference between the various vibrational levels of S_1 and S_0 are usually very similar, the emission spectra of a molecule mirrors the absorption spectra but at longer wavelength.
In general the emission of photons is as fast as the absorption (10^{-15}). However, the S_1 state of excited molecules has a lifetime of a few nanoseconds before any transition occurs. This leads to a exponentiation decay of fluorescence with a characteristic time (average lifetime of S_1) when molecules are excited by a very short light pulse.

Intersystem Crossing

The third possibility for a de-excitation process within the lifetime of the singlet S_1 state is intersystem crossing (ISC) to the excited triplet state T_1. Although this process is in principle forbidden due to the different spin multiplicities (spin-forbidden transition) it is still possible when spin-orbit coupling is large enough. In fact the transition is often fast enough (10^{-7}-10^{-9}) to compete with the other two de-excitation processes. Spin-orbit coupling is caused by overlapping wavefunctions of excited states even when their spin multiplicity is different. This effect is enhanced in the presence of heavy atoms (e.g. Br, Pb) and can be therefor even favor intersystem crossing.

Phosphorescence

The lowest vibrational level of T_1 has, compared with the S_1, a relatively long lifetime since all de-excitation processes are spin-forbidden. Anyhow, due to spin-orbit coupling they are possible and in solutions at room temperature non-radiative de-excitation is favored. Collision with solvent molecules lead to a relatively fast relaxation via intersystem crossing and vibrational relaxation to the S_0 state. However, at low temperatures or if the molecule is embedded in a regid matrix this deactivation processes are less likely and the lifetime of T_1 is long enough to enable phosphorescence. This radiative relaxation from the T_1 state can be observed on time-scales up to seconds or even minutes under theses conditions.
Since the energies of triplet states T_1 are generally lower than those of singlet states S_1 the phosphorescence spectrum is located at higher wavelength (lower energy) than the fluorescence emission.

Delayed Fluorescence

For delayed fluorescence to happen it is necessary that reverse intersystem crossing (rISC) from T_1 to S_1 occurs. This process can take place if the energy difference between the two states is relatively small and the lifetime of T_1 is long enough. Since the transition has to happen from

an excited vibrational level of T_1 to get to the S_1 state there are two possibilities to activate the lowest vibrational level. On the one hand the electron can be thermally activated (E-type) which leads to increasing efficiency with increasing temperature. The second possibility is triplet-triplet annihilation (P-type) where the activation happens because of the collision of two activated molecules in the T_1 state. This allows one of the molecules to return to the S_1 state and takes place in concentrated solutions.
After repopulation of the S_1 state the same deactivation processes discussed above (IC, fluorescence and ISC) can happen again. The only difference between the delayed fluorescence emission compared with the prompt fluorescence is the characteristic lifetime which is in the same region than for phosphorescence since it depends also manly on the lifetime of the triplet state.

2.1.2 Intermolecular Deactivation Processes [4]

Next to intrinsic de-excitation processes also intermolecular deactivation processes can occur. This possibility, where an excited molecule (fluorophor) M^* interacts with a second molecule Q, is commonly referred to as "quenching". Quenching leads to a decrease of the fluorescence intensity, the quantum yield and in some cases also the decay time. There are different mechanisms involved in this bimolecular interaction. The de-exitation can be based on the transfer of energy, electrons or protons, the formation of excimers or exciplexes or the collision with heavy atoms (e.g. halogenids) or paramagnetic molecules (e.g. O_2, NO). In this context the existence of intramolecualr deactivation processes should be mentioned as well (e.g. intramolecular charge transfer, internal rotation, intramolecular proton transfer). These processes of course affect the fluorescence characteristics but since they play a miner role or behave similar to intermolecular processes they are not discussed in detail.

In general there are several different scenarios how the interaction of the excited molecule M^* with the quencher Q can happen.
Case A: Q is in an large excess compared to M^*. In this case the probability that M^* and Q are in close proximity, so that their incineration is significant, during the time of excitation is high. Therefore no mutual approach of the two molecules is necessary. When the probability of the quencher molecule being within the encounter distance of M^* is less than 1, this situation is described as static quenching (see section 2.1.2). When the probability is equal to 1 the concentration of Q does not have any influence on the kinetics of the deactivation process and the reaction can be considered of pseudo-first order. This is normally the case for photoinduced proton transfer (PPT) reactions in aqueous solutions since water is the quencher in this case.
Case B: Q is not in an large excess compared to M^*. In this case mutual approach of the two molecules is not possible within the lifetime of M^* in the given (viscous) medium. However

quenching still can occur if the interaction distance to enable quenching is longer than the collisional distance. This is the case for long-range non-radiative energy transfer which is possible for distances up to 80 Å.

Case C: Q is not in an large excess compared to M* and mutual approach is possible during the lifetime of M*. This bimolecular process is diffusion-controlled and is called dynamic quenching(see section 2.1.2). If the concentration of Q is high, static quenching can happen additionally (see section 2.1.2).

Dynamic Quenching

As mentioned above, the quenching rate constant k_Q for dynamic quenching is consider to be time independent in a first approximation. Dynamic quenching reduces the fluorescence intensity and also the decay time. The fluorescence decay time τ can be described like that:

$$\frac{\tau_0}{\tau} = 1 + k_Q \, \tau_0 \, [Q] \tag{2.2}$$

I this equation τ_0 represents the decay time in the absence of a quencher, whereas [Q] gives the quencher concentration.

Since the relation of $\frac{\tau_0}{\tau}$ is equal to the relation of the steady-state fluorescence intensities ($\frac{I_0}{I}$) and the fluorescence quantum yields ($\frac{\phi_0}{\phi}$) the equation can be further extended.

$$\frac{\phi_0}{\phi} = \frac{\tau_0}{\tau} = \frac{I_0}{I} = 1 + K_{SV} \, [Q] \tag{2.3}$$

This equation is the so called Stern-Volmar relation. In this relation the product of k_Q and τ_0 is substituted by the Stern-Volmar constant K_{SV}.

Static Quenching

As mentioned above, situations in which the quenching process is not depending on molecular transport (no mutual approach of Q and M*) are called static quenching. For this situations it is characteristic that the ratio of lifetimes ($\frac{\phi_0}{\phi}$) is unchanged at different concentrations of the quencher, whereas the intensity ratio ($\frac{I_0}{I}$) behaves according to Stern-Volmar like for dynamic quenching. To explain this behavior the concept of the sphere of effective quenching has been proposed. This concept states that in order for static quenching to happen the quencher Q has to be already inside an encounter sphere of the excited molecule M* since it is not possible for Q to move there within the lifetime of M* in viscous media. Therefore only the amount of quenched molecules changes with the concentration of the quencher. The average lifetime on the other hand is unchanged since the decay of the unquenched excited molecules M* is independent of the quencher. A typical example for static quenching is the formation of non-fluorescecnt complexes in the ground state.

Simultaneous Dynamic and Static Quenching

Both dynamic and static quenching can happen simultaneously when the molecular transport (mutual approach of Q and M*) is generally possible like in the case of dynamic quenching. Static quenching starts to play a role at increasing concentrations of Q (Q is even without mutual approach within the encounter radius of M*). Therefore it leads to a deviation from the linear Stern-Volmar plot at high concentrations of Q. Simultaneous quenching is often associated with quenchers forming complexing agents which do not emit photons.

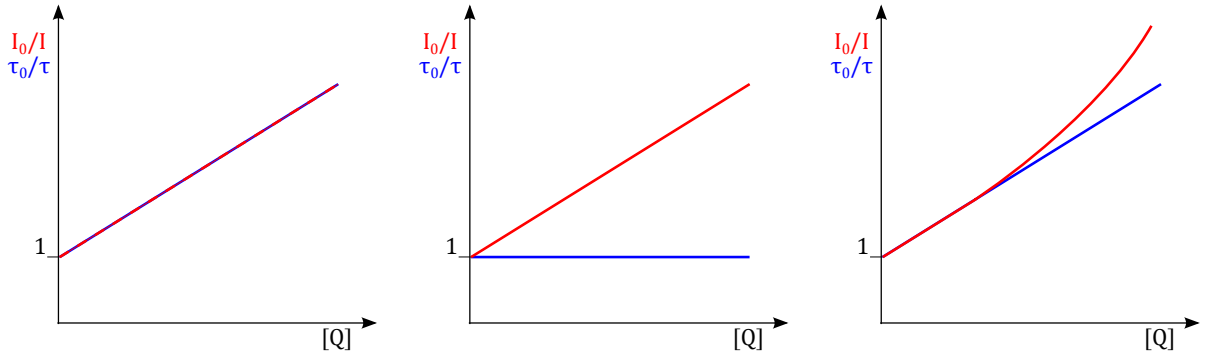

(a) Dynamic Quenching (b) Static Quenching (c) Dynamic and Static Quenching

Figure 2.2: Stern-Volmar plots illustrating the different quenching situations.

Photoinduced Electron Transfer (PET)

PET is one of the most common quenching mechanism and is involved in various organic photochemical reactions. For example it plays a major role in photosynthesis and is also used for organic photovoltaic devices. PET is therefor a well studied mechanism and is more predictable compared with other quenching processes like ISC and electron exchange. The redox potential of the excited molecule and the quencher hereby provide information of possible electron transfers. In general the excited molecule can act as a electron donor as well as an acceptor although oxidative electron transfers (M* being the donor) are more common. In fig. 2.3 both transfer are shown in a simplified scheme and one can see that oxidative and reductive properties of a molecule can be enhanced due to excitation.

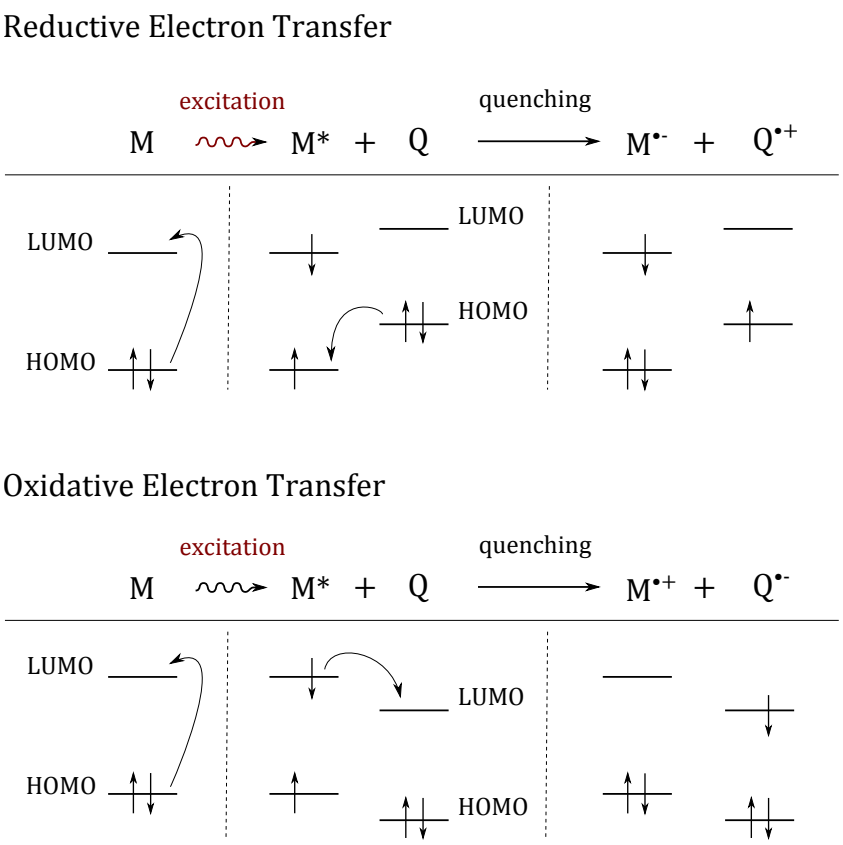

Figure 2.3: Reductive and oxidative electron transfers.

Formation of Excimers and Exciplexes

The terms excimer and exciplexe both refers to excited bimolecular species, whereas excimers ("**exci**ted di**mer**") consist of dimers and exciplexes ("**exci**ted com**plex**") of complexes in the excited state. They are formed by collision of an excited molecule M* with either an identical unexcited molecule or an unlike molecule which acts as a electron donor or acceptor (A or D).

$$
\begin{aligned}
{}^1M^* + {}^1M &\rightleftharpoons {}^1(MM)^* \\
{}^1M^* + A &\rightleftharpoons {}^1(MA)^* \\
{}^1M^* + D &\rightleftharpoons {}^1(MD)^*
\end{aligned}
$$

Excimers posses also fluorescence properties which are not necessarily weaker than the original ones. Their emission is bathochromically shifted and has no vibrionic levels like the emission of the monomer does.
Since the formation is based on the collision of the molecules these processes are diffusion-controlled and the photophysical effects are therefore detectable mainly at relatively high concentrations. Temperature and viscosity are of course important parameters since thy have a huge influence on the number of collisions which can happen during the excited-state lifetime.

Photoinduced Proton Transfer (PPT)

Typical PPT reactions are happening in aqueous solutions where water molecules act as electron acceptor or donor counterparts for the excited molecule. Therefore this processes are not diffusion controlled.
Since the electronic properties of a molecule in the excited state differ from the ones in the ground state also acidic and basic properties can be changed due to the electronic redistribution. Especially the cases where acids and bases get stronger upon excitation are interesting since this behavior triggers photoinduced proton transfers. For example the pKa value of a proton donor group (e.g. an OH substituent of an aromatic ring) can be dramatically decreased compared to the pKa in the ground state leading to much stronger acidic behavior. In the same way an increase of the pKa value of proton acceptors (e.g. heterocyclic nitrogen atom) leads to stronger basic properties.
The possibility for PPT to happen depends again on the lifetime of the excited molecule and the ratio between the rates for proton transfer and competitive deactivation processes. The simplest case of PPT with no geminate proton recombination is shown in fig. 2.4 for an acid which gets stronger with excitation ($pKa^* < pKa$). It is noteworthy that in contrast to the deprotonation rate k_1, which is of pseude-first order, the reprotonation rate k_{-1} is a second-order rate constant and therefore diffusion-controlled. Because of this it is pH-dependent and if the pH value of the solution is smaller than 2 the back-reaction is fast enough so it has to be taken into account. In fact it is in the same order than the excited-state lifetime of most organic bases and PPT can't be considered as an effective quenching process anymore.

The pKa^* value can be theoretically predicted by the Förster cycle (fig. 2.5) which takes

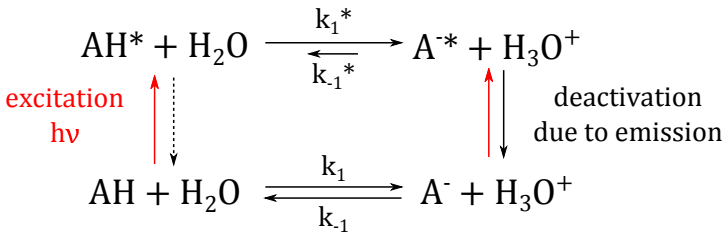

Figure 2.4: Processes happening in a simple PPT.

spectroscopic measurements of the involved species into account. Assuming that the ionization entropies of the excited state and the ground state are equal eq. 2.4 can be transformed in eq. 2.5.

$$N_a h\nu_{AH} + \Delta H^{0*} = N_a h\nu_{A^-} + \Delta H^0 \tag{2.4}$$

$$pKa^* - pKa = 2.1 \cdot 10^{-3} \left(\tilde{\nu}_{A^-} - \tilde{\nu}_{AH}\right) \tag{2.5}$$

In this equations N_a is the Avogadro's number, $h\nu$ is the energy difference of the 0-0 transition between the excited state and the ground state, ΔH is the standard molar ionization enthalpies and $\tilde{\nu}$ is the wavenumber corresponding to the 0-0 transition.
According to eq. 2.5 pKa* is lower than pKa, if the emission band of the basic form is located at higher wavelengths than that of the acidic form. Therefore AH* is a stronger acid than AH.

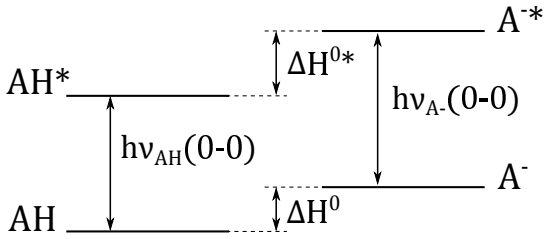

Figure 2.5: Förster cycle.

Excitation Energy Transfer (EET)

An excited molecule (D*) can transfer its stored energy to an another molecule (A). In general it is differentiated between homotransfer, where the donor and the acceptor molecule are of the same kind, and heterotransfer where the interaction happens between two different molecules. Further EET can be classified into radiative or non-radiative transfer.

(a) Radiative Energy Transfer
Radiative energy transfer is a two step process where the excited molecule emits photons which are subsequently reabsorbed by another molecule. Therefor the distance between the molecules has to be larger than the wavelength of the emitted photon. The emission spectra of the donor molecule overlaps with the absorption spectra of the acceptor molecule and in this region the fluorescence intensity is decreased. this type of energy transfer is commonly revered to as inner filter effect. There is no further interaction between the molecules required. Anyhow there is no analytic tool using this transfer and in application this effect is rather unwanted. It can be avoided by working with low dye concentrations in media which doesn't absorb in the area of interest.

(b) Non-Radiative Energy Transfer
Non-radiative energy transfers occur without emission of photons at distances shorter than the wavelength. For it to happen molecular interactions are needed and a overlap of the emission spectra of te donor and the absorption spectra of the acceptor is needed. The overlap grantees that in both molecules transitions occur with the exact same energy which than can be coupled (i.e. are in resonance). Therefor this type of transition is often also revered to as RET (resonance energy transfer). RET does not chance the appearance of the fluorescence spectrum and just

the intensity is decreased.
According to the type of molecular interaction one differentiated between two mechanisms called Förster's and Dexter's mechanism. On the one hand coulombic (e.g. dipole - dipole) interactions lead to FRET (Förster resonance energy transfer). It is effective over distances up to 10 nm and while the electron of the donor is returning from the LUMO to the HOMO, an electron in the acceptor is promoted from the HOMO to the LUMO. This is just true for spin-allowed transitions since for spin-forbidden ones FRET is negligible. In this cases only resonance transitions according to Dexter's mechanism can be observed. They happen due to intermolecular orbital overlap and are effective over distances of < 1 nm. Anyhow, in spin-allowed transitions FRET is predominate even at small distances.

2.2 Optical Chemical Sensors

Optical chemical sensor, often also revered to as optodes, have made a steep rise in both academia and industry in recent years. They are widely applied in fields like biomedical research [5, 6], biotechnology [7, 8], marine biology [9, 10], biological and toxicological screening [11, 12] and food packaging [13]. Optodes are capable of monitoring various parameters and respond quite selectively to different chemical species like oxygen, pH, CO_2, glucose and various ions.
Optical chemosensors gain information about analytes with fully synthetic receptors which interact with electromagnetic radiation. They can generally be separated into three functional units: A recognition element (i.e. receptor) which identifies and interacts with the analyte, a transducer element which converts the chemical recognition in a measurable optical signal and a detector element which recognizes changes in the optical signal, converts them into electrical signals and provides them to a read-out unit. [14]

Like most analytical tools optodes should be sensitive and selective towards the analyte, have a linear response, a wide dynamic range and a good reproducibility. Moreover, optical sensors should additionally show high luminescence brightness, have a good mechanical and chemical stability, obtain high photostability and be versatile in their scope. Other important requirements, especially for industrial applications, are that the sensors should be cheap, robust, easy to use and small.
In general analytical tools based on luminescent are great in tackling those task since they naturally have a high sensitivity. They are also quite selective and can cover a whole variety of different measurements like intensity and decay time measurements or kinetic studies.[15] Moreover, the temporal and spatial resolution [16, 17] of fluorescent techniques can be changed and they enable the observation of various wavelength.

2.3 Fluorescent pH Indicators

The measurement of pH values is traditionally done electrochemically and glass electrodes provide accurate results in most cases. Anyhow, since they can't be miniaturized and are susceptible for electromagnetic interferences there are enough application where their use is not sufficient.
Optical sensors based on fluorescent pH sensitive indicator dyes are therefore a great alternative. They are easy to miniaturize, highly sensitive within their dynamic range, robust and inexpensive. However, they have also some drawbacks like their cross-sensitivity to ionic strength, especially at low salinity levels [18] which lead to s shift of the calibration plot. This is due to pH being defined as the negative decadic logarithm of the activity of protons H^+ rather then the negative decadic logarithm of the H^+ concentration. Both values are related over activity coefficients (f_A, f_B) as one can see in the Henderson-Hasselbalch equation (eq. 2.6).

$$pH = pKa + log\frac{[A^-]}{[HA]} + log\frac{f_{A^-}}{f_{HA}} \tag{2.6}$$

The activity coefficients depend on factors like the ionic strength and the interaction of the indicator dye with its microenvironment. Because the results of optical measurements display the concentration of protons (respectively the concentration of deprotonated or protonated indicator dye molecules) and not, like electrochemic measurements, the activity, this above mentioned cross-sensitivity exists. However, if low charged indicator dyes are embedded in uncharged hydrogel matrices this effect can be minimized and reliable optical pH measurements are possible.[19–22]
On this point it should be emphasized that measured pKa values of indicator dyes are "apparent" since they strongly depend on the interaction of the dye with environmental medium and micro-heterogeneouse media (i.e. solvent and matrix).[23]
Another difference of optical pH sensing to electrochemical measurements is the appearance of the calibration curve. It has a sigmoidal shape with its highest signal change close to the apparent pKa of the sensor. The dynamic range of fluorescent pH indicators is normally limited to about ± 1.5 pH units. This is quite narrow but therefore leads to a high sensitivity around the pKa. Since in many applications monitoring of the pH just within a small window is necessary (e.g. biotechnological systems ~pH 6.5, physiological applications ~pH 7.4, marine systems ~pH 8) this limits their application just to a certain degree.

In general fluorescent pH sensitive indicator dyes can be classified depending on their de-excitaion mechanism:

2.3.1 A: Fluorophores that Undergo PPT [4]

Most fluorophores based on photoinduced photon transfer are much more acidic in the excited state and have therefore a lower pKa value than in the ground state. Consequently excitation of the acidic form of the indicator dye is followed by quick excited-state deprotonation at pH values around the pKa of the ground state. Therefore the emitting form is always the basic form of the fluorophore and the fluorescence spectrum of these dyes is unchanged in contrast to the absorption spectrum.
Prominent example of this class of dyes are pyranine and hydroxycoumarins. Pyranine and its derivatives have pKa values around 7, provide good photostability but are generally very sensitive to ionic strength and have quite low excitation wavelength. [24, 25] Hydroxycoumarins have found their application in intracellular pH sensing.[26, 27]

2.3.2 B: Fluorophores that Undergo PET [4]

The non-protonated form of indicator dyes which undergo PET exhibit very small fluorescence quantum yields due to internal quenching by the transfered electrons. Protonation of the dyes suppresses the electron transfer and the fluorescence is therefore largely increased. Fluorescence and absorption spectra ot theses class of fluorophores are generally independent of the pH value. Most of theses indicator dyes consist of a fluorophore linked with a amine moiety with a methyl spacer. At high pH values the lone pair of the amine is transfered to the aromatic backbone of the dye and the fluorescence gets internaly quenched as described above. At lower pH values the amin gets protonated and therefore has no electrons left for a possible transfer. This mechanism provides potentially higher sensitivity than PPT based indicators.

2.3.3 C: Fluorophores that Exhibit neither PPT nor PET [4]

This class of fluorophors show a spectral shifts of the absorption and the emission spectra with varying pH. It is characteristic that thereby both spectra behave similar which means that when increasing the pH, the absorption and emission bands of the acidic form should decrease with a concomitant increase in the absorption and emission bands of the basic form. Prominent representatives of this class of dyes are SNAFL and SNARF dyes as well as xanthene dyes like fluorescein derivatives and eosin Y.

2.4 Optical pH Sensing Methods

The simplest form of optical pH sensing is done by the measurement of the luminescence intensity. Unfortunately this methods has quit some disadvantages due to the influence of factors like light source intensity, concentration of the fluorophore, photobleaching or leaching of the indicator dye, ambient light, scattering and detection efficiency. Also temporal or spatial inhomogeneities have a huge influence on the measurement. To overcome this problems several different ratiometric or time-resolved techniques can be used.
Ratiometric measurement is the most applied technique nowadays. Different methods can be used for either a single fluorophores or for a combination of dyes. For single indicator dyes a pH dependent ratio of fluorescence intensities is measured between either two excitation or two emission wavelength. This method requires dyes where the acidic and de basic form of the indicator dye have different spectral behavior (typically fluorophores which exhibit neither PPT nor PET like above mentioned fluorescein, SNAFL or SNARF dyes). The use of PET-based indicator dyes for ratiometric measurements is just possible when a additional reference dye is added since they don't exhibit a spectral shift between the acidic and the basic form.
Classical lifetime measurements require bulky and expensive equipment since pH sensitive fluorophores exhibit just very short lifetimes. Therefore a phase modulation technique called dual lifetime referencing (DLR) can be used to avoid the high costs. This method was first published by Huber et al. for chlorine sensors. [28] DLR is based on two different luminophores which are simultaneously excited at the same wavelength but exhibit different decay times. In the case of pH measurements additionally to the pH sensitive dye, which has a quite short lifetime, a phosphorescent reference dye is used. The principle of DLR is shown in fig. 2.6.

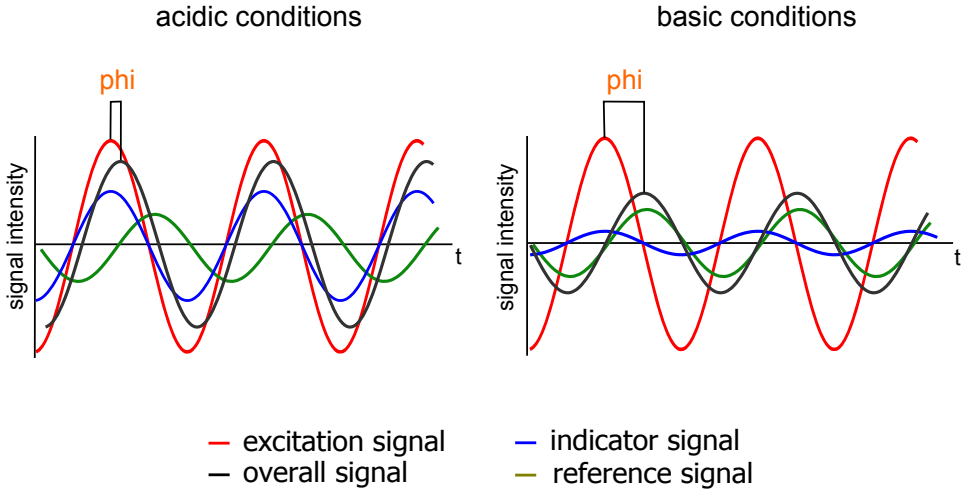

Figure 2.6: Principle of DLR for pH measurements.

DLR measures the phase shift ϕ of the overall signal with respect to the excitation signal. At

acidic conditions the fluorescence signal of the pH indicator is strong, which leads to small phase shift of the overall signal. When the fluorescence signal is quenched at basic conditions and the overall signal consists mainly of the phosphorescent signal of the reference dye, the phase shift gets larger due to the longer lifetime of the reference dye.
As long the ratio of indicator to reference dye stays constant the DLR measurement is independent of ambient light and variations of luminophore concentration or fluctuations of the light source and the photodetector.

2.5 Integration of Optical Sensors in Microfluidic Systems

2.5.1 Microfluidic Systems

Nowadays microfluidic systems are created as "lab-on-a-chip" devices where all necessary components are already integrated on the chip respectively on a small number of subsequent chips. One of the main problems of this technology is the integration of the necessary analytical tools since miniaturization leads to a couple of challenges like a decreased number of analyte molecules compared to traditional devices due to reduced sample volumes. Therefore a high sensitivity of the used methods is needed, especially since the analyte concentration may not be changed during measurement. Another important factor is that the device has to be able to work at such small dimensions, which is not possible for all existing sensing technologies. Since most microfluidic devices are used as disposals, their costs play a really important role. For all these challenges fluorescent sensors offer great solutions, especially since their integration can be accomplished rather simple.

2.5.2 Sensor Formates

Different sensor formates for the application of optical sensors have been developed making them a versatile platform which can be integrated into microfluidic chips. The decision for one formate should always be made according to the measurement requirements and be coordinated with the detection method. For example spatial resolution needs different formates and read-out units than single-point measurements. Another important factor is the type of microfluidic device which is used since the possibilities for integration are different for self-constructed chips and commercially available ones.
In fig. 2.7 the four general sensor formates are shown. Although soluble probes should not be referred to as sensors, they will be discussed briefly within this chapter since they have been used for microfluidc applications.

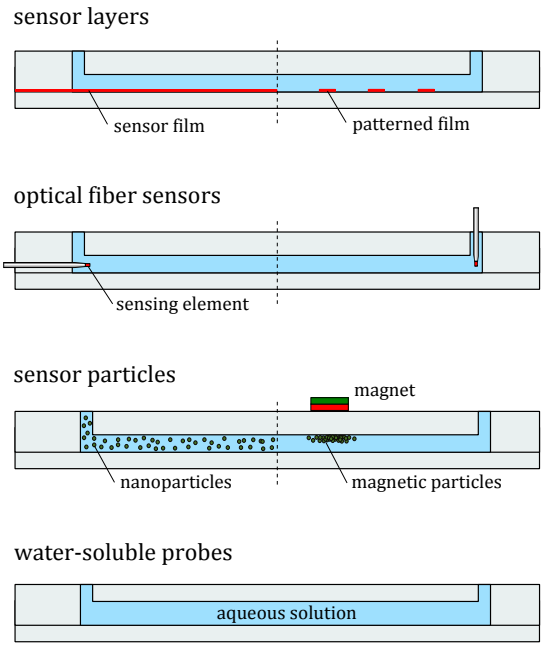

Figure 2.7: Various sensor formates for the integration into microfluidic systems.

Sensor Layers

Sensor layers are the widest applied format and are usually made by deposition of a sensor cocktail (solution of matrix material, indicator and additives) on a substrate via knife coating, spin-coating, spray coating, screen printing inkjet or pin-printing. Afterwards the wet film is allowed to dry or polymerize. An additional curing process is also possible. The used layers can be either homogeneous or pattered and their fabrication is usually compatible with microfabrication techniques.
Another advantage of this concept is that the sensor layers do not need additional effort once they are applied and that they can be used for single point measurements as well as for imaging applications. A drawback however is that the integration into ready-made chips is till now not possible and therefore only people who fabricate their one microfluidic devices are able to use this format. Moreover, the requirements for long-term stability of the sensor material are way higher than for other formates since photobleaching and leaching effects limit the usability of chips with integrated layers.

Optical Fiber Sensors

Optical fiber sensors are another useful sensor format since they can be used at poorly accessible sites and under harsh or hazardous conditions. They normally consist of an sensing element (matrix material and indicator dye) attached to an optical fiber, which serves as a waveguide

for the excitation and emission light. Optical fiber sensors are typically fabricated by dip-coating from a sensor cocktail and subsequent removal of the solvent. The sensor material can additionally be cured or polymerized.
Although fiber sensors are due to their nature limited in their resolution and can basically just perform single-point measurements, it is still possible to measure gradients by using an array of sensors.[29]

Sensor Particles

Sensor beads exhibit outstanding properties when it comes to flexibility concerning integration into microfluidic chips. They can simply be added to the fluid like dissolveable indicators but they have way superior properties regarding selectivity since the indicator is encapsulated into a suitable matrix. There are many different procedures to prepare sensor particles at a micro- or nano-scale.[30] For example it is possible to get polymeric particles via precipitation [31, 32] or straight from polymerization with adjacent staining of the particles. Another possibility is the adsorption of indicator molecules to already existing particles [24] or grinding of indicator-loaded bulk matrix material.
Next to different polymers serving as a matrix for nanoparticles, also silica can be used. As Korzeniowska et al. reviewed recently there are a lot of areas where fluorescent silica nanoparticles are applied. For example they are used for cell imaging and intracellular sensing of oxygen, pH and ionic species.[33] A combination of polymeric material and silica can also be used to achieve beneficial properties (e.g. core-shell particles). As Wang et al. have shown, imaging of the pH in bacterial growth is possible with this particles.[34] Even measurements of various parameters within living cells are possible with so-called PEBBLE sensors.[35]
Another big advantage of sensor particles is that in microfluidic systems the requirements concerning long-term stability (e.g. photobleaching) are not that high since the particles are constantly replaced. Anyhow, this sensor format bares other challenges like a the need for extraordinary brightness of the sensor particles since the reduced channel depths lead to insufficient emission intensities. Another problem is the stability of the colloids because sedimentation of particles may lead to drift.
One possibility to tackle the task of insufficient intensity values is by introducing magnetic properties to the sensor beads. [36] The particles can than be collected with a magnet at the channel wall leading to sensor spots with increased brightness compared to nanoparticle dispersions.

Water-soluble Probes

Another possibility to integrate sensing functionalities into microfluidic devices are water-soluble probes. As mentioned above, in a strict sense they should not be referred to as sensors. But since this concept is used in microfluidics they are mentioned here as well for the sake of completeness. Their main problem is that they suffer, due to the missing of an encapsulation matrix, from environmental interferences. This limits the performance of water-soluble probes drastically. Another disadvantge of the missing matrix is that certain parameters like sensitivity and selectivity can not be tuned. The most promising solution to get ride of some of these huge drawbacks is the covalent linkage to other molecules for example to branched molecules (dendrimers).[37]

2.5.3 Read-Out Units

Miniaturization of optical components in recent years led to new devices and enabled fluorescent sensing to boost its field of application. New cheap excitation sources (LED) and detection devices (photodiodes, CCDs - charge-coupled devices) made it a cost efficient technology which is also very flexible.
Generally there are two approaches to enable optical sensing on microfluidic devices. There is the off-chip approach, where excitation and detection are done at a macro-scale and are coupled to a micro-scale detection area, and there is the on-chip approach, where excitation and detection are miniaturized and directly integrated into the microfluidic chip. The benefit of the off-chip approach is application of traditional and well established sensing technologies which have low levels of background signal. The aim of the on-chip approach is the replacement of bulky and expensive equipment by micro-optical electromechanical systems (MOEMS). This development seems promising but has not arrived for all applications yet.

The off-chip approach can be further separated by the way in which excitation and detection sources are coupled with the microfluidic chip. Depending on the system this leads to different resolutions.
The most used sensor platforms for single-point measurements are fiber optical sensors. The sensing material can be applied directly on the fiber or the fiber can be used to couple light through the wall of a microfluidic chip to an embedded sensor layer or spot. Another method to couple light into a chip and measure the changes of en embedded sensor layer is with a planar waveguide. This leads of course also to a single-point measurement and provides the average value over the whole area. To get high spatial resolutions imaging techniques are best suited. These require microscopes and normally CCD-chips are used as detection device.

3 Materials and Instruments

3.1 Materials

All chemicals used during the work process are listed with their suppliers below. They were used without further purification, except for styrene, which was filtered over aluminum oxide to remove the stabilizer. Dyes and polymers which are not commercially available were supplied by the Institute for Analytical Chemistry and Food Chemistry at Graz University of Technology or synthesized as part of this work.

Table 3.1: Used polymer matrices.

Polymer		**Supplier**
Abbreviation	**Name**	
PSPVP	Poly(styrene-block- vinylpyrrolidone) (38 % w/w emulsion in water)	Sigma Aldrich
RL100	Eudragit® RL100 (12.15 % w/w of quaternary ammonium groups, MW 15000)	Degussa
PAcM	Poly(4-acryloylmorpholine- co-styrene- co-N-(3-(dimethylamino)propyl) acrylamide) (15 % w/w of quaternary ammonium groups)	synthesized
PViCl-PAN	Poly(vinylidene chloride-co- acrylonitrile) (20 % w/w polyacrylonitrile, MW 150000)	Polysciences
D4	Hydromed® D4	AdvanSource biomaterials
Mylar®	Poly(ethylene terephthalate) support	Goodfellow

Table 3.2: Used dyes.

Dye		Supplier
Abbreviation	**Name**	
ClOHbutoxy-complex	(Z)-4-(5-((5-(4-butoxyphenyl)-3-phenyl- 2H-pyrrol-2-ylidene)amino) -1-(difluoroboranyl)-4-phenyl- 1H-pyrrol-2-yl)-2-chlorophenol	synthesized
FOHbutoxy-complex	(Z)-4-(5-((5-(4-butoxyphenyl)-3-phenyl- 2H-pyrrol-2-ylidene)amino) -1-(difluoroboranyl)-4-phenyl- 1H-pyrrol-2-yl)-3-fluorophenol	TU Graz
OHbutoxy-complex	(Z)-4-(5-((5-(4-butoxyphenyl)-3-phenyl- 2H-pyrrol-2-ylidene)amino) -1-(difluoroboranyl)-4-phenyl- 1H-pyrrol-2-yl)-phenol	TU Graz
$PtTPTBPF_4$	Platinum(II)meso-tetra(4-fluorophenyl)tetrabenzoporphyrin	TU Graz
Macrolex® Red	3-(benzothiazol-2-yl)-7-(diethylamino)-2-oxo-2H-1-benzopyran-4-carbonitrile	Simon & Werner GmbH
Lumogen® Red	N,N-Bis(2,6-diisopropylphenyl)-1,6,7,12-tetraphenoxyperylene- 3,4:9,10-tetracarboxdiimide	Kremer Pigmente

Table 3.3: Used buffer substances.

Buffer		used pH range	Supplier
Abbreviation	**Name**		
H_3PO_4	phosphoric acid	pH 2.4 - 3.2	Carl Roth
AcOH	acetic acid	pH 3.2 - 4.8	Carl Roth
MES	2-(*N*-morpholino)ethanesulfonic acid	pH 4.8 - 6.0	Carl Roth
MOPS	3-(*N*-morpholino)propane-1-sulfonic acid	pH 6.0 - 7.6	Carl Roth
HEPES	2-[4-(2hydroxyethyl)piperazin-1-yl]ethanesulfonic acid	pH 7.6 - 8.4	Carl Roth
CHES	2-(Cyclohexylamino)ethanesulfonic acid	pH 8.4 - 10.0	Carl Roth
CAPS	3-(Cyclohexylamino)-1-propanesulfonic acid	pH 10.0 - 11.2	Carl Roth

Table 3.4: Other used chemicals.

Chemicals		Supplier
Abbreviation	**Name**	
ClOH-acetophenone	3´-chloro-4´-hydroxyacetophenone	TCI
butoxyacetophenone	4´-butoxyacetophenone	TCI
benzaldeyde	benzaldeyde	ABCR
CH_2NO_2	nitromethane	Sigma Aldrich
NH_4Ac	ammoniumacetate	Sigma Aldrich
BF_3Et_2O	boron trifluoride diethyl etherate	Sigma Aldrich
DIPEA	diisopropylethylamine	Sigma Aldrich
styrene	styrene	Sigma Aldrich
acryloylmorpholine	4-acryloylmorpholine	Sigma Aldrich
aminoacrylamide	*N*-(3-(dimethylamino)propyl)acrylamide	ABCR
CH_3I	methyl iodide	ACROS Organics
AIBN	azobisisobutyronitrile	ACROS Organics
glucose	glucose	Carl Roth
GOx	glucose oxidase from aspergillus niger	Sigma Aldrich
$CoCl_2$	cobalt(II) chloride	MERK
Na_2SO_3	sodium sulfite	Carl Roth
NaCl	sodium chloride	VWR
Na_2SO_4	sodium sulfate	VWR
K_2SO_4	potassium sulfate	Carl Roth
NaOH	sodium hydroxide	Carl Roth
KOH	potassium hydroxide	Carl Roth
K_2CO_3	potassium carbonate	Sigma Aldrich
HCl	hydrochloric acid	VWR
silica gel		Acros
TLC slide	thin layer chromatography slide (silica gel 60)	Merk

Table 3.5: Used solvents.

Solvent		Supplier
Abbreviation	**Name**	
acetone	acetone	Brenntag
CH	cyclohexane	VWR
hexane	n-Hexane	VWR
MeOH	methanol	VWR
EtOH	ethanol	Brenntag
THF	tetrahydrofurane	VWR
CH_2Cl_2	dichloromethane	Fisher Scientific
propanol	isopropanol	Sigma Aldrich
EtOAc	ethylacetate	VWR
octane	isooctane	MERK

3.2 Instruments

Characterization of the synthesized dye, the sensor foils and the sensor beads was done with following instruments.

NMR Spectra

^{1}H-NMR spectra were recorded with a 300 MHz instrument from Brucker with trimethylsilane (TMS) as a standard. DMSO-d_6 (purchased from Eurisotop) was used as deuterated solvent.

pH Measurement

The pH values of the buffer solutions were controlled with a digital pH-meter from METTLER Toledeo (Seven Easy) equipped with a "InLab Routine Pro" glass electrode. It was calibrated at 20 °C with standard buffers of pH 7.01, pH 4.01 and pH 10.01 from Hanna instruments.
The used buffer solutions were prepared with the buffer substances mentioned above (table 3.3) and adjusted to the desired pH value with 1M NaOH or 1M HCl. The ionic strength was controlled with NaCl as background electrolyte.

Absorption Spectra

Absorption measurements were performed on a Carry 50 UV/Vis spectrometer from Varian. All spectra were acquired in the "fast"-mode (equals 1 point per nm) and the background was corrected with pure solvent.

Emission Spectra

Emission spectra were recorded on a Hitachi F-7000 fluorescence spectrometer equipped with a red-sensitive photomultiplier R928 from Hamamatsu. All spectra were compensated with a wavelength dependent correction factor acquired from the halogen lamp calibration.

Size Measurement

Size measurements of sensor beads were performed on a particle size analyzer Zetasizer Nano ZS from Malvern.

DLR Measurement

The phase angle of the luminescent signals was measured with a Piccolo2 from PyroScience. It was equipped with a focusing lens attached to a 2 mm POV from ESKA (grade: ck-80). The fiber-optic oxygen meter was, if not stated otherwise, operated with 100 % LED intensity, a 400x amplification factor, 32 ms measuring time and a phase-modulation of 8000 Hz.

NIR Imaging

The imaging setup consists of a commercial available RGB-NIR camera JAI AD-130GE equipped with a 3 CCD lens (Video V25 C 1/2" 0.5x Adapter). It was mounted on a microscope used with a LD Plan-Neofluar 20x/0,4 Korr Ph2 lens from Zeiss. For excitation the 579 nm band of an HBO-lamp was used together with a XF1044 excitation filter. Further more a D6 dichromatic mirror and a RG610 emission filter was used. The software platform "common vision blox" (CVB 2011) from Stemmer Imaging was used to adapt the measuring software. For image processing Matlab R2009a was used.

4 Experimental

4.1 Synthesis of the ClOHbutoxy-complex

4.1.1 Synthesis of the (2E)-1-(3´-chloro-4´-hydroxyphenyl)-3-phenylprop-2-en-1-one

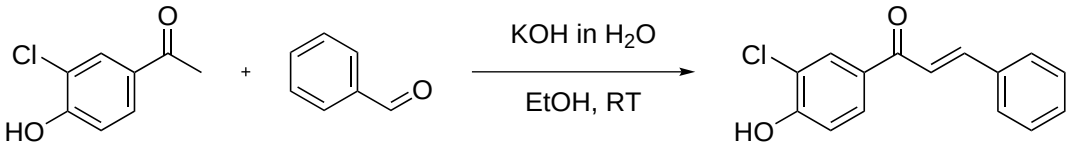

Figure 4.1: Reaction scheme for the formation of ClOH-chalcone.

ClOH-acetophenone (2.5 g, 14.63 mmol) was dissolved in 12.5 ml EtOH and benzaldehyde (1.64 ml, 16.09 mmol) was added. KOH (2.45 g, 43.88 mmol) was dissolved in 12.5 ml H_2O and added drop-wise over 10 minutes. The solution was stirred over night at room temperature. 15 ml of 1 M HCl were added to the suspension and further acidified with HCl conc. to pH 1. This yielded in precipitation of product, which was filtered and washed with H_2O to gain 3.32 g (88 % yield). The product was use without further purification.

4.1.2 Synthesis of (2E)-1-(4-butoxyphenyl)-3-phenylprop-2-en-1-one

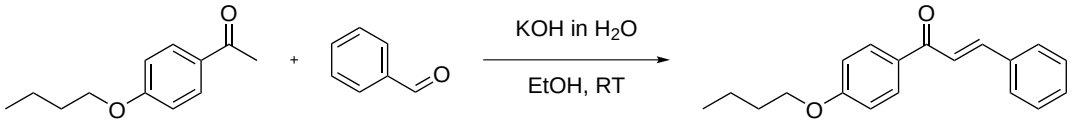

Figure 4.2: Reaction scheme for the formation of butoxy-chalcone.

Butoxyacetophenone (1.49 g, 7.73 mmol) was dissolved in 6 ml EtOH and benzaldehyde (0.864 ml, 8.5 mmol) was added. KOH (1.3 g, 23.18 mmol) was dissolved in 6 ml H_2O and added drop-wise over 5 minutes. The solution was stirred for 3.5 h at room temperature. 6 ml of 1 M HCl were added to the suspension and it was further acidified with HCl conc. to pH 1. The resulting

precipitate was filtered and washed with H_2O to gain 2.05 g product (95 % yield). It was used without further purification.

4.1.3 Synthesis of 1-(3´-chloro-4´-hydroxyphenyl)-4-nitro-3-phenylbutan-1-one

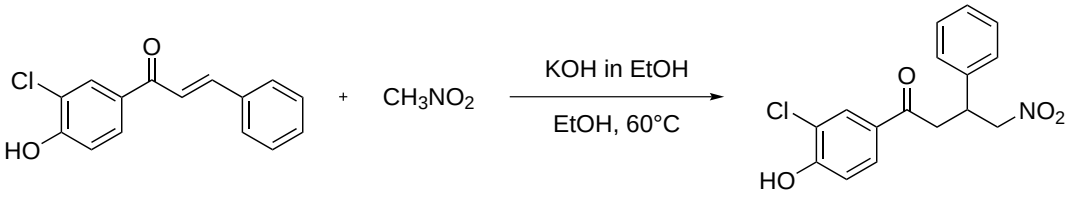

Figure 4.3: Reaction scheme for the formation of ClOH-nitrochalcone.

ClOH-chalcone (3.32 g, 12.8 mmol) was dissolved in nitromethane (13.7 mL, 256.5 mmol) and diluted with KOH (864 mg, 15.4 mmol) dissolved in 7 ml EtOH. The solution turned orange and white precipitate was formed which was dissolved with 100 ml EtOH and 60 ml MeOH. The solution was stirred at 60°C for 4 h and afterwards the solvent was removed under reduced pressure. The residual was dissolved in EtOAc and saturated NaCl solution. Afterwards the mixture was acidified with 4 M HCl to pH 1 and the phases separated. The aqueous phase was washed with 200 ml EtOAc and in the next step the organic phases were combined, dried over Na_2SO_4 and the solvent removed under reduced pressure. The product was gained in quantitative yield (4.02 g) and used without further purification.

4.1.4 Synthesis of 1-(4-butoxyphenyl)-4-nitro-3-phenylbutan-1-one

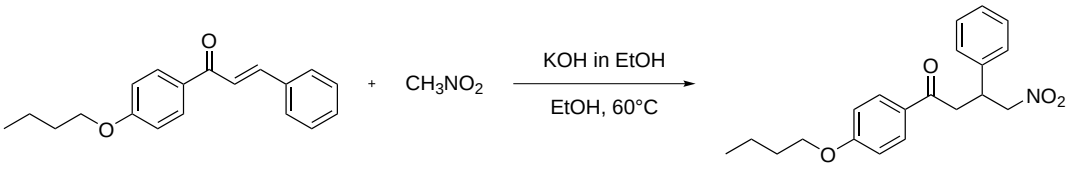

Figure 4.4: Reaction scheme for the formation of butoxy-nitrochalcone.

Butoxy-chalcone (2.05 g, 7.31 mmol) was dissolved in nitromethane (7.9 mL, 146.2 mmol) and diluted with KOH (82 mg, 1.46 mmol) dissolved in 10 ml EtOH. The solution was stirred at 60°C for 4 h and afterwards the solvent was removed under reduced pressure. The residual was dissolved in EtOAc and a saturated NaCl solution. The mixture was acidified with 4 M HCl to pH 1 and the phases were separated. The aqueous phase was washed with 200 ml EtOAc and afterwards the organic phases were combined, dried over Na_2SO_4 and the solvent removed

under reduced pressure. The product was gained in quantitative yield (2.55 g) and used without further purification.

4.1.5 Synthesis of (Z)-4-(5-((5-(4-butoxyphenyl)-3-phenyl-2H-pyrrol-2-ylidene)amino)-4-phenyl-1H-pyrrol-2-yl)-2-chlorophenol

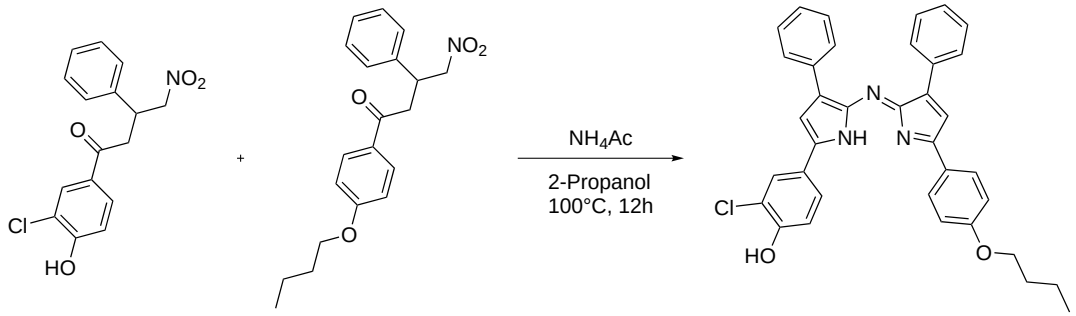

Figure 4.5: Reaction scheme for the formation of ClOHbutoxy-ligand.

ClOH-nitrochalcone (2.93 g, 9.16 mmol) and butoxy-nitrochalcone (2.55 g, 7.46 mmol) were dissolved in 100 ml isopropanol and ammonium acetate (20.12 g, 261 mmol) was added. The solution was stirred at reflux over night and turned blue. The solvent was removed under reduced pressure and the residue was redissolved in CH_2Cl_2 and a saturated NaCl solution. The phases were separated and the organic phase was washed several times with H_2O until it was clear. Afterwards the solution was dried over Na_2SO_4. Silica-gel (20 g) was added to the dry solution and the solvent was removed under reduced pressure. The product was purified on a silica-gel column with n-hexane and CH_2Cl_2 as eluents. Yield: 1.49 g (35 %). Rf = 0.13 with CH and CH_2Cl_2 mixed 1:1 as eluents. ^{1}H - NMR (300 MHz, DMSO-d_6) δ: 8.07 (d, J = 6.7 Hz, 5 H); 7.98 (d, J = 8.6 Hz, 2 H); 7.89 - 7.82 (m, 1 H); 7.58 (s, 1 H); 7.53 (s, 1 H); 7.42 (dt, J = 15.3 Hz, 7.0 Hz, 6 H); 7.18 (d, J = 8.5 Hz, 1 H); 7.14 - 7.06 (m, 2 H); 4.09 (t, J = 6.4 Hz, 2 H); 1.75 (p, J = 6.5 Hz, 2 H); 1.48 (h, J = 7.2 Hz, 2 H); 0.97 (t, J = 7.3 Hz, 3 H)

4.1.6 Synthesis of (Z)-4-(5-((5-(4-butoxyphenyl)-3-phenyl-2H-pyrrol-2-ylidene)amino) -1-(difluoroboranyl)-4-phenyl-1H-pyrrol-2-yl)-2-chlorophenol

The ClOHbutoxy-ligand (1.41 g, 2.47 mmol) was dissolved in CH_2Cl_2 (abs.) under inert atmosphere (N_2). Afterwards diisopropylethylamine (DIPEA) (4.2 ml, 24.7 mmol) and BF_3 (4.57 ml, 37.0 mmol) were added and the formation of fume (HF) was observed. After 3 h green precipitate was noticed and a TLC showed the formation of product. The solution was stirred over night at room temperature under N_2 atmosphere. H_2O and CH_2Cl_2 were added to the

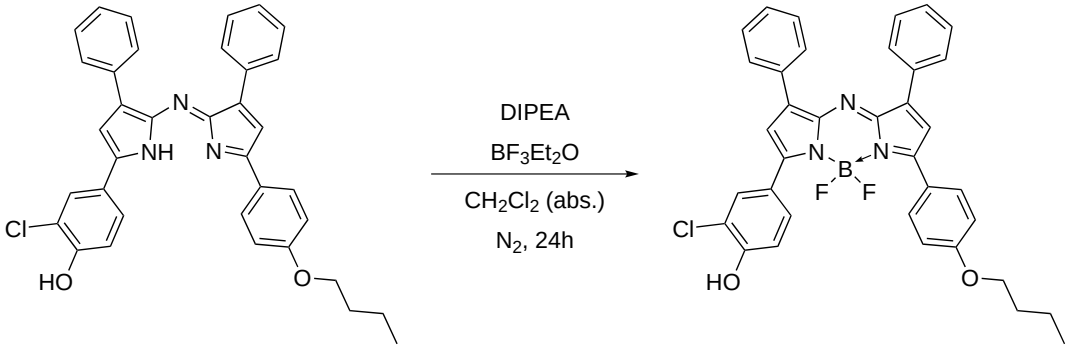

Figure 4.6: Reaction scheme for the formation of the ClOHbutoxy-complex.

solution, the phases were separated and the aqueous phase was washed with CH_2Cl_2. The combined organic phases were dried over Na_2SO_4, silica-gel (15 g) was added to the dry solution and the solvent was removed under reduced pressure. The product was purified on a silica-gel column with CH and CH_2Cl_2 as eluents. Yield: 370 mg (25 %). Rf= 0.43 with CH and CH_2Cl_2 mixed 1:2 as eluents.
For further purification the product was dissolved in CH_2Cl_2 and $MgSO_4$ was added to remove traces of free ligand. $MgSO_4$ was collected on a filter and the organic solvent under reduced pressure. The product was recrystallized from THF and isooctane. ^{1}H - NMR (300 MHz, DMSO-d6) δ: 8.26 - 8.13 (m, 7 H); 8.07 - 7.99 (m, 1 H); 7.62 (d, J = 6.1 Hz, 2 H); 7.58 - 7.46 (m, 6 H); 7.13 (t, J = 8.1 Hz, 3 H); 4.12 (t, J = 6.4 Hz, 2 H), 1.75 (p, J = 6.6 Hz, 2 H); 1.47 (h, J = 7.4 Hz), 2 H); 0.96 (t, J = 7.4 Hz, 3 H)

4.2 Preparation of Sensor Layers

1 g of polymer cocktail, containing 100 mg D4 dissolved in 1 ml EtOH/H_2O (9:1), was stained with 0.5 ml of a stock solution of aza-BODIPY in THF (c = 0.5 mg/ml). The mixture was knife-coated with a 3 mil coating knife from Byk with a application distance of 76 µm on a dust-free Mylar® foil as support. After evaporation of the solvents, an approximately 7.5 µm thick sensor layer is yielded.

4.3 Preparation of Nanoparticles

4.3.1 PSPVP Particles

This core-shell particles (see fig. 5.3(a)) were stained according to [24]. Different aza-BODIPY dyes (fig. 5.1) were used in varying concentrations to stain the shell and obtain pH sensitive

particles. In order to enable DLR measurements the core of some PSPVP particles were stained with $PtTPTBPF_4$, an oxygen sensitive, phosphorescent dye. (see fig. 5.9(b))
pH sensitive particles with a dye concentration of 0.25 % were made by diluting approximately 500 mg of aqueous PSPVP colloid (38% w/w) with 40 ml of EtOH and 20 ml of H_2O to swell the particle shell. Stock solutions with a concentration of 0.5 mg/ml in isopropanol were made of the different aza-BODIPY dyes. The appropriate amount of stock-solution (e.g. 900 µL for 474 mg PSPVP colloid) was diluted with 10 ml of EtOH and added drop-wise to the vigorous stirring PSPVP particle colloid over 5 minutes. Afterwards EtOH was removed under reduced pressure and the particles were either freezedryed or the colloid was concentrated to a particle concentration of 5 % (approx. 3.8 ml total volume). To synthesis particles with 0.5 % or 1 % dye the procedure was exactly the same, except that the double or fourfold amount of the indicator dye stock was used.
To stain the core of the PSPVP reference particles with $PtTPTBPF_4$ approximately 1000 mg of the aqueous colloid (38% w/w) was diluted with 50 ml H_2O and 30 ml THF. A stock solution with a concentration of 1 mg/ml $PtTPTBPF_4$ in THF was prepared. The appropriate amount of stock solution for a dye concentration of 0.5 % within the particle (e.g. 1900 µL for 995 mg PSPVP colloid) was diluted with 20 ml of THF. The dye solution was added to the PSPVP particle colloid drop-wise under vigorous stirring over 5 minutes. Afterwards THF and parts of H_2O were removed under reduced pressure and the colloid brought to a total volume of 38 ml which equals a particle concentration of 1 %.
For NIR imaging purposes the shell of PSPVP particles was stained with both, a pH sensitive aza-BODIPY dye (OHbutoxy-complex) and either Macrolex® Red or Lumogen® Red as a red emitting reference. Therefore approximately 500 mg of the aqueous colloid (38% w/w) was diluted with 40 ml of EtOH and 20 ml of H_2O. Stock solutions of the OHbutoxy-complex, Lumogen® Red and Macrolex® Red with concentrations of 0.25 mg/ml in isopropanol were prepared. The appropriate amounts of stock solutions for dye concentrations of 0.25 % for the OHbutoxy-complex and 1 % for Lumogen® Red or Macrolex® Red within the particle were mixed and brought to a total volume of 15 ml with EtOH (e.g. 1.9 ml of the OHbutoxy-complex stock and 7.6 ml of one reference dye stock for 500 mg PSPVP colloid). Afterwards the dye solution was added to the PSPVP particle colloid drop-wise under vigorous stirring over 5 minutes. EtOH and isopropanol were removed under reduced pressure and the aqueous colloid was freezedryed.

4.3.2 RL100 Particles

The precipitation of pH sensitive RL100 particles (fig. 5.3(b)) was done as described in [32]. Therefore stock solutions of the aza-BODIPY dyes with exactly 1 mg/ml in acetone were made. 10 ml of a 10 mg/ml solution of RL100 polymer in acetone was diluted with 40 ml of acetone.

Particles with a dye concentration of 0.25 % were made by adding 250 µl of indicator stock solution. (To fabricate particles with 0.5 % and 1 % of indicator dye, the double or fourfold amount of stock solution was used.) Afterwards the solution was stirred vigorously and the sixfold amount of H_2O (300 ml) was added within 5 seconds. Acetone was removed under reduced pressure and the mixture concentrated until a particle concentration of 0.5 % was reached (equals 20 ml of total volume).

4.3.3 PAcM Particles

Synthesis of the Polymer

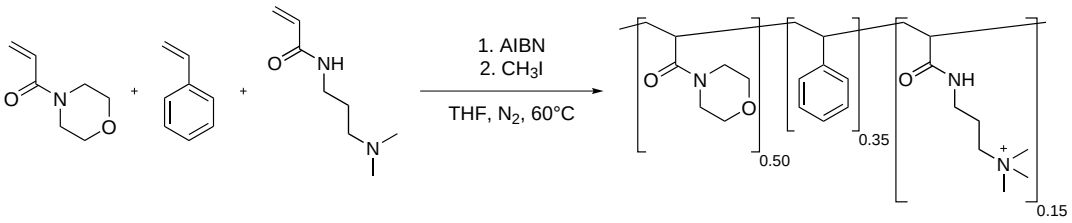

Figure 4.7: Reaction scheme for the formation of PAcM.

The polymer was synthesized via radical polymerization. Therefore styrene (0.92 g, 8.83 mmol ≙ 35% w/w), which was filtered over Al_2O_3 to remove the stabilizer, 4-acryloylmorpholine (1.31 g, 9.28 mmol ≙ 50% w/w) and *N*-(3-(dimethylamino)propyl)acrylamide (0.39 g, 2.49 mmol ≙ 15% w/w) were dissolved in 8 ml THF abs. The solution was deoxygenized for 10 minutes with N_2, AIBN (40 mg, 0.24 mmol) was added and the mixture heated to 55 °C under inert atmosphere. Since there was no change in the viscosity after 2 h, another 20 mg (0.12 mmol) of AIBN were added. The reaction was cooled to room temperature, stirred over night and diluted with 5 ml THF abs. the next day. After deoxygenizing again for 15 minutes with N_2, 30 mg (0.18 mmol) of AIBN were added and the reaction heated to 65 °C. Since now the solution was getting more viscose, CH_3I (467 µL, 7.47 mmol), diluted in 6 ml THF, was added after 2 h. The solution was diluted with another 10 ml THF and stirred for 40 minutes. Afterwards K_2CO_3 (352 mg, 2.55 mmol) was added and the reaction cooled to room temperature. The mixture was diluted with 100 ml H_2O and NaCl was added until the polymer precipitated. The precipitate was separated via centrifugation and washed several times with H_2O to remove the salt. Hereby the polymer dissolves partly in the water and therefore several fractions were taken. The polymer was further purified via extraction with CH_2Cl_2 and H_2O.

Preparation of the Particles

The preparation of PAcM particles (fig. 5.3(c)) was done by dissolving 100 mg of the polymer in 20 ml of a mixture of acetone and THF (4:1). H_2O was added until the turbidity was gone (approx. 20 drops to dissolve remaining NaCl). Afterwards 0.5 ml of a aza-BODIPY stock solution in acetone with a concentration of 0.5 mg/ml was added to yield particles with a dye concentration of 0.25 %. (For the preparation of particles with a dye concentration of 0.5 % and 1 %, the double and fourfold amount of stock solution was used.) The mixture was diluted with acetone to an overall volume of 50 ml. Afterwards the solution was stirred vigorously and the fivefold amount of H_2O (250 ml) was added within 5 seconds. Acetone was removed and the mixture concentrated under reduced pressure until a particle concentration of 0.5 % was reached. (approx. 20 ml of total volume.)

4.3.4 PViCl-PAN Particles [31]

PViCl-PAN reference particles (fig. 5.3(d)) were made by dissolving 200 mg of PViCl-PAN in 100 ml acetone and adding 3 ml of a $PtTPTBPF_4$ stock solution in acetone with a concentration of 1 mg/ml to yield particles with a dye concentration of 1.5 %. Afterwards 300 ml of H_2O were added drop-wise under vigorous stirring. Acetone was removed and the mixture concentrated under reduced pressure until a particle concentration of 0.07 % was reached. (equals 300 ml of total volume)

4.4 Measurements

4.4.1 Dye Characterization

Absorption Spectra

Absorption spectra of the dyes are obtained by diluting stock solutions containing 0.5 mg/ml in THF with the 100-fold amount of EtOH, yielding in solutions with a dye concentration of 5 µg/ml. To control the pH of the final solution, buffer stocks, using adequate buffer substance for the aimed pH value (see table 3.3), with a concentration of 50 mM were made. The salinity of the final solution was controlled by adding a NaCl stock solution with a concentration of 450 mM. Two parts of buffer stock were mixed with 3 parts of NaCl solution and 5 parts of the dye stock solution to yield the final solutions which was measured. This 1:1 mixture of EtOH and water contained a dye concentration of 2.5 µg/ml, 10 mM of buffer and 135 mM of NaCl. For the measurement 1 cm single-use cuvettes from Sarstedt (PMMA) were used.
The absorption spectra were recorded for different pH values. For the determination of the

pKa value of the dye the absorption at the maxima were plotted against the pH value and the sigmoidal curve fitted with a Boltzmann equation.

$$y = A_2 + \frac{(A_1 - A_2)}{(1 + e^{\frac{x-x_0}{dx}})} \tag{4.1}$$

In this Boltzmann equation A_1 is the maximum of the curve and A_2 the minimum. The value dx represents the slope at x_0 at which the point of inflection lies. This point represents the pKa values of the pH sensitive dyes.

Emission Spectra

To obtain the emission spectra the same solutions which are described above were used. The measurements were also performed in the 1 cm single-use cuvettes. The adjustments for the fluorimeter are shown in table 4.1.

Table 4.1: Measurement settings for emission spectra.

Dye	λ_{Ex}	scan speed	Ex Slit	Em Slit	PMT Voltage
ClOHbutoxy-complex	660 nm	1200 nm/min	5.0 nm	5.0 nm	950 V
FOHbutoxy-complex	640 nm	1200 nm/min	5.0 nm	5.0 nm	950 V
OHbutoxy-complex	640 nm	1200 nm/min	5.0 nm	5.0 nm	900 V

The emission spectra were recorded at various pH values for each dye. The corrected fluorescence intensities at the maxima of the spectra were plotted against the pH values of the buffer solutions and the resulting sigmoidal curve was fitted with a Boltzmann equation (see eq. 4.1) to get the apparent pKa value of the dye in its excited state.

Molar Extinction Coefficient

Stock solutions with a dye concentration of 5 mg/ml in THF were made for each dye. These stocks were acidified with 1 M HCl and further diluted with THF to yield three different samples of each stock with concentrations of 5 µg/ml, 3.75 µg/ml and 2.5 µg/ml. The absorption spectra of the solutions were taken and the extinction at the maxima (693 nm for the ClOHbutoxy-complex, at 685 nm for the FOHbutoxy-complex and at 698 nm for the OHbutoxy-complex) plotted against the molar concentration of the dyes according to the Lambert–Beer law (eq. 2.1). From the slopes of the linear fits, represented by $\epsilon_\lambda \cdot d$, the molar extinction coefficients were calculated.

4.4.2 Sensor Layer Characterization

Emission Spectra

A well established Hydromed® D4 matrix [22] was chosen as a standard to enable the comparison of the photophysical properties of aza-BODIPY indicator dyes entrapped into a matrix. The sensor layer on a Mylar® foil was cut into a rectangular pieces which fit exactly into the diagonal of a 1 cm glass cuevette. During the whole measurement the foil was not moved and the cuevette was filled with various buffer solutions with different pH values. The buffer solution were changed after each measurement and the foils were washed with water in between.
The pH of the buffer solutions was controlled with adequate buffer substances (see table 3.3) used as a 50 mM stock solution. They were diluted with a 1.5-fold amount of a 450 mM NaCl solution, in order to control the salinity, and a 2.5-fold amount of water. This yields in a 10 mM buffer solution with a NaCl concentration of 135 mM.
For all measurements the same adjustments were used. λ_{Ex} was set to 650 nm, a scan speed of 1200 nm/min was used, excitation and emission slits were set to 5.0 nm and a PMT voltage of 850 V was used.
After collecting the fluorescence spectra at various pH values the corrected intensities at the maximas of the spectra were plotted against those values. The resulting sigmoidal curves were fitted with a Bolzmann equation (see eq. 4.1) and the resulting points of inflections were calculated since they describe the apparent pKa values of the dyes entrapped in a D4 matrix.

4.4.3 Particle Characterization

Emission Spectra

For the measurement of the emission spectra of the different particles, 50 mM stock solutions with various pH values were prepared from adequate buffer substances (see table 3.3). The stocks were further diluted with a 1.5-fold amount of a 450 mM NaCl solution in order to control the salinity and a 2.5-fold amount of water. Nine parts of the resulting buffer solutions were mixed with one part of prepared 0.5 % particle stocks in 1 cm single-use cuvettes from Sarstedt. The resulting 0.05 % particle solutions, containing 9 mM buffer and 121.5 mM NaCl, were measured with the fluorimeter with a PMT voltage of 950 V and 1200 nm/min scan speed. Further adjustments for the different particle types and the different dyes are shown in table 4.2.

The maximal intensities of the corrected emission spectra were plotted versus the pH of the measured particle colloids. The apparent pKa values of the different particles with the entrapped

Table 4.2: Used Measurement settings for emission spectra.

Particle Type	Dye	λ_{Ex}	Ex Slit	Em Slit
PSPVP	ClOHbutoxy-complex (0.25 %)	675 nm	10.0 nm	10.0 nm
PSPVP	FOHbutoxy-complex (0.25 %)	675 nm	10.0 nm	10.0 nm
PSPVP	OHbutoxy-complex (0.25 %)	675 nm	10.0 nm	10.0 nm
Eudragit® RL100	ClOHbutoxy-complex (0.25 %)	650 nm	5.0 nm	5.0 nm
Eudragit® RL100	FOHbutoxy-complex (0.25 %)	660 nm	5.0 nm	5.0 nm
Eudragit® RL100	OHbutoxy-complex (0.25 %)	660 nm	5.0 nm	5.0 nm
PAcM	ClOHbutoxy-complex (0.25 %)	675 nm	5.0 nm	5.0 nm
PAcM	FOHbutoxy-complex (0.25 %)	675 nm	5.0 nm	5.0 nm
PAcM	OHbutoxy-complex (0.25 %)	675 nm	5.0 nm	5.0 nm

pH sensitives dyes were calculated from the sigmoidal fits of the Boltzmann equation (see eq. 4.1).

Particle Size

The size of the precipitated particles was determined with uncolored particles due to the fact that the pH sensitive dyes absorb in the red region of the electromagnetic spectrum and therefore would interfere with the red laser source of the Zetasizer. RL100, PAcM and PViCl-PAN particles were made according to section 4.3.2, section 4.3.3 and section 4.3.4 but without adding any dye stock. The colloids were diluted to a particle concentration of 0.5 % with water. PSPVP particles were not measured since their size is known.[38]
The measurement was performed with the Zetasizer with following adjustments: As a refractive index for the polymer 1.490 was estimated and it was assumed that the polymers don't absorb light. The measurement temperature was set to 25°C and the equilibration time for it to 120 seconds. This temperature results in an viscosity index of 0.8872 cP and an refractive index of 1.330 for water. It was estimated that the viscosity of the sample is equal to water since the dilution is quite high. The disposable cuvettes from Sarstedt were measured at a 173° backscatter angle. The duration was chosen automatically and three measurements for each sample were performed.

True Dye Concentration within the Particles

To estimate the true dye concentration in the particles, absorption spectra of RL100 and PAcM particle solutions were taken. Due to the fact that PSPVP colloids are to disperse to take

proper absorption spectra, no attempts were made to investigate the true concentration of the dye within this sort of particles.
For the preparation of the samples the particle stock solutions (c(particle)= 0.5 %) were diluted with acidified water (pH 1) to a particle concentration of 0.05 %. The samples were measured in a glass cuvette for small sample volumes.
To calculate the true dye concentration within the particles, the Lambert-Beer law (see eq. 2.1) was transformed to equation 4.2.

$$c = \frac{E_\lambda}{\epsilon_\lambda * d} \tag{4.2}$$

With the pathlength d being 1 cm and the molar absorption coefficients (measured according to section 4.4.1), the dye concentration can be calculated from the maximal absorption intensity of the absorption spectra.

Cross Sensitivity to Oxygen

To check the cross sensitivity of the PViCl-PAN reference particles for oxygen, with respect to the pH value, six samples of each an acidic buffer (~pH 3), a neutral buffer (~pH 7) and a basic buffer (~pH 11) were prepared. The samples contained concentrations of 0.007 % of PViCl-PAN reference particles stained with 1.5 % of $PtTPTBPF_4$, 9 mM of buffer substance and 121.5 mM of NaCl as a background electrolyte. Three samples of each pH value were deoxygenized with a little bit of $NaSO_3$ prior the measurement which was performed with a Piccolo2 equipped with a focusing lens. It was measured through the glass wall of the carefully stirred vial (avoiding oxygen intake for the deoxygenized samples) with following settings: light modulation frequency of 4000 Hz, 100 % LED intensity, 400 x amplification, 128 ms measuring time, 1 point per second data acquiring and data smoothening over 3 values.
For the data analysis FireEval, a python based program provided by Christoph Staudinger, was used and the mean phaseangle values of the measurements were compared.

Cross Sensitivity to Ionic Strength

For the determination of the cross sensitivity to the salinity three additional sets of buffer solutions with different concentrations of NaCl were prepared. Each buffer contained 11.11 mM of an adequate buffer substance (see table 3.3) and either 5.55 mM, 55.55 mM or 166.66 mM of NaCl. These buffers were mixed 9:1 with stock solutions of the different particle types containing 0.25 % of OHbutoxy-complex. The RL100 particle stock had a particle concentration of 0.5 %, the PSPVP colloid 5 % and the PAcM particle stock contained also 0.5 % particles. Therefore the resulting samples had buffer concentrations of 10 mM, particle concentration of either 0.05 % (RL100, PAcM) or 0.5 % (PSPVP), and NaCl concentrations of 5 mM, 50 mM or

150 mM.
The measurement was performed on the fluorimeter in single use cuvettes from Sarstedt with following measurement settings. The excitation wavelength λ_{Ex} was set to 675 nm, a scan speed from 1200 nm/min and a PMT voltage from 950 V were used. For the RL100 and PAcM colloids excitation and emission slits of 5 nm were chosen, for the PSPVP particles slits of 10 nm were used.
The corrected, maximal emission intensities of the various pH values were normalized and ploted against the according pH value. The resulting sigmoidal curves were fitted with a Boltzmann equation (see eq. 4.1) and compared for the different salinities. For this comparison also the data acquired in section 4.4.3 for the investigation of the emission properties were used.

4.4.4 Microfluidic Measurements

Chips and Set-up

All data acquisition was done with a Piccolo2 from PyroScience mentioned in chapter 3.2. For the microfluidic measurements different types of chips were used. Figure 4.8 shows those chips, their properties and the companies which provided them. For each type of microfluidic chip a different, house-made chip holder was used. The whole set-up is shown in figure 4.9.

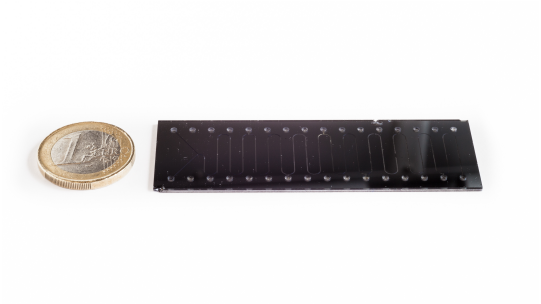

(a) Sillicium meander chip provided by iX-factory; channel width: 200 µm, channel depth: 400 µm

(b) Sillicium chamber chip provided by iX-factory; channel width: 100 µm, channel depth: 200 µm

(c) Glass microreactor from Micronit; channel width: 150 µm, channel depth: 150 µm, internal volume: 6 µl; Product code: R150.332.2

(d) Teardrop micromixer from Micronit; channel width: 200 µm, channel depth: 150 µm, internal volume: 2 µl; Product code: TD26

(e) Microfluidic glass chip from iX-factory (thin cover glass); channel width: 1000 µm, channel depth: 300 µm

Figure 4.8: Different microfluidic chips which were used during this work.

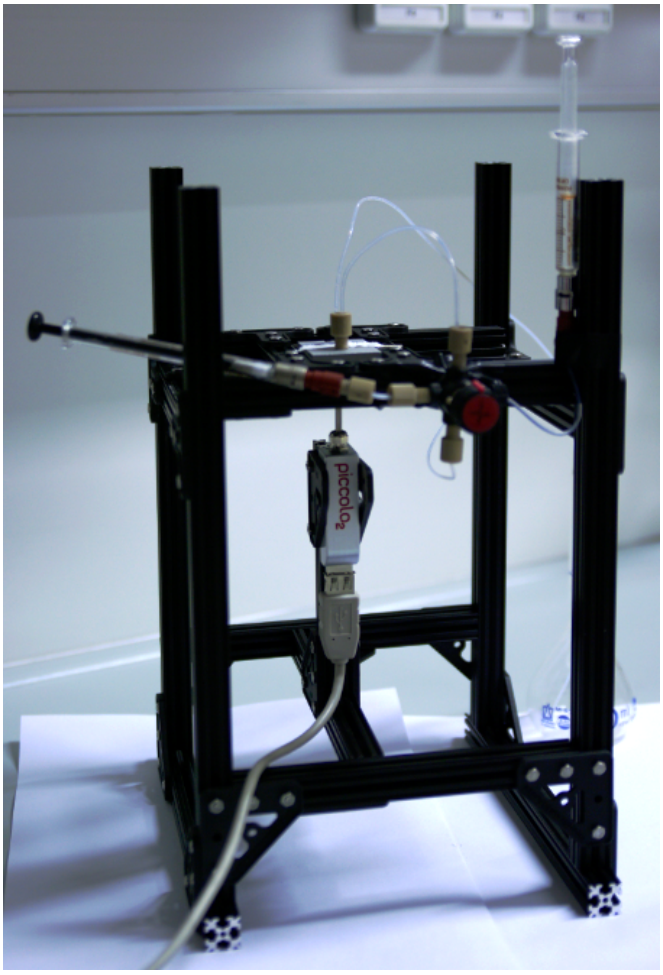

Figure 4.9: Measurement set-up; including framework, chip holder, microfluidic glass chip from iX-factory, Piccolo2, a 2/2-way valve and two syringes.

Method Development

The first step for developing a measurement method was the measurement of reasonable particle concentrations (from 0.1 % to 1 %) of PSPVP particle containing 0.25 % indicator dye. The measurement was performed in a glass chip (channel depth of 300 µm, see fig. 4.8(e)), with a Piccolo2 equipped with a focusing lens under acidic conditions. Therefore following settings were used: 100 % LED intensity, an amplification factor of 400, a measurement time of 32 ms and a modulation frequency of 4000 Hz.
RL100 particle were also measured with the same settings and the same dye concentration but with a particle concentration of 0.05 %, which is a tenth of the maximal particle stock concentration.
In the next step different particle concentrations of the reference dye ($PtTPTBPF_4$) entrapped in PSPVP particles with a dye concentration of 0.5 % were measured with the same adjustments to find a matching intensity for the indicator particles.

The first DLR measurements were carried out at acidic, neutral and basic conditions with particle concentrations of 0.5 % PSPVP particles stained with 0.25 % indicator dye and 0.015 % PSPVP colloid stained with 0.5 % of $PtTPTBPF_4$ as reference. The samples were measured with the settings described above, except that the modulation frequency was varied between 2000, 4000 and 8000 Hz.
The DLR measurement showed a poor resolution due to a lack of reference signal and the best explanation is a poor measurement of the intensity values for the reference particles in the first place since they were performed without the framework. Various concentrations of reference PSPVP particle containing 0.5 % $PtTPTBPF_4$ were therefore measured again. The settings were unchanged and modulation frequencies of 8000 and 12000 Hz were used.

The second set of DLR measurements was performed just under acidic and basic conditions with the same settings as the first measurement. The modulation frequency was varied between 8000 and 12000 Hz. The used particle concentrations were 0.5 % for PSPVP indicator particles, 0.05 % for RL100 indicator particles and 0.025 % for the PSPVP reference particles. Indicator dye concentrations in the particles were 0.25 % and the reference dye concentration was 0.5 %.

The problem with $PtTPTBPF_4$ in PSPVP particles as a reference is that these particles are sensitive to oxygen since PSPVP is O_2 permeable. Therefor the pH measurement would be cross-sensitive to oxygen which is not desirable. To avoid this problem a different matrix for the reference particles was chosen. PViCl-PAN particles should not be oxygen permeable and were measured with the above stated adjustments with a modulation frequency of 8000 Hz at air saturated and at deoxygenized conditions (Na_2SO_3). The samples contained 0.007 % of particles (a tenth of the stock) dyed with 1.5 % of $PtTPTBPF_4$.
After the measurement of the new reference particles the new and final DLR measurment

systems was checked by measuring acidic an basic samples containing 0.007 % of PViCl-PAN reference particles stained with 1.5 % of $PtTPTBPF_4$ and either 0.5 % of PSPVP particles, 0.05 % of RL100 particles or 0.05 % of PAcM particles (Since properties of PAcM particles are very similar to RL100 the same concentration was used.) containing 0.25 % of indicator dye. The adjustments for the Piccolo2 were the same as stated above and a modulation frequency of 8000 Hz was used.

Calibration

The different pH sensitive particles were characterized via DLR measurements with PViCl-PAN particles, stained with 1.5 % of $PtTPTBPF_4$, used as a reference. During the development of the method it was shown that in general the best mixture between pH sensitive particles and reference particles is a 1:1 mixture of the particle stock solutions. The particle concentration of this stock solutions were 0.07 % for the reference particles (PViCl-PAN), 5 % for the PSPVP colloid and 0.5 % for RL100 and PAcM particles, no matter which pH sensitive dye in what concentration was used.
For the calibration curve buffer stocks with varying pH values, containing 10 mM of an adequate buffer substance (see table 3.3), and 135 mM NaCl as a background electrolyte were used. Those buffer stocks were mixed with the premixed particle stocks in a ratio of 8:2 yielding in samples containing 8 mM puffer substance, 108 mM NaCl, 0.007% PViCl-PAN particles and eighter 0.5% PSPVP, 0.05% RL100 or 0.05% PAcM particles containing 0.25% of indicator dye.
Measurement data were acquired with a Piccolo2 from PyroScience, operated with an focusing lens and the standard adjustments described in section 3.2. The measurements were performed in a 1 mm broad, 300 µm deep glass chip from iX-factory shown in fig. 4.8(e). The colloidal solutions were brought into the chip manually with a syringe and the chip was flushed with water after each measurement. Before the measurement the background value of water was taken and was automatically subtracted during the following measurements.
For finding the plateaus within the measurment data, FireEval, a phyton based program written by Christoph Staudinger, was used. The cotangents of the measured average phase angle Φ from each plateau was plotted against the respective pH value and the resulting sigmoidal curve was fitted with a Boltzmann equation (see eq. 4.1) to get the apparent pKa value of the indicator entrapped in the particles.

Reproducibility

For the reproducibility measurement two puffer stock solutions with pH 5.90 and pH 6.99 ($c(buffer) = 10\,mM$, $c(NaCl) = 135\,mM$) were mixed with a particle stock solution containing

0.025 % of RL100 colloid, stained with 0.25 % of FOHbutoxy-complex, and 0.035 % of PViCl-PAN reference particles, stained with 1.5 % of $PtTPTBPF_4$. The mixing ratio was 8:2 and therefore the yielded solutions contained 0.05 % of pH sensitive particles, 0.007 % of reference particles, 8 mM buffer substance and 108 mM NaCl as a background electrolyte.
The solution was transported with a syringe pump from WPI with a speed of 50 µL/min through a 300 µm deep glass chip from iX-factory, shown in fig. 4.8(e). The DLR measurement was performed with a Piccolo2 from PyroScience operated with the standard settings described in section 3.2. Before the measurement the background value of water was taken and automatically subtracted during the following measurements. Three values each were taken at three different positions for each sample. Between each measurement the system was flushed with water. The plateaus of the phase angles within the measurement data were found with FireEval, a phyton based program written by Christoph Staudinger. The mean value and the standard deviation of the cotangents of the phase shift for each pH value were calculated. With the Boltzmann equation of the according calibration curve (see fig. 5.12(b)) of the used particle system these values were transformed into pH values.

Drift Measurements

Drift measurements were primarily performed in an iX-factory meander silicium chip with a channel depth of 400 µm and a channel width of 200 µm shown in fig. 4.8(a). For the measurement the particle stock solution of the various particles were mixed with a buffer stock solution (c(buffer) = 10 mM, c(NaCl) = 0 mM) with an pH of 6.36 inside the microfluidc chip with a ratio of 1:9. The particle stock solutions had concentrations of 0.07 % for the PViCl-PAN reference particles (containing 1.5% of $PtTPTBPF_4$), 5 % for PSPVP colloid and 0.5 % for RL100 and PAcM particles (each containing 0.25% of OHbutoxy-complex). For the transport of the liquids through the chip two Tecan Cavro syringe pumps were used. One, equipped with a three-way valve and a 5 ml syringe (pump 2), was pumping the buffer stock and was operated at 1.8 µL/sec. The second one, equipped with a 9 port valve system and a 1 ml syringe (pump 1), was transporting the particle stocks with 0.2 µL/sec. Therefore the final solutions in the chip contained 9 mM buffer substance and either 0.007 % of PViCl-PAN reference particles, 0.5 % of PSPVP colloid, 0.05 % of RL100 particles or 0.05 % of PAcM particles. Each particle type was measured for 45 minutes and the signal intensity was monitored to examine the drift. Between the different particle types the chip was washed with acetone and water. For programing the pump cycles "Bernoulli", a LabView based software written by Tobias Able, was used. In fig. 4.10 the sequence used for the measurement is shown.

Drift measurements were also performed for PViCl-PAN particles (stained with 1.5 % of $PtTPTBPF_4$) and for PSPVP reference particles (stained with 0.5 % of $PtTPTBPF_4$) in a meander glass chips from Micronit (shown in fig. 4.8(c)) to see the influence of the chip material

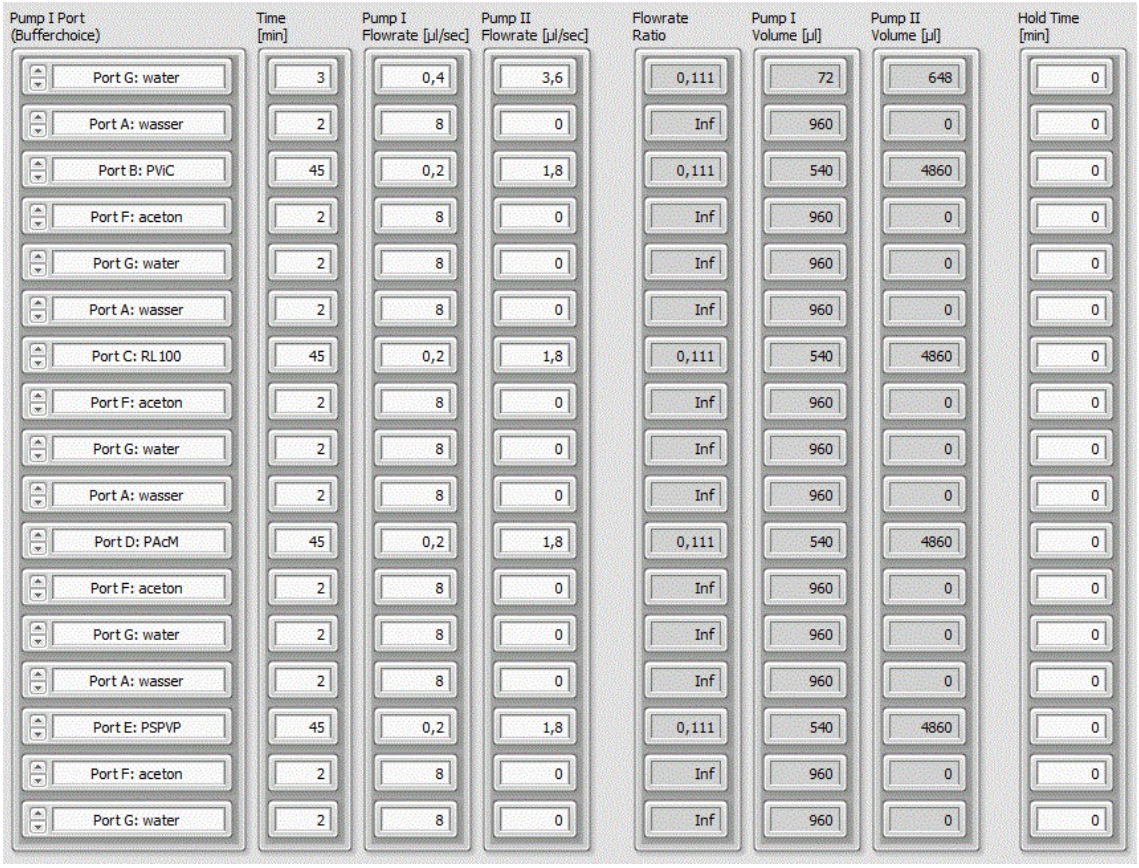

Pump I Port (Bufferchoice)	Time [min]	Pump I Flowrate [µl/sec]	Pump II Flowrate [µl/sec]	Flowrate Ratio	Pump I Volume [µl]	Pump II Volume [µl]	Hold Time [min]
Port G: water	3	0,4	3,6	0,111	72	648	0
Port A: wasser	2	8	0	Inf	960	0	0
Port B: PViC	45	0,2	1,8	0,111	540	4860	0
Port F: aceton	2	8	0	Inf	960	0	0
Port G: water	2	8	0	Inf	960	0	0
Port A: wasser	2	8	0	Inf	960	0	0
Port C: RL100	45	0,2	1,8	0,111	540	4860	0
Port F: aceton	2	8	0	Inf	960	0	0
Port G: water	2	8	0	Inf	960	0	0
Port A: wasser	2	8	0	Inf	960	0	0
Port D: PAcM	45	0,2	1,8	0,111	540	4860	0
Port F: aceton	2	8	0	Inf	960	0	0
Port G: water	2	8	0	Inf	960	0	0
Port A: wasser	2	8	0	Inf	960	0	0
Port E: PSPVP	45	0,2	1,8	0,111	540	4860	0
Port F: aceton	2	8	0	Inf	960	0	0
Port G: water	2	8	0	Inf	960	0	0

Figure 4.10: Used sequence for executing the measurement. Pump I (equipped with 9-way valve): Port A: water, Port B: PViCl-PAN stock, Port C: RL100 stock, Port D: PAcM stock, Port E: PSPVP stock, Port F: acetone, Port G: water; Pump II (equipped with a 3-way valve): buffer pH 6.36

on the drift and to have a direct comparison between the two sorts of reference particles. Therefore 9 parts of a buffer stock solution (c(buffer) = 10 mM, c(NaCl) = 0 mM) with a pH of 6.97 were mixed with one part of either a 0.07 % PViCl-PAN colloid or a 1 % PSPVP particle solution within the chip. The same set-up and adjustments concerning the Piccolo2 and the pumps were used as described above. Therefore the measured solutions also contained 9 mM buffer substance and either 0.007 % of PViCl-PAN particles or 0.1 % of PSPVP reference particles. The solutions were measured each for about 30 minutes and the signal intensity was monitored to examine the drift. Between the different particles the chip was washed with acetone and water.

4.4.5 NIR Imaging [39]

For NIR imaging a colloid stock with 5 % particle concentration was prepared from the freezedryed PSPVP particles, containing 0.25 % OHbutoxy-complex and 1 % Lumogen® Red. Buffer stocks with varying pH values were prepared from adequate buffer substances (see table 3.3) with a concentration of 10 mM, containing 135 mM NaCl as a background electrolyte. One part of colloid was mixed with nine parts of buffer stock yielding samples containing particle concentrations of 0.5 %, buffer concentrations of 9 mM and 121.5 mM NaCl. The samples were filtered with a 0.8 µm syringe filter from Carl Roth in order to receive more homogeneous images.
The samples were measured within a 300 µm deep glass chip from iX-factory (see fig. 4.8(e)) at a flow speed of 5 µl/min. For the sample transport a syringe pump from WPI was used. The measurement was carried out with the set-up described in section 3.2. The samples were excited with the 579 nm band of a HBO lamp.
During the excitation two images were recorded by the camera under low ambient light conditions to minimize the background signal. The images had a 12 bit resolution and a size of 1296 (h) x 966 (v) pixels which equals 0-4095 greyscale values. One image was acquired in the near infrared and contained the analyte-dependent information. The other image was taken in the visible color range with three channels (red, green and blue; each comprising 12 bit) where the red channel contained the analyte-independent information ($\widehat{=}$ reference signal). Images were not only taken from the samples, but also from water as a blank and its values were subtracted during data processing from all sample values. Each image was recorded under identical conditions with a shutter time of 1100 ms for the NIR image and 500 ms for the color image.
The ratiometric images of the samples were calculated by dividing the analye-dependent signal (NIR image) by the analyte-independent signal (red channel of the color image). This process was done pixel by pixel with a Matlab script provided by Josef Ehgartner.
To obtain the calibration curve the mean values and the standard deviations of a certain region within the ratiometric images (region of interest) were plotted against the pH values of the samples. The resulting sigmoidal curve was fitted with a Bolzmann equation (see eq. 4.1) and the apparent pKa of the particles is therefore represented by the point of inflection of this curve.

5 Results and Discussion

5.1 Synthesis of the aza-BODIPY Dye [40]

In general there are two different strategies known for the synthesis of azadipyrromethene chromophors. One method is using 2,4-diarylpyrroles as precursors and introduce a nitroso moiety in the 5 position. Afterwards condensation with a second pyrrole forms the unsymmetrical derivative.[41] The second method is the reaction of nitromethane adducts of chalcones with ammonium salts.[42] Hereby a mixture of symmetrical and unsymmetrical derivatives can be obtained by using different chalcone derivatives. As Jokic et al. have pointed out, the conversion of diarylnitroketones over pyrrols to 5-nitrosopyrroles (and the isolation of these compounds) is not necessary in the second method. Since the separation of the symmetrical and the unsymmetrical product is a quite easy task the second method was chosen as synthetic strategy. The whole pathway for the three different dyes which were used during this work is shown in fig. 5.2. The ClOHbutoxy-complex was successfully synthesized for the first time within the work of this thesis whereas the FOHbutoxy-complex and the OHbutoxy-complex were both made by Martin Strobl. The structures of all three used pH sensitive indicator dyes are shown in fig. 5.1.

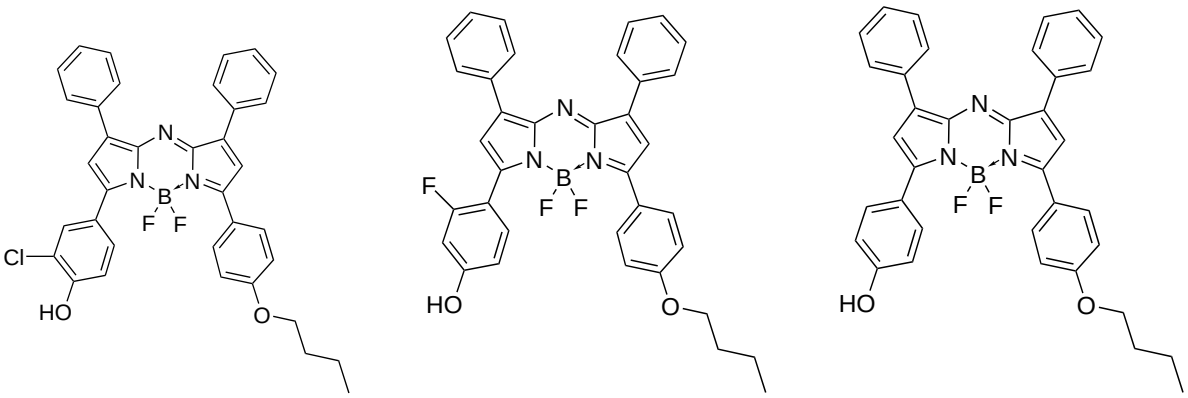

(a) ClOHbutoxy-complex (b) FOHbutoxy-complex (c) OHbutoxy-complex

Figure 5.1: Used pH sensitive indicator dyes based on an aza-BODIPY structure

For the used approach diaryl α,β-unsaturated ketones (chalcones) were made via Claisen-Schmidt condensation from the according aldehyde and acetophenone using KOH as a base with about 90% yield. Nitromethane was added, with the help of KOH as a base, via Michael addition to those chalcones yielding 1,3-diaryl-4-nitrobutan-1-ones in essentially quantitative yields after aqueous work-up and were used without further purification. The condensation with ammonium acetate of the two different chalcone species was done under reflux in isopropanol and yielded one third (theoretical yield: 50%) of the unsymmetrical azadipyrromethenes via a cascade of events (in situ formation of the pyrrole and corresponding nitroso-pyrrole, and subsequent condensation of those two entities [43]) after purification via chromatography. The last step was the complexation of the azadipyrromethene with boron trifluoride and DIPEA as a base with about 25% yield after column chromatography.[43]

The improvement of the synthesized dyes is the introduction of the butoxy moiety. It enhances the solubility in organic compounds which is not only advantageous during synthesis but should also help staining polymeric materials due to the increased lipophilicity. It is also believed that this apolar functionality improves the longterm stability of the sensor materials due to the hindrance of migration processes within the matrix and therefore aggregation of the dyes is less likely.
As Jokic et al. have shown, the pKa value of these pH sensitive dyes can be adjusted by the introduction of different electron pulling or pushing functionalities. The general rule is, the more electron pulling character a substituent has, the lower is the pKa value of the dye. Moreover the photostability of the dye is increased by electron withdrawing groups. Since the hydroxy moiety of the dyes is responsible for the pH sensitive character, it is also essential at which positions the substituents are located.(e.g. +M and -M effects) Another fact, which should be kept in mind for the design of dyes is, that there should be no substituents which can possibly carry charges (except the one essential hydroxy group). This has basically three reasons. First, more complicated acid-base equilibriums are avoided and there are only two possible forms of the indicator. The second reason is, that more charges within a dye lead to higher polarity. This would enhance the solubility of the dye in water and therefore could cause more troubles concerning leaching. The third reason is, that with less charges the interaction with other electrolytes is expected to be lower and therefore the effect of the ionic strength on the sensing properties should be minimized.[19]

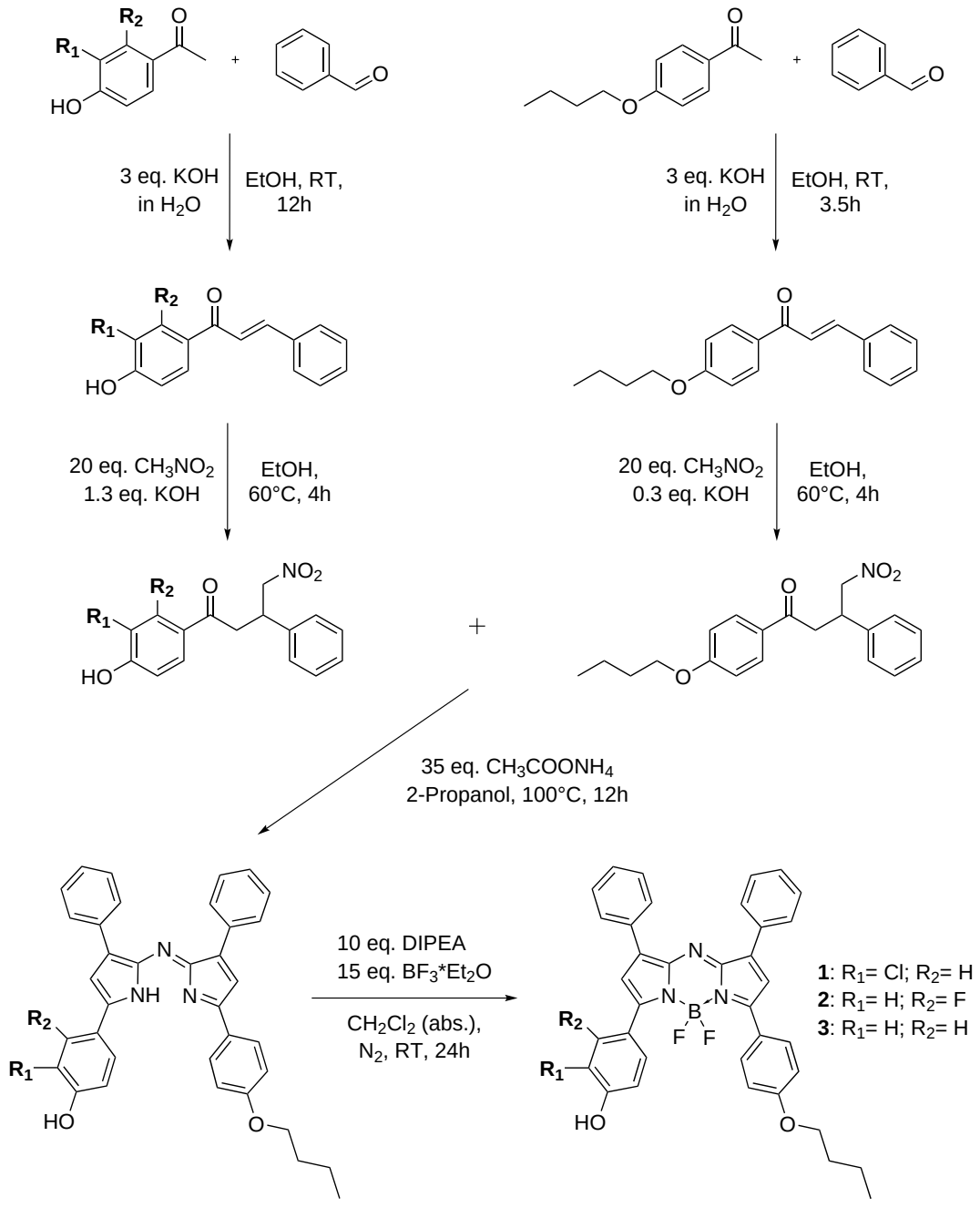

Figure 5.2: Synthetic pathway for different pH sensitive aza-BODIPY dyes.

5.2 Preparation of the Sensors

The most important property of a sensor material for a pH sensor is the permeability for water respective protons since the concentration of hydronium cations is measured. Another important factor is, how easy the immobilization of the dye within the matrix can be achieved and if the procedure can be upscaled easily to obtain large quantities of the sensor material.[24] The most favorable entrapment methods therefore are staining of existing particles or the precipitation of sensor beads from dyed polymer solutions. In fig. 5.3 the various particles used during this work are shown with their chemical composition.

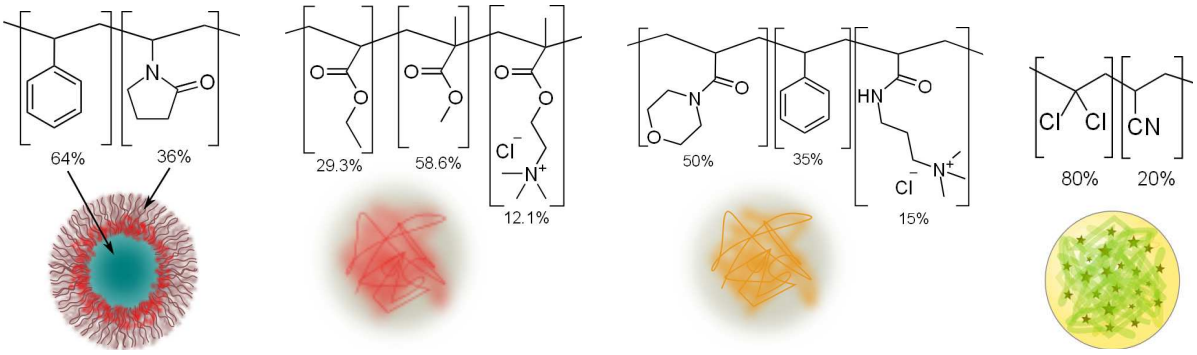

(a) PSPVP (b) Eudragit® RL100 (c) PAcM (d) PViCl-PAN

Figure 5.3: Chemical structure of the different used particles.

5.2.1 D4 Sensor Layer

Hydromed® D4 is a commercial available, ether-based hydrophilic polyurethane. It is uncharged, highly proton-permeable and has a water uptake from about 50 %.[40] The dye was incorporated by physical entrapment and the material was used as a about 7.5 µm thick (dry state), knife coated sensor layer with Mylar® foil as support.

5.2.2 PSPVP Particles

PSPVP particles (shown in fig. 5.3(a)) are specified by the manufacturer as poly(styrene-block-vinylpyrrolidone) nanobeads which consist of 64 % w/w of styrene and 36 % w/w of vinylpyrrolidone and have a size of less then 500 nm. They have a core-shell structure where the hydrophobic polystyrene blocks form the core and the hydrophilic poly(vinylpyrrolidone) parts form the shell.[38] This shell is interacting with the solvent and is the reason for the high stability of the beads against aggregation. This is also true for solutions with high ionic

strength or even more complex media.[24]
Both parts can be stained separately with lipophilic dyes using two different procedures. For staining the shell the colloid is dispersed in a ethanol/water mixture (70:30 v/v) and for staining the core a mixture of THF/water (50:50 v/v) is used. In both procedures the organic solvent is removed under reduced pressure and therefore the indicator dye is forced into the particle. In general oxygen and temperature indicators should be immobilized in the core, whereas indicators for ions should be located in the shell since only the shell is permeable for charged species. Due to this proton permeability of the shell pH sensitive indicators should be either located there or in the intermediate region [24],[38]. It has been shown that the average size of PSPVP particles is about 245 nm and that they have a ζ-potential from -12.1 mV which indicates a slightly negative charge.[38] According to Borisov et al. this charge is however caused by ionic stabilizers such as ascorbic acid and not by the beads per se. It was also reported that PSPVP beads can be freeze-dried and re-dispersed in an ultrasonic bath.[38] However, within this thesis it was discovered that if the colloid was concentrated under reduced pressure and elevated temperatures (above 50°C) parts of the particles started to stick to the wall of the flask and form aggregates. Also the redispersibility after freeze-drying was not perfect and there were always some aggregates. Therefore it was never possible to state the exact concentration of particles within a colloid.

5.2.3 RL100 Particles

Eudragit® RL100 (shown in fig. 5.3(b)) is a positively charged acrylate polymer which forms nanaoparticles with an average size of around 30 nm when precipitated from acetone with water.[32] According to the manufacturer it is a copolymer made out of ethyl acrylate, methyl methacrylate and trimethylammonioethyl methacrylate chloride with a ratio of 1:2:0.2. For reproducible results it is important that the water is added with a constant speed over a constant time. Due to the positive charges of the polymer the deprotonated form of the indicator dye (negatively charged) is better stabilized within this matrix and it is expected that therefore the apparent pKa of the entrapped dyes is lowered. Moreover it is expected that, because of this already charged environment, additional charges (e.g. from dissolved salts) don't have such a big influence on the indicator dye anymore. However, it is known that RL100 particles have a much higher tendency to aggregate if the colloid is stored at high concentrations then for example PSPVP particles. A maximal particle concentration of 0.5 % could be handled without difficulty in the past.

5.2.4 PAcM Particles

PAcM particles (shown in fig. 5.3(c)) consist of a statistical copolymer made out of three different components by radical polymerization. It contains of 50 % w/w 4-acryloylmorpholine which represents the hydrophilic part of the polymer and is responsible for the interaction with the solvent and the proton permeability. The second component is styrene. Its share is 35 % w/w and this hydrophobic molecule is supposed to form the core of the particle and works as the anchor platform for lipophilic dyes. The other 15 % w/w are composed out of methylated *N*-(3-(dimethylamino)propyl)acrylamide. This component is positively charged and therefor responsible for the formation of stable nanobeads when precipitated from acetone with water. By varying the share of the components the properties of the particles can be changed quite drastically. The used composition of the polymer within this thesis is based on the experiences which was made with this material in our lab. In general the properties of this material are quite similar to Eudragit® RL100. Since it carries even more positive charges the apparent pKa should also be significantly lower than in PSPVP. However, experiments have shown that this is not the case. A possible explanation is the different size of the particles. For a closer discussion see section 5.4.1.

5.2.5 PViCl-PAN Particles

PViCl-PAN particles (shown in fig. 5.3(d)) consist of 20% w/w acrylonitrile moieties and are reported to be impermeable to oxygen.[31] Therefor they were used as reference particles stained with an oxygen sensitive dye ($PtTPTBPF_4$) for DLR measurements. The main problem with this material is, that it tends to aggregate at the presence of electrolytes. However, since it was reported that low particle concentrations (lower than 0.025%) seem to have almost no aggregation behavior[31] and there was no better O_2 impermeable particle matrix available, PViCl-PAN was used even with this known disadvantage.

5.3 Photophysical Properties of the Dyes

The class of commonly called "aza-BODIPY" dyes is a subset of the parent BODIPY dye system in which the C^8-position is substituted by a nitrogen atom.[43] This substitution causes a quit large bathocromic shift for the absorption and florescence spectrum (about 80 nm).[44] Almost all known aza-BODIPY's posses 3,3,5,5-aryl substituents and the substitution with phenylrings is the most common and widely studied derivative.[43] It was first presented in literature in 1994 where its exceptional fluorescent properties were mentioned.[45]
Aza-BODIPY dyes can receive a sensitivity towards pH by introduction of a hydroxy moiety. This fluorescent sensitivity is due to the PET effect of the basic (deprotonated) form of the molecule. As explained in section 2.1.2 the negatively charged oxygen is donating a electron to the excited aromatic backbone of the dye enabling deactivation via fluorescence of the excited state. Therefore the deprotonated form of the dye is non fluorescent and the florescence intensity reflects the concentration of protonated dye molecules in the excited state. Since the ratio of protonated to deprotonated dye molecules depends on the pH value of a solution, it can be determined with an appropriate calibration curve.

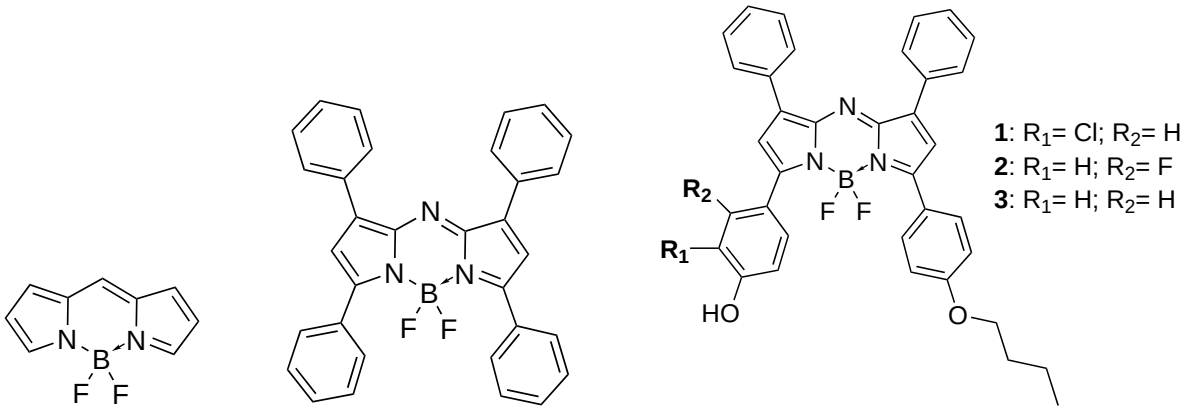

(a) BODIPY scelleton (b) 3,3,5,5-phenyl aza-BODIPY (c) General structur of used aza-BODIPY's.

Figure 5.4: Used aza-BODIPY pH indicator dyes and their parent systems.

5.3.1 Absorption Spectra of the ClOHbutoxy-complex

The simple aza-BODIPY dye (see fig. 5.4(b)) exhibits its maximal absorption at 650 nm.[44] Due to the +M effect of the additional hydroxy and ether group the spectrum is shifted further to longer wavelength. The maximum for the ClOHbutoxy-complex is at 688 nm under acidic conditions. This is in the red region of the visible light and lies therefore in the so-called biological window from 650 nm till 1000 nm. This NIR region is preferable due to the fact that

red light has a larger penetration depth in biological tissues, is getting less absorbed and causes no harm to cells in comparison with widely used UV light. There is also less autofluorescence in this region.[44] The deprotonated form of the dye (under basic conditions) has an even higher electron density in the π-system and therefore the maximum is shifted to 750 nm.
The calibration curve shows an pKa value of 7.51 for the protonated form of the dye and 7.50 for the deprotonated form. This difference lies within in the range of the experimental error. Since the pKa of indicator dyes used for most biological applications should be general around 7 and it is expected that the apparent pKa of the dye entrapped in a matrix is lower due to the FRET effect, this seems like a promising result.

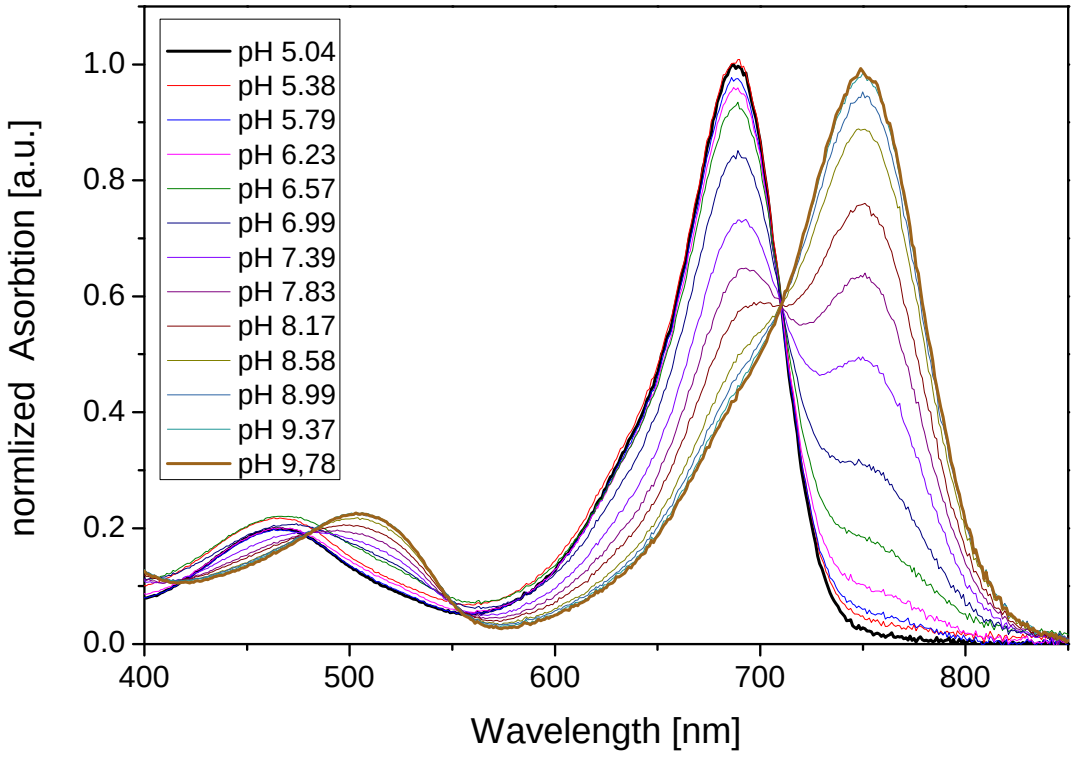

Figure 5.5: Absorption spectra of the ClOHbutoxy-complex in EtOH/H_2O 1:1 at various pH values.

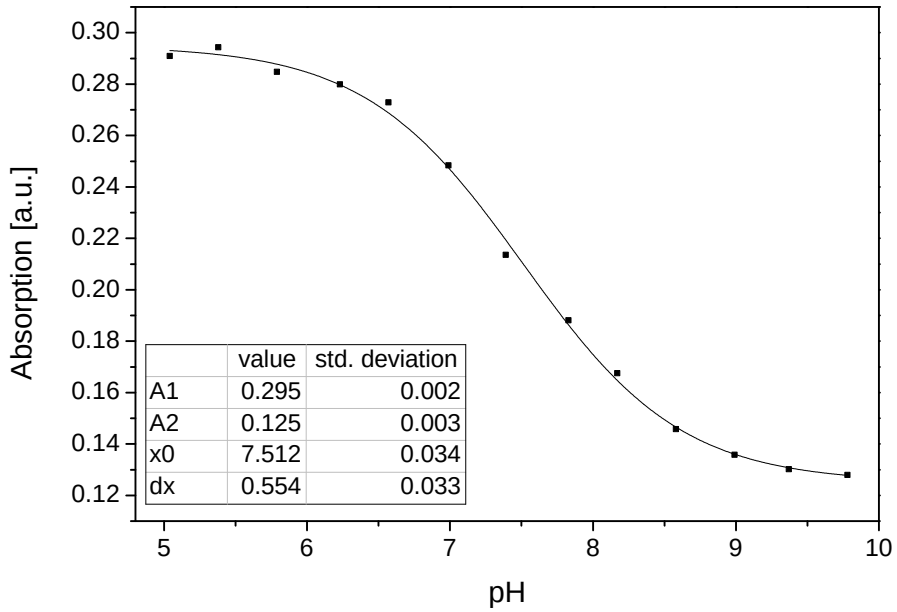

(a) Calibration curve for the protonated form of the indicator dye. $\lambda_{max} = 688\,\text{nm}$.

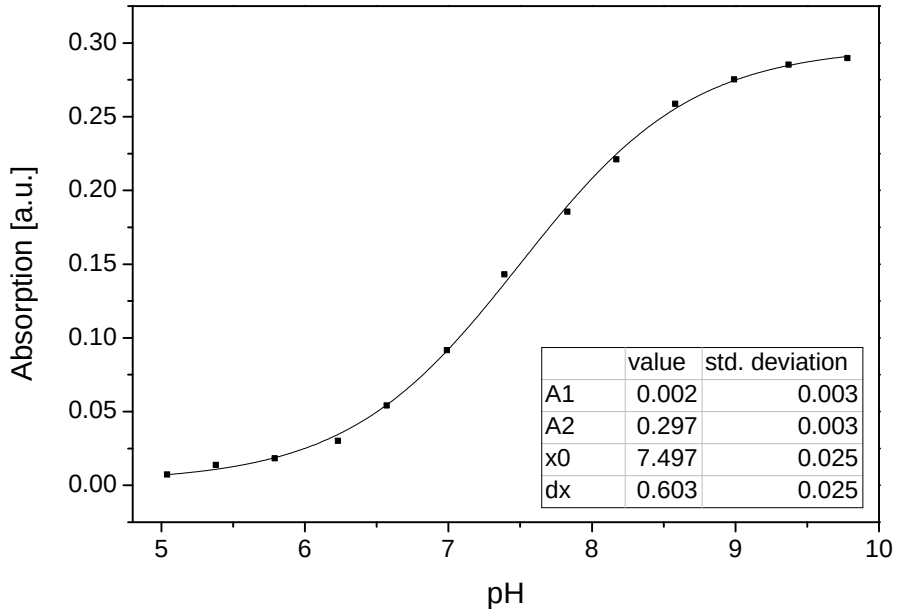

(b) Calibration curve for the deprotonated form of the indicator dye. $\lambda_{max} = 750\,\text{nm}$.

Figure 5.6: Calibration curves the absorption spectra of the ClOHbutoxy-complex.

5.3.2 Fluorescence Spectra of the ClOHbutoxy-complex

As described above, the emission spectra for pH sensitive aza-BODIPY dyes does not change depending on the pH value since only the acidic (protonated) form emits light and therefore only the intensity changes with the pH value. The emission spectra has its maximum at a wavelength of 724 nm which is in the NIR region of the electromagnetic spectrum. Therefore the fluorescence signal has the advantage of hardly being absorbed by biological materials and suffers from less interferences.

The sigmoidal calibration curve shows a apparent pKa value of 7.42. The difference ($\Delta = 0.09$), compared with the pKa value gained via the absorption spectra, is because this apparent pKa is based on fluorescence and therefor provides information about the excited state. This means that this apparent pKa is, technically speaking, the pKa of the excited state.

5.3.3 Comparison of the Different aza-BODIPY Dyes

As one can see in fig. 5.8(b) the apparent pKa value of the indicator dye can be influenced with the substitution pattern on the aromatic ring. The general rule therefore is, that the higher the electron density within the aromatic system is, the higher the pKa values get. The OHbutoxy-complex with no other electron withdrawing group therefore has the highest apparent pKa value with 8.78. It is followed by the FOHbutoxy-complex with an apparent pKa of 8.71 which is surprisingly close to the unsubstituted complex. One possible explanation is, that the -I-effect of the fluorine is less pronounced due to the formation of a hydrogen bond to the hydrogen atom in close proximity. The ClOHbutoxy-complex has, as stated above, an apparent pKa value of 7.42. This huge shift over more than one pH unit can be explained by the -I-effect of the chlorine with no possibility for hydrogen bonding. Furthermore its +M-effect increases the electron density in the ortho-positions of the chlorine where the hydroxy-group is located and therefore weakens the O-H-bond.
In fig. 5.8(a) the absorption spectra under acidic conditions and the emission spectra of the three used aza-BODIPY dyes are shown. It is noteworthy that the maxima of the FOHbutoxy-complex are not between the other two complexes like one could expect from the order of the pKa values. Another interesting aspect of the comparisons of the spectra is that the FOHbutoxy-complex has the largest stock shift ($\Delta = 43nm$) of the three dyes. This is beneficial since this means that the excitation light and the absorption light can be easier separated.

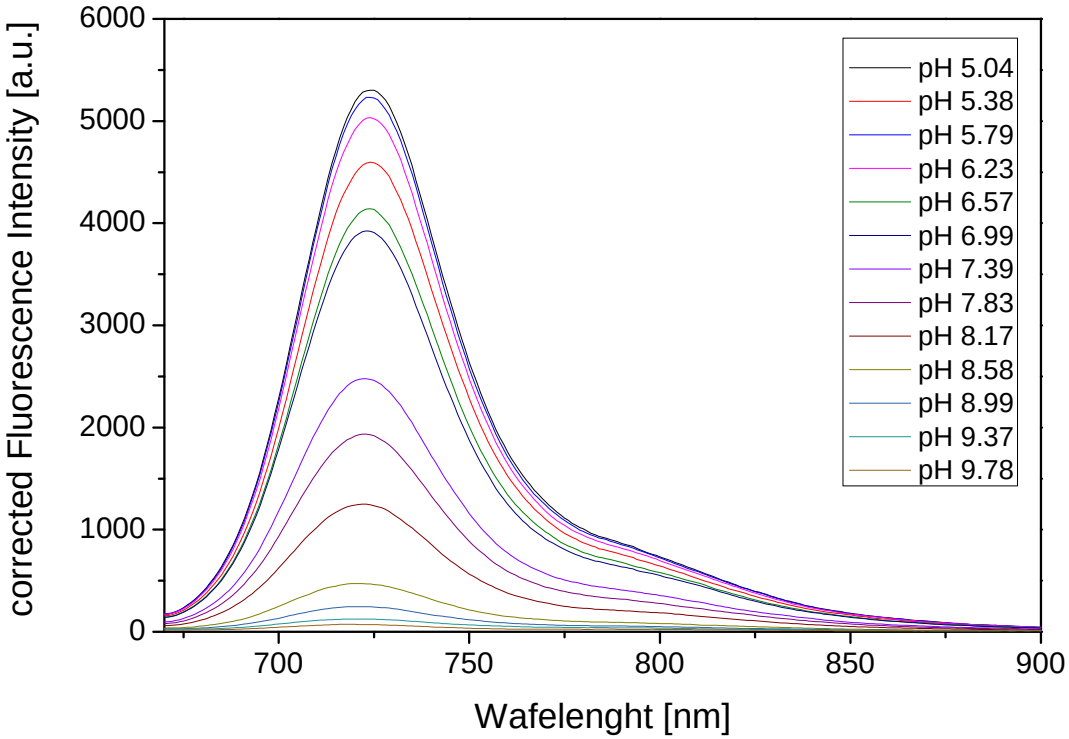

(a) Emission spectra of the ClOHbutoxy-complex at various pH values.

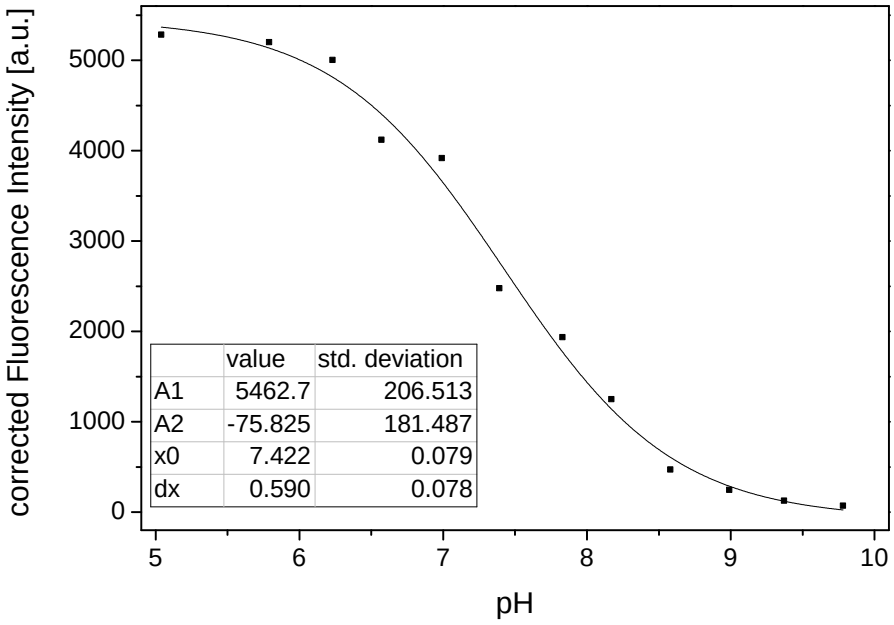

(b) Calibration curve.

Figure 5.7: Emission spectra of the ClOHbutoxy-complex in EtOH/H_2O 1:1 and the according calibration curve.

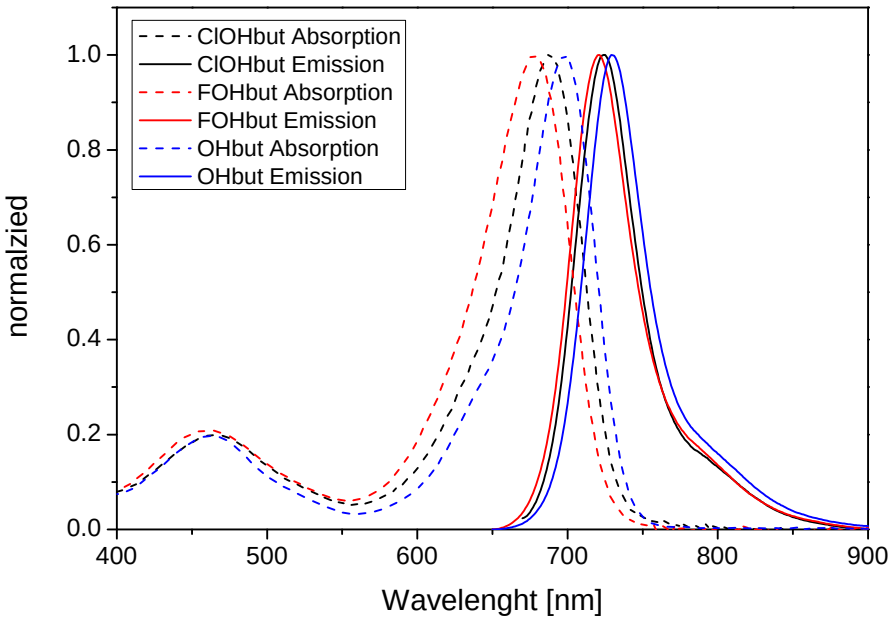

(a) Normalized absorption and emission spectra of the used dyes.

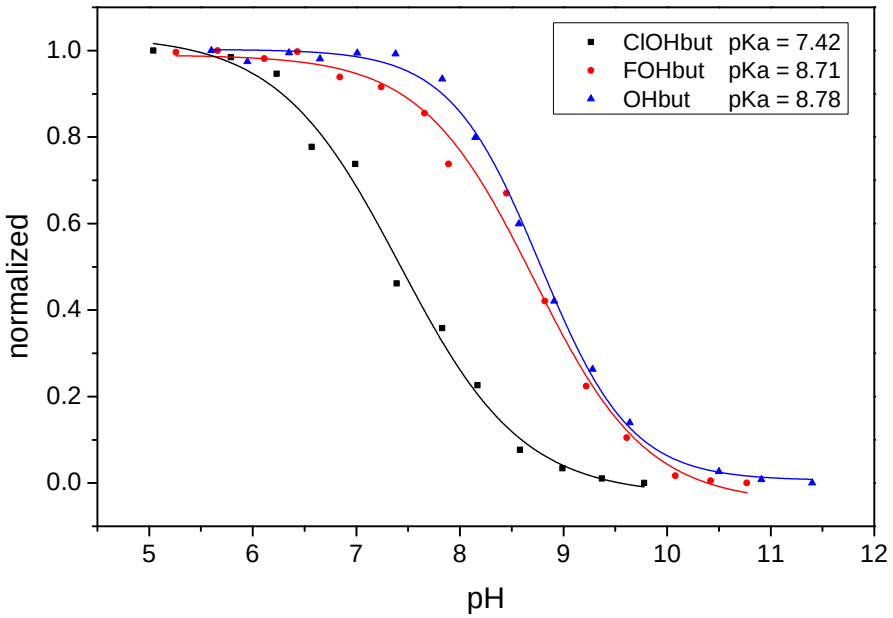

(b) Calibration curves based on fluorescence spectra.

Figure 5.8: Comparison of the photophysical properties of the used indicator dyes. All spectra were recorded with EtOH/H_2O 1:1 as solvent.

5.3.4 Extinction Coefficients of the aza-BODIPY Dyes

BODIPY dyes normally exhibit quite high molar absorption coefficients of over 80 000 $M^{-1}cm^{-1}$.[44] This is also true for the used dyes. The highest molar absorption coefficient of the tree used indicators has the OHbutoxy-complex. But with the standard deviation kept in mind there is almost no difference between them. They are all around 90 000 $M^{-1}cm^{-1}$ and therefore in the expected range.

Table 5.1: Molar absorption coefficient for used aza-BODIPY dyes.

indicator dye	$\epsilon_{\lambda max}$	Std dev
ClOHbutoxy-complex	93 517.9 $M^{-1}cm^{-1}$	$\pm$ 1.25 %
FOHbutoxy-complex	89 418.3 $M^{-1}cm^{-1}$	$\pm$ 2.68 %
OHbutoxy-complex	95 529.9 $M^{-1}cm^{-1}$	$\pm$ 6.08 %

5.3.5 Spectral Properties of $PtTPTBPF_4$ [46]

$PtTPTBPF_4$ is a oxygen sensitive platin complex of a fluorinated benzoporphyrin. It can be exited with blue or red light and exhibits an efficient NIR phosphorescence. The structure and the spectral proprieties are shown in fig. 5.9.

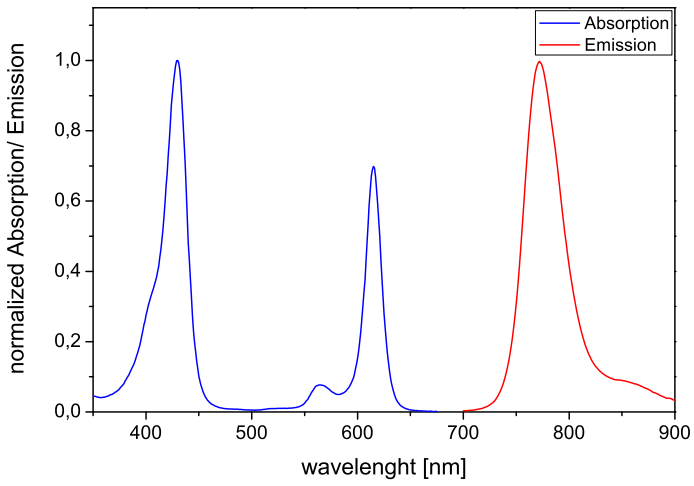

(a) Spectral properties of $PtTPTBPF_4$ in toluene.

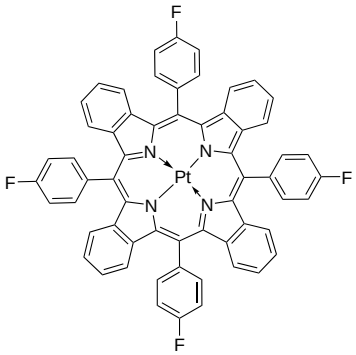

(b) Chemical structur of $PtTPTBPF_4$.

Figure 5.9: Structure and spectral properties of the oxygen sensitive reference dye.

The Soret band of the dye has its maximum at 430 nm (blue light) were it has an absorption coefficient of 212 000 $M^{-1}cm^{-1}$. The Q-bands of the phorphyrin are at 565 and 615 nm (red light). Their $\epsilon_{\lambda\,max}$ (16 300 and 146 000 $M^{-1}cm^{-1}$) are extremely high compared to the absorption coefficients of "clasical" porphyrines which are typical around 20 000 $M^{-1}cm^{-1}$. The maximal emission is at 773 nm. The quantum yield for the phosphorescence is reported with 0.60 and the lifetime τ with 50 µs.

5.4 Properties of the Sensors

5.4.1 pH Sensing Properties

The indicator dyes entrapped into various matrices show different pH sensing behavior as shown in fig. 5.10. In general the entrapment leads always to a decrease of at least 0.9 pKa values. This is due to the shielding the matrix provides against proton penetration. This effect is of course stronger when the matrix is positively charged. Another effect, which is responsible for an additional shift of the apparent pKa, is the FRET effect (Förster resonance energy transfer effect, see section 2.1.2). It appears if dye molecules are in close proximity. Since hydrophobic dyes favor the formation of domains with a higher dye concentration within a matrix, this leads to closer proximity of the molecules and therefore to FRET.

As one can see in table 5.2 the apparent pKa has the lowest value when the indicator is entrapped in RL100 particles. This can be explained by the positively charged quaternary ammonium groups which are present in the polymer matrix (6.25 % n/n; 12.15 % w/w). The positively charged matrix provides a higher barrier for the also positively charged protons and therefore there is a huge shift in the apparent pKa. The positive charge also lead to a stabilization of the basic form of the indicator and therefore the apparent pKa is shifted even further to a lower pH value. However, it was found that PAcM particles show almost no shift compared to PSPVP particles which are not positively charged even tough they exhibit, under the assumption that polymerization was successful, more quaternary ammonium groups (12.2 % n/n; 15 % w/w) than RL100. This indicates that the size of the particles, and the difference in the volume to surface ratio, plays an important role since it is the main difference between RL100 and PAcM particles. As in section 5.4.2 shown, RL100 particles are a lot smaller than PAcM or PSPVP particles. Therefor their surface to volume ratio is much higher and the dye molecules are forced closer together when trying to avoid contact with water. Consequently the FRET effect is more pronounced and the apparent pKa is lower.

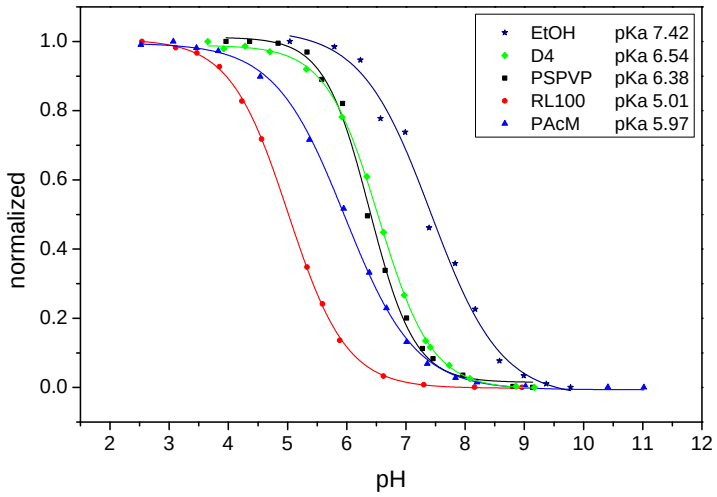

(a) Calibration curves of the ClOHbutoxy-complex.

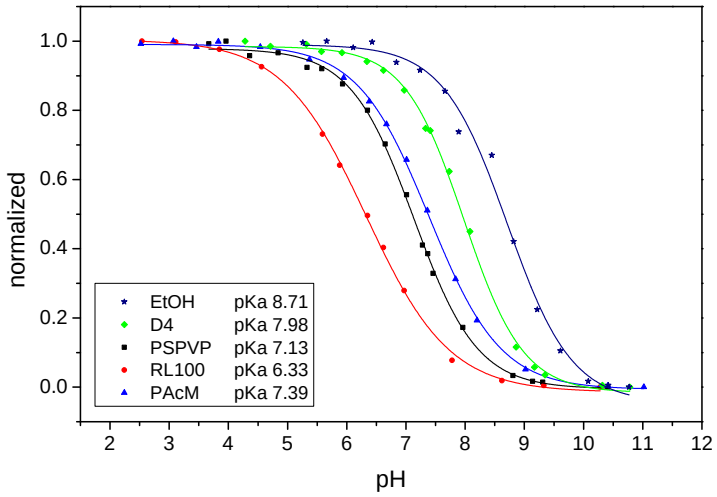

(b) Calibration curves of the FOHbutoxy-complex.

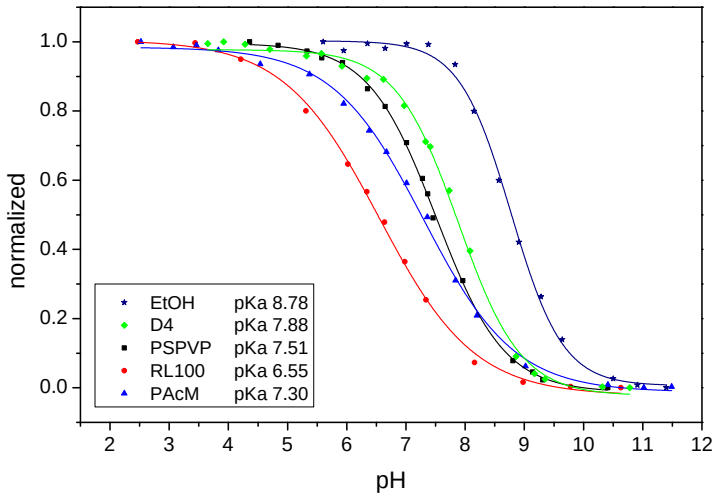

(c) Calibration curves of the OHbutoxy-complex.

Figure 5.10: Behavior of the indicator dyes entrapped in various matices with a concentration of 0.25 %.

Table 5.2: Apparent pKa values of the indicator dyes in various matrices with a dye concentration of 0.25 %.

Indicator Dye	EtOH/H_2O	D4	PSPVP	RL100	PAcM
ClOHbutoxy-complex	7.42	6.54	6.38	5.01	5.97
FOHbutoxy-complex	8.71	7.98	7.13	6.33	7.39
OHbutoxy-complex	8.78	7.88	7.51	6.55	7.30

Another important factor which has an influence on the FRET effect and therefore can change the apparent pKa, is the actual dye concentration. As one can see in fig. 5.11(a) the apparent pKa drops about 0.5 pH values when dye concentration is increased from 0.25 % to 1 %. Because the FRET effect becomes more pronounced at higher dye concentrations and a inner-filter effect develops, the maximal fluorescence intensity doesn't scale linear with the dye concentration. Depending on the size of the particles (surface to volume ratio), there is a maximal dye concentration at which the intensity does not increase anymore. As fig. 5.11(b) shows, a dye concentration of more than 0.25% is just in the case of PAcM particles beneficial to improve the fluorescence intensity of the particles. This can be explained again with the particle size, the different volume to surface ratio and only the shell being stained in the case of PSPVP particles.

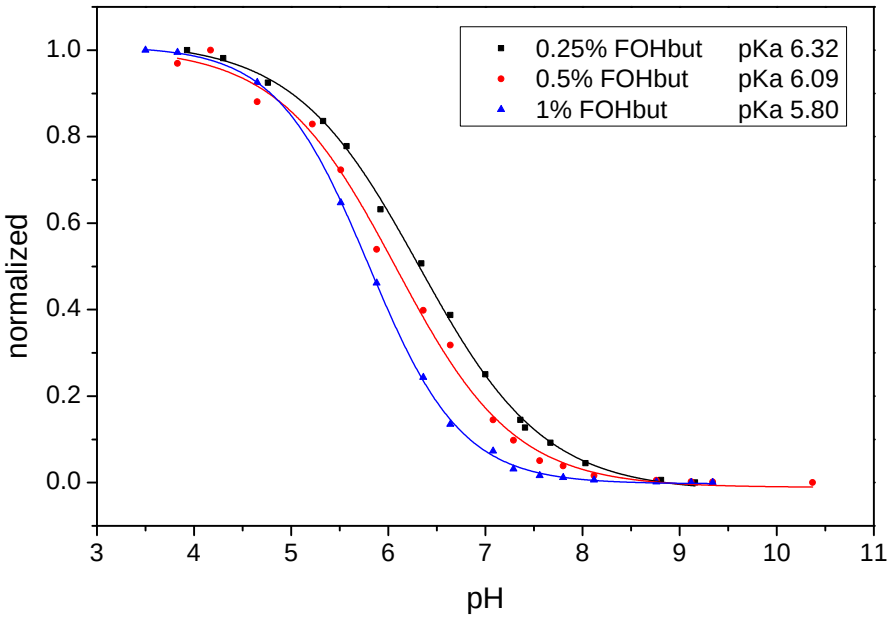

(a) Calibration curves of different concentrations of the FOHbutoxy-complex entrapped in RL100 particles.

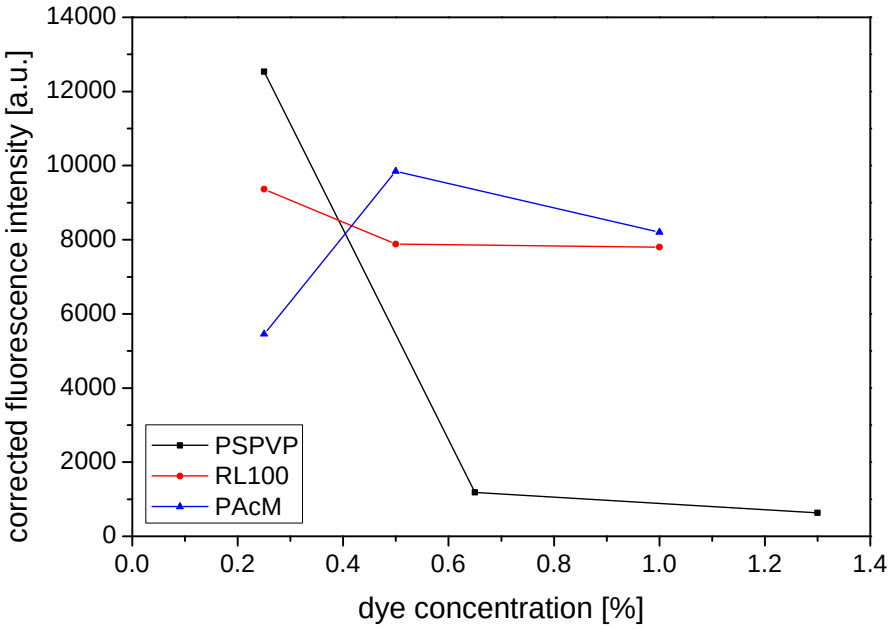

(b) Fluorescence intensities of various dye concentrations in differen particles. FOHbutoxy-complex in PSPVP; FOHbutoxy-complex in RL100; OHbutoxy-complex in PAcM

Figure 5.11: Influence of the dye concentration within the particles on the photophysical properties of the pH sensitive beads.

5.4.2 Size of the Particles

Particle size measurements were carried out for RL100, PAcM and PViCl-PAN beads due to the fact that the size of PSPVP particles is already known (average size = 245 nm [38]). As one can see in table 5.3 the precipitated particles RL100 and PAcM don't have a homogeneous particle size. However, there wide distribution doesn't really matter with regards to the sensing properties as long as the size distribution is reproducible and the particles are not too big. The approximately 550 nm fraction of the RL100 beads probably didn't form during precipitation and is more likely a result of aggregation due to elevated temperatures during the concentration of the particle stock.

Table 5.3: Results of the size measurement

Particle	Peak 1	Share 1	Peak 2	Share 2	Peak 3	Share 3
RL100	26.9 nm	59.5 %	6.1 nm	28.7 %	586.7 nm	8.5 %
PAcM	384.7 nm	55.6 %	6.8 nm	24.4 %	37.5 nm	17.3 %
PViCl-PAN	251.0 nm	100 %				

5.4.3 Estimated Dye Concentration

As argued above the dye concentration is a critical parameter for the sensor characteristic since it can shift the apparent pKa quite drastically due to the FRET effect. Another problem which appeared during the concentration of the particle stocks is, that because of the elevated temperatures parts of the particles stick to the wall. Therefore the exact concentration of the particles in the solution is not known. To estimate the dye concentration, absorption spectra were taken of the two clear particle types. The data is presented below in table 5.4.

These data show that the estimated values, especially of the higher concentrations, are quit far of the mark. This measurement is of course just a ruff estimation since there are several problems with it. For example the influence of the polymeric matrix is not taken into account at all. Another problem is that the maximal absorption has a bathochromic shift when the dyes are entrapped in the beads. This causes problems since the molar absorption coefficient is technically speaking just defined for one wavelength. Even if all these troublesome effects are not taken into account, one can not know what causes the reduced dye concentration since there are at least two possible errors. The first would be the imprecise concentration of the indicator stocks which can have a huge influence. This error would probably at least follow a trend and could therefore be determined. The second error might be a reduced particle concentration due to loss of particles during the concentration of the stocks. This would lead to lower signals

Table 5.4: Estimated indicator dye concentration in various particles.

indicator dye	Particle Type	aimed c(dye)	estimated c(dye)
ClOHbutoxy-complex	RL100	1 %	0.38 %
	RL100	0.5 %	0.35 %
	RL100	0.25 %	0.20 %
	PAcM	0.25 %	0.27 %
FOHbutoxy-complex	RL100	1 %	0.78 %
	RL100	0.5 %	0.32 %
	RL100	0.25 %	0.28 %
	PAcM	0.25 %	0.17 %
OHbutoxy-complex	RL100	0.5 %	0.39 %
	RL100	0.25 %	0.21 %
	PAcM	1 %	0.64 %
	PAcM	0.5 %	0.42 %
	PAcM	0.25 %	0.17 %

than expected and is not reproducible at all. Moreover this error has probably the stronger influence.

5.4.4 Cross Sensitivity to Oxygen

The at various conditions measured phaseangles of the PViCl-PAN reference particles are shown in table 5.5. As one can see, the biggest difference between O_2-saturated and unsaturated solutions can be observed at acidic conditions. This indicates that the polymeric structure of the particle is less dense under acidic conditions and therefor shows a slightly higher permeability for O_2. Since under acidic conditions just one third of the overall signal is due to reference particles, the estimated error of the phase angle is about 0.4 %. Keeping in mind this error just occurs at a maximal difference in the oxygen concentration it can be neglected when there are just small variations.

Table 5.5: Φ values of PViCl-PAN reference particles at various conditions.

	acidic pH	neutral pH	basic pH	Δ
O_2 saturated	44.82°	44.85°	45.15°	0.33°
O_2 free	45.40°	45.26°	45.25°	0.15°
Δ	0.58°	0.38	0.10	

5.4.5 Cross Sensitivity to Ionic Strength

As it was expected, the RL100 particles show almost no cross sensitivity towards the salinity of the solution. This is can probably be explained by the already charged environment the indicator dye is located in. Therefore the PAcM particles should also show almost no cross sensitivity. Anyhow, the experiments showed that this is not the case and that the cross sensitivity is even higher then for PSPVP particles. This is quite surprising since PAcM particles exhibits more positive charges than the RL100 polymer. A possible explanation for this might be, that the particle size of PAcM is, due to aggregation, more sensitive to the salinity. A change of the particle size leads to a different apparent pKa, as already discussed in section 5.4.1, and therefore to a pronounced cross sensitivity.

Table 5.6: Apparent pKa values of 0.25 % OHbutoxy-complex entrapped in various matrices at various salinities.

Salinity	**15 mM**	**60 mM**	**116 mM**	**160 mM**
PSPVP	7.75	7.41	7.42	7.21
RL100	6.59	6.56	6.55	6.49
PAcM	6.31	6.94	7.30	7.02

5.5 Microfluidic Measurements

5.5.1 Method Development

The first measurements were performed without the later used framework (see in fig. 4.9) and therefore the measured values were quite unstable. Anyhow, it could be shown that PSPVP colloids show signal intensities of about 10 mV at a concentration of 0.1 %. At concentrations of 0.5% around 30 mV and at 1 % about 50 mV could be observed (measurement with a modulation of 4000 HZ). Compared to an 13 mV background these values are not very high, especially when keeping in mind that this is the maximum under acidic conditions. Anyhow, since the particle concentration for applications is limited, according to experience, to about 1 % using higher concentrations is not an option to improve the signal intensities.
Because reference particles have to be added for DLR measurements and also for economic (use of less sensor material) and handling reasons (particle stock concentrations of 5 %) it was decided to use PSPVP indicator colloids at a concentration of 0.5 % for further measurements. RL100 indicator particles show a maximal intensity between 30 and 40 mV under acidic conditions at a concentration of 0.05 %. Since the maximal concentration of the RL100 stock

solutions due to aggregation reasons is 0.5 % and the intensity values at 0.05 % are in the same region as for 0.5 % PSPVP colloids it seams reasonable to used them at this concentration. The PSPVP reference particles were measured at concentrations of 0.05 %, 0.025 % and 0,015 %. The samples showed intensities of 110 mV, 67 mV and 36 mV under acidic, air saturated conditions. Since the intensity ratio between pH dependent signal and reference signal should be about 50 %: 50 % as explained in section 2.4, 0.015 % of reference particles were used to realize the first DLR system.

Table 5.7: Measured intensities and phase angles for the first DLR system at differed modulation frequencies. 0.5% PSPVP particles and 0.015 % of reference PSPVP particles

pH	**2000 Hz**		**4000 HZ**		**8000 Hz**	
	intensity	Φ	**intensity**	Φ	**intensity**	Φ
background	13.4 mV		13.2 mV		-	
acidic	51 mV	5.0°	48.8 mV	5.5°	39.5 mV	6.1°
neutral	-	-	38.2 mV	6.6°	33.7 mV	8.7°
basic	9.1 mV	21.1°	10.2 mV	20.5°	7.0 mV	34.0°
Δ	41.9 mV	16.1°	38.6 mV	15°	32.5 mV	27.9°

Form the gained data of the first DLR system one can see, that the difference in the phase angle between acidic and basic conditions is quite small (approx. 15°) for modulation frequencies of 2000 and 4000 Hz. This would lead to a quite poor resolution of the sensor system. A modulation of 8000 Hz showed better results covering almost the double range ($\Delta\,\Phi = 27.9°$). It can also be observed that the signal intensity is generally dropping with higher modulation frequencies and that the ratio of reference signal to pH dependent signal is not ideal. From the intensity values at basic conditions one can see that the ratio of the reference particles is not high enough and is even lower than the subtracted background. The best explanation therefore is that the above given values for the intensities of reference particle concentrations are incorrect since their measurements were still performed without the framework.

As closer investigations show (table 5.8) the intensity of the reference particles are indeed smaller than the first measurements have shown. Therefore, for the second DLR system, a higher concentration of reference particle was used. Since equally strong signals would cause a smaller difference in the phase angles than seen in the first DLR system and that observed shift is barley satisfying, the aim was to have about one third of the signal intensity from the reference particles and not more. Therefore a particle concentration of 0.025% for the reference particles containing 0.5% $PtTPTBPF_4$ and 0.05% of RL100 particles respective 0.5 % PSPVP particles stained with 0.25% indicator dye were used for the second DLR system.

Table 5.8: Measured intensities and phase angles for PSPVP reference particles containing 0.5 % of $PtTPTBPF_4$ for various particle concentrations.

c(particle)	**8000 Hz**		**12000 HZ**	
	intensity	Φ	**intensity**	Φ
0.01 %	6.0 mV	38.0°	4 mV	50.0°
0.015 %	8.8 mV	39.0°	6.7 mV	50.0°
0.02 %	13 mV	39.0°	9.3 mV	49.8°
0.05 %	36.5 mV	39.3°	24.7 mV	49.7°

Table 5.9: Measured intensities and phase angles for the second DLR system at differed modulation frequencies. 0.5% PSPVP particles, 0.05% RL100 particles and 0.025 % of PSPVP reference particles

	RL100		**PSPVP**	
pH	**8000 Hz**	**12000 HZ**	**8000 Hz**	**12000 HZ**
background	11.2 mV	8.1 mV	11.1 mV	-
acidic	40.5 mV, 12.5°	31.3 mV, 13.6°	49 mV, 10.4°	37.6 mV, 11.2°
basic	10.7 mV, 42.5°	7.4 mV, 48.9°	9.8 mV, 39.5°	6.9 mV, 48.5°
Δ	29.8 mV, 30°	23.9 mV, 35.3°	39.2 mV, 29.1°	30.7 mV, 37.5°

As one can see, the higher modulation frequency has a larger difference in the phase angles, but at the cost of a lower signal intensity (also the background decreases). Since the gained difference in Φ is not that big and signal intensities are in general troubling low, it was decided to use a frequency modulation of 8000 Hz as a standard adjustment. It can also be observed, that the aimed intensity for the reference signal was again not reached. The expected value was around 15 mV for a modulation of 8000 Hz and the DLR measurements showed just around 10 mV. This might be explained by a look at the absorption spectra of the indicator dyes under basic conditions. (e.g. see fig. 5.5) Since it is bathochromically shifted to about 750 nm it exhibits quite an overlap with the emission spectra of the $PtTPTBPF_4$ complex (see fig. 5.9(a)). This might lead to reabsorption of the emitted light and therefore to the apparent loss of reference signal.

Due to the sensitivity of the PSPVP reference particle to oxygen, PViCl-PAN was used instead as a reference matrix since it has almost no permeability for O_2. As in table 5.10 shown, the difference in the phase angle is quite small between air saturated and deoxygenized conditions (less then 5% between the extrema).

Table 5.10: Measured intensities and phase angles for PViCl-PAN reference particles containing 1.5 % of $PtTPTBPF_4$ at a particle concentration of 0.007 %.

	intensity	**phase angle**
air saturated	31.3 mV	60.0°
deoxygenized	31.2 mV	62.9°

Because PViCl-PAN is barley permeable to O_2, the lifetime of $PtTPTBPF_4$ in this matrix is longer than in PSPVP. Therefor the phase angle is higher and this means that for the DLR system a higher ratio of reference signal can be used since the shift of the phase angle should still be sufficient. As shown above, the pH dependent signals are, at the used concentrations, between 30 and 40 mV for PSPVP and RL100 particles. PAcM particles behave quite similar to RL100 particles and also show around 30 mV of signal intensity under acidic conditions at a concentration of 0.05 %. Keeping in mind that the reference signal might be a little reduced again, a concentration of 0.007 % for the PViCl-PAN particles seems quite good as a standard concentration.

Table 5.11: Measured intensities and phase angles for the final DLR systems. Background noise for the used set-up: 8.7 mV.

pH	**PSPVP**		**RL100**		**PAcM**	
	intensity	**Φ**	**intensity**	**Φ**	**intensity**	**Φ**
acidic	71.9 mV	25.1°	66.9 mV	24.2°	48.6 mV	28.6°
basic	34.9 mV	56.9°	31.8 mV	57.6°	26.9 mV	57.0°
Δ	37 mV	31.8°	35.1 mV	33.4°	21.7 mV	28.4°

The results of the final DLR systems are satisfying. The minimal signal intensity with about 30 mV is almost four times higher than the background of the system and a shift of the phase angel from about 30° between acidic and basic conditions provides a sufficient resolution. Following adjustments were used from now on as a standard. The Piccolo2 equipped with a focusing lens was operated with a LED intensity of 100 % , an amplification factor of 400, a measurement time of 32 ms and a modulation frequency of 8000 Hz. The standard particle concentrations are shown in table 5.12.

Table 5.12: Used standard particle concentrations with standard dye concentrations for the sensor particles.

matrix	application	c(particle)	c(dye)
PViCl-PAN	reference	0.007 %	1.5 % $PtTPTBPF_4$
PSPVP	pH dependent	0.5 %	0.25 % indicator dye
RL100	pH dependent	0.05 %	0.25 % indicator dye
PAcM	pH dependent	0.05 %	0.25 % indicator dye

5.5.2 Calibration Curves

In table 5.13 the measured apparent pKa values for the indicator dyes entrapped in different polymeric matrices are shown. The comparison of this data with the apparent pKa values gained via fluorescence measurement (table 5.2) shows good agreement.

Table 5.13: Apparent pKa values of the indicator dyes in various matrices measured via DLR in a microlfuidic chip.

Indicator Dye	PSPVP	RL100	PAcM
ClOHbutoxy-complex	6.39	5.17	6.04
FOHbutoxy-complex	7.38	6.34	7.36
OHbutoxy-complex	7.61	6.74	7.30

Miner differences might be due to not using the exact same particle stock or due to aging of the particles. Since it is almost impossible that different batches have exactly the same photophysical properties due to variations in the dye concentration and particle size this is not surprising.
Aging of the particles means a change of the properties with ongoing storage time. There are a couple of known effects which can cause aging. On the one hand it is possible that the indicator dye entrapped in the particle migrates within the matrix. This can change the polarity of the environment the dye is located in and also may enhance the FRET effect if the dye molecules aggregate. Another reason for aging can be the agglomeration of the particles. This would change the particle size and influences, as discussed in section 5.4.2, the apparent pKa value. Even if aza-BODIPY dyes are known for their excellent photostability [44], bleaching still has to be considered as a possible aging effect as well as leaching which is theoretically possible.
A typical responds curve of a measurement with the resulting calibration curve is shown in fig. 5.12 for 0.25 % FOHbutoxy-complex entrapped in RL100 particles.

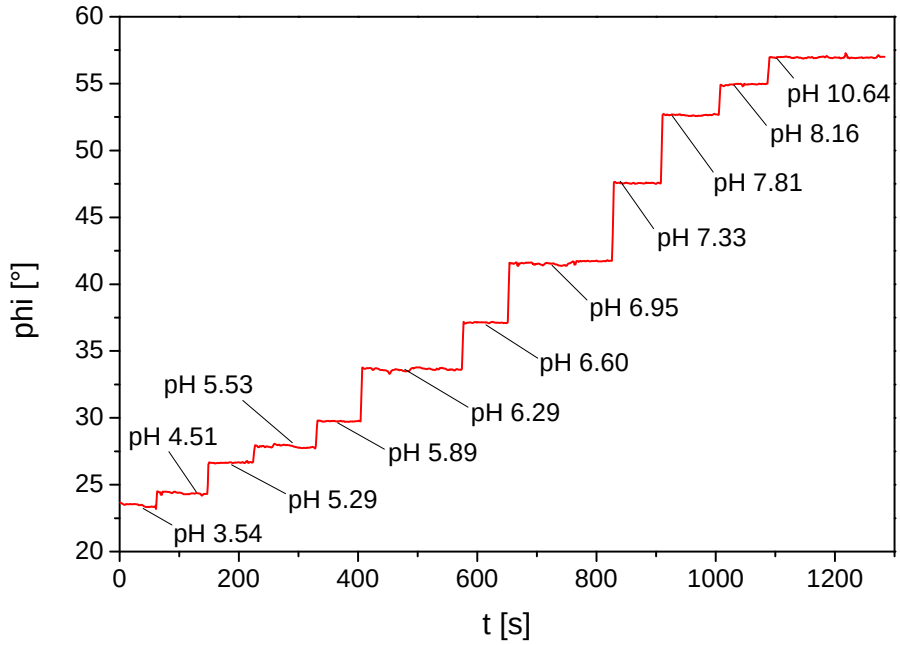

(a) Responscurve of the FOHbutoxy-complex etrapped in RL100 particles.

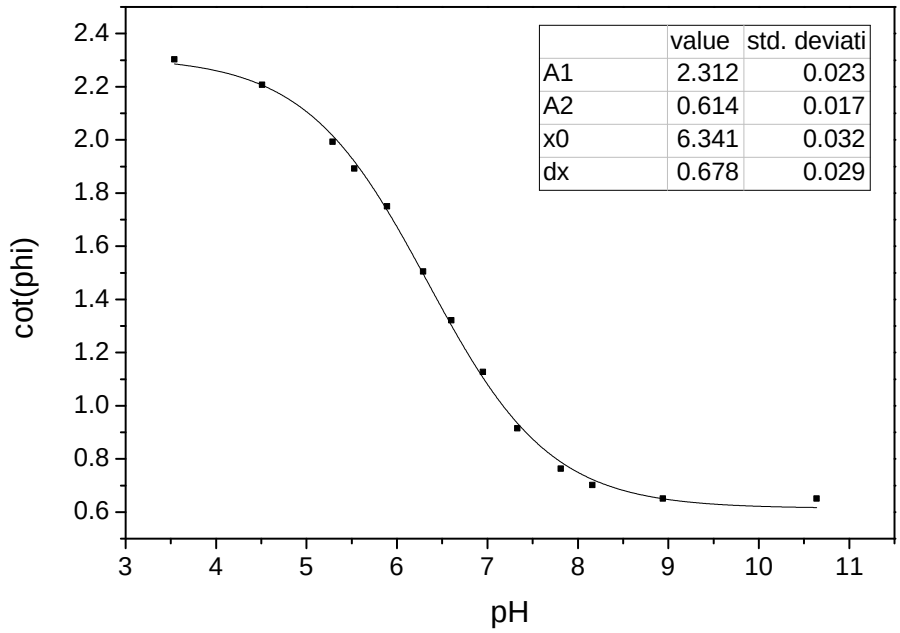

(b) Calibration curve.

Figure 5.12: Typical response curve of the FOHbutoxy-complex (0.25%) entrapped within RL100 particles with PViCl-PAN reference particles stained with 1.5 % of Pt-TPTBP-F_4 in a 300 µm deep i-X factory glass chip.

5.5.3 Reproducibility of pH Measurements

In table 5.14 the measured values of the three positions in the microfluidic chip at the two different pH values are shown. Each value is based on three measurements. The pH of the used buffers was chosen in a fashion that both values are about 0.5 pH values above respectively beneath the pKa value of the used DLR system to cover the linear range. Since RL100 particles stained with the FOHbutoxy-complex were used the apparent pKa of the system was at 6.34.

Table 5.14: Via DLR measured and calucalted values for pH 5.90 and 6.99 at three different positions.

	pH 5.90			**pH 6.99**		
	Φ	**cot(Φ)**	**pH**	**Φ**	**cot(Φ)**	**pH**
position 1	31.04	1.662	6.018	43.15	1.067	7.028
position 2	30.99	1.665	6.013	43.40	1.058	7.047
position 3	30.97	1.666	6.011	43.25	1.063	7.035

In table 5.15 the overall results of all nine measurements are shown and the standard deviation is very small. This shows that the realized DLR system has an excellent reproducibility. When transfered with the according calibration curve (fig. 5.12(b)) to pH values the standard deviation is only about one-hundredth of a pH unit. The accuracy is, with a error of about one-tenth, also not bad. The offset can be explained by the fact that the used calibration curve was taken several days before this measurement. Therefore small changes could have happened to the particle stocks and with an improved calibration even better results are possible.

Table 5.15: Data for the reproducibility of the DLR measurement.

reproducibility	**cot(Φ)**	**measured pH**	**Δ pH**
pH 5.90	1.664 ± 0.006	6.014 ± 0.011	0.12
pH 6.99	1.062 ± 0.005	7.037 ± 0.011	0.05

5.5.4 Longterm Measurements within Microfluidic Chips

Reported aggregation and sedimentation of particles [31] might be an issue when performing longer lasting experiments. Such possible behavior was checked by measuring the particles over a longer time at a constant flow. To exclude the ionic strength as the reason for possible

sedimentation, no background electrolyte was used for this experiment. Further the particle stocks were mixed with the buffer inside the chip to exclude the time of dilution as a factor and get very reproducible conditions.

The response curves of the measurements are shown in fig. 5.13. One can see that there is a heavy drift in the intensity of the PViCl-PAN reference particles showing that they accumulate inside the chip. There is also a noticeable drift in the phase angle. It is decreasing which means that the lifetime of the dye is getting shorter. The reason for this is probably the heavy light load the particles, which are stuck inside the channel, are exposed to. This can lead to photodegradation of the matrix due to produced singlet oxygen which causes an increased oxygen permeability and therefore the Φ drops.
PAcM particles also show a slight drift of the intensity as one can see in fig. 5.13(b). However, it is by far not as drastically as for PViCl-PAN particles. Nevertheless the drift is around 10 % within half an hour an can therefore not be neglected.
As fig. 5.13(c) shows, the intensity of the PSPVP particles takes much longer to equilibrate than the one of the other colloids. After equilibration it is more or less stable and at the end of the measurement it is slightly deceasing which is kind of unexpected. This indicates that the colloid is stable during the time in the chip, but that the particle stock in the reservoir might suffer from inhomogeneity. The maximal differences in the intensity signal is around 10% and needs to be addressed for successful longtime measurements.

To eliminate the chip material as a reason for the strong intensity drift of the PViCl-PAN reference particles, the same experiment was conducted in a Micronit glass chip (see fig. 4.8(c)). But as in fig. 5.14(a) shown, the PViCl-PAN particles have the same drift behavior in the glass chip than in the silicium chip. This might be due to the fact that both materials have negatively charged SiO_2 groups on their surface which might interact with the matrix material. Therefore polymeric chips or coating of the chips might reduce the aggregation of the particles within the chip and enable the developed system to be used also over a longer time period. Another possibility to address this problem is the application of surfactants like PEG (polyethylene glycol) to cancel the interaction between the chip material and the particle matrix.
The PSPVP reference particles (see fig. 5.14(b)) show no significant drift over the measured time and behave basically the same then in the silicium chip. PSPVP are therefore the most stable matrix. However, their intensity signals still suffer from fluctuations which are probably caused by inhomogeneities within the sensor beads. This inhomogeneities are most likely caused by elevated temperatures during the concentration process or by the freeze-drying process leading to particle aggregation. Anyhow, with proper referencing this problems should be manageable.

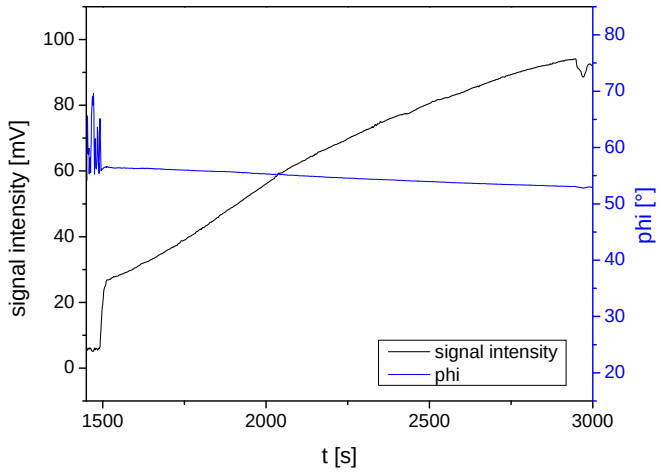

(a) Drift measurement of PViCl-PAN particles.

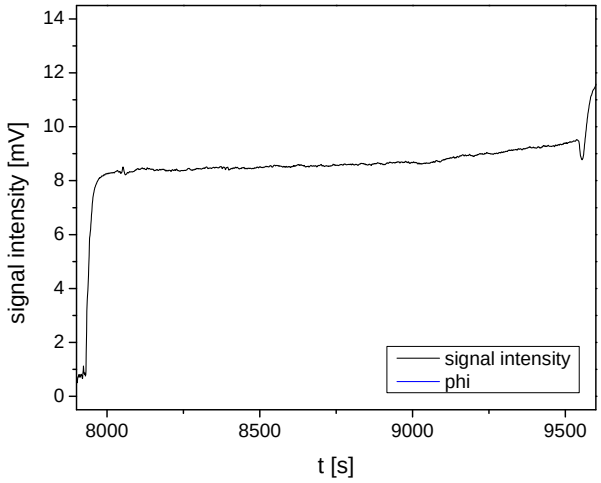

(b) Drift measurement of PAcM particles.

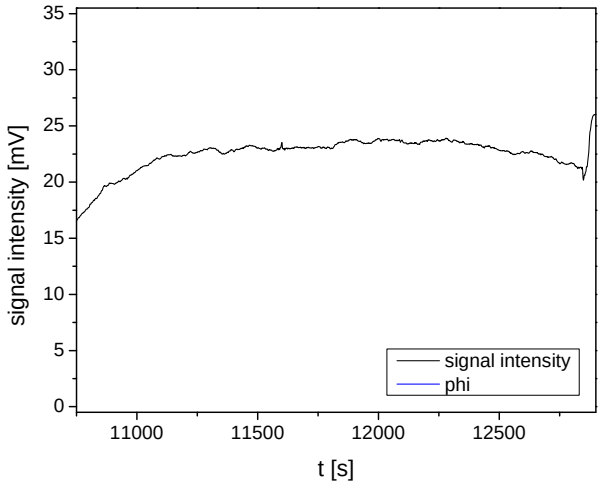

(c) Drift measurement of PSPVP particles.

Figure 5.13: Longterm measurements of the different particle types with in a 400 µm deep Si meander chip from iX-factory (see fig. 4.8(a)) with a flow rate of 2 µl/sec.

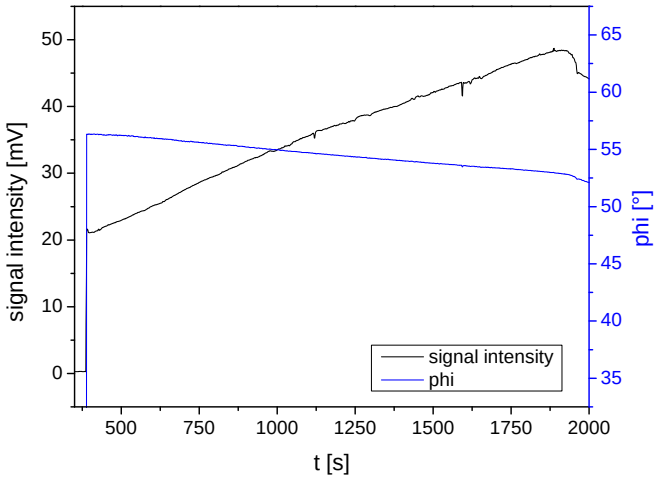

(a) Drift measurement of PViCl-PAN particles.

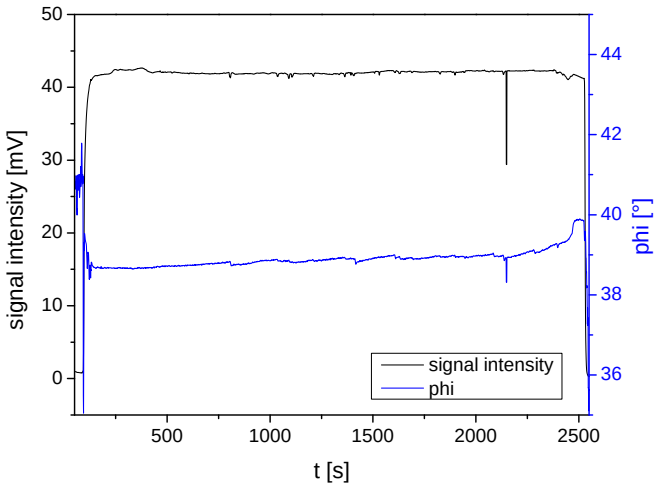

(b) Drift measurement of PSPVP reference particles.

Figure 5.14: Longterm measurements of the two different types of reference particles within a 300 µm deep Micronit glass chip (see fig. 4.8(c))with a flow rate of 2 µl/sec.

5.6 NIR Imaging

Lumogen® Red was used as a reference dye for the imaging system and also to realize the energy transfer to the pH sensitive indicator dye which does not absorb around 579 nm where the excitation with the orange band of a HBO lamp happened. As in fig. 5.15 shown, Lumogen® Red exhibits good absorption at 579 nm and is emitting at 610 nm. It doesn't match the absorption of the indicator dye perfectly but since the LED of the Piccolo2 is also just exciting at 620 nm and the light intensities are higher with the microscope set-up, reasonable results are expected.

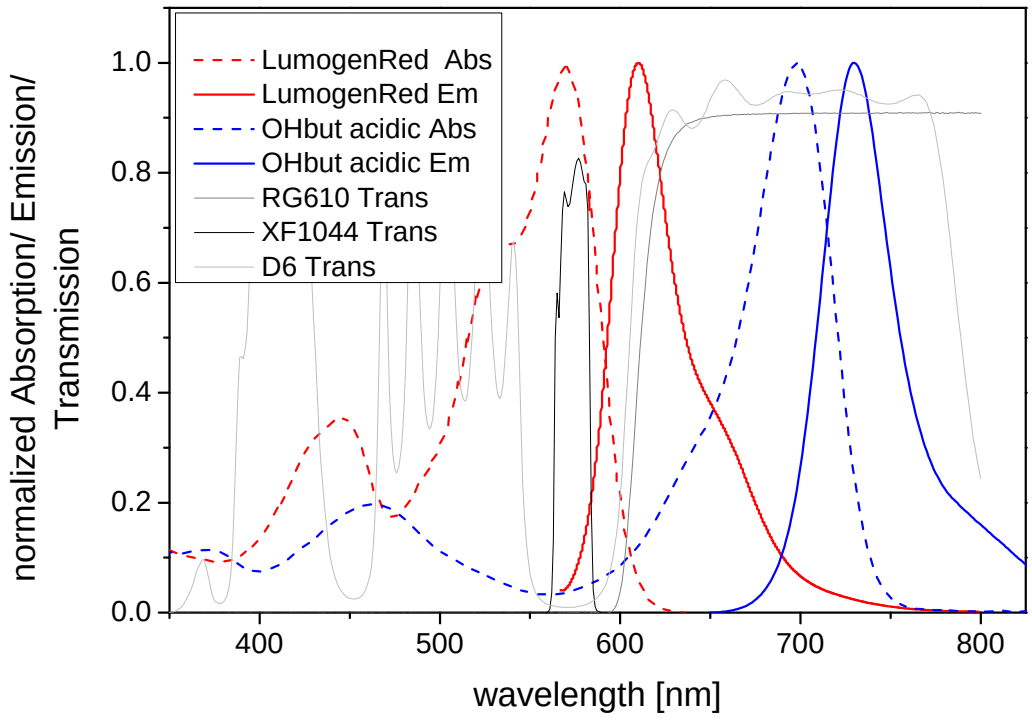

Figure 5.15: Spectral properties of Lumogen® Red and the OHbutoxy-complex combined with the transmission of the used optical filters.

In fig. 5.16 the recorded calibration curve of the realized NIR imaging system is shown. It exhibits an apparent pKa value of about 7.54. This is quite close to the apparent pKa of the DLR system where OHbutoxy-complex is entrapped in PSPVP particles (apparent pKa = 7.61) showing that the Lumogen® Red entrapped within the same particle doesn't influence the properties of indicator dye a lot. However, the standard deviation within the images is quite large under acidic conditions. The reason therefore is probably the weak indicator signal due to the issue of its poor absorption at 610 nm. This leads to longer shutter time for the NIR image

than for the color image, which means that light inhomogeneities have more influence and also inhomogeneities in the particle flow are not referenced out.

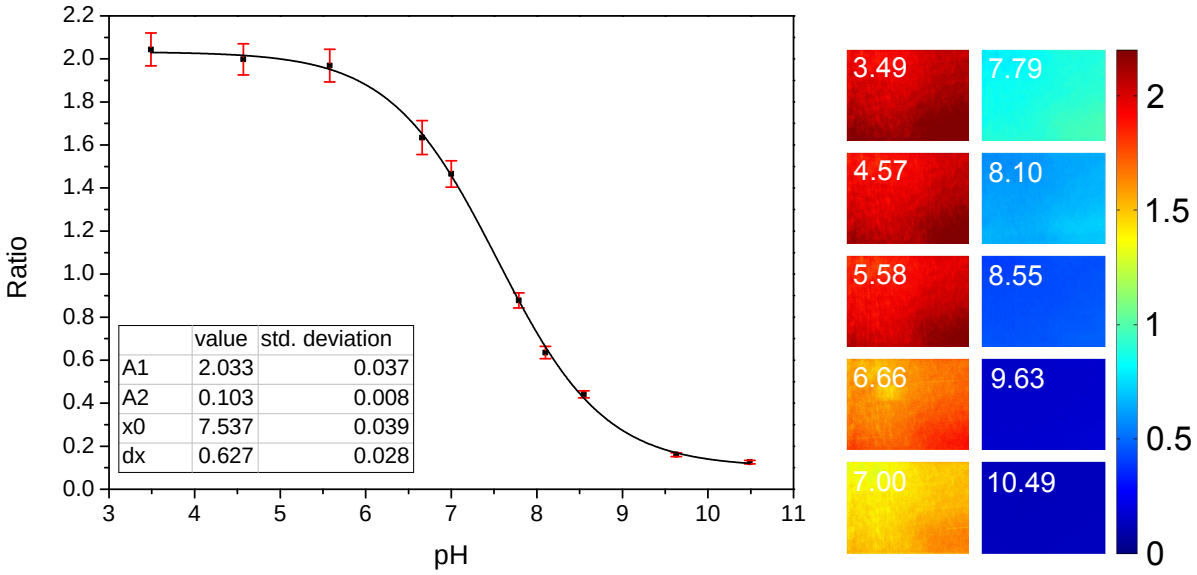

(a) Calibration curve of the NIR imaging system.

(b) Ratiometric images.

Figure 5.16: NIR imaging system based on the OHbutoxy-complex and Lumogen® Red entrapped in PSPVP particles.

6 Conclusion and Outlook

In general this thesis shows that it is possible to apply pH sensitive nanobeads in microfluidic systems and measure the pH within the chips based on a DLR system of aza-BODIPY dyes and $PtTPTBPF_4$ over a broad range (pH 3.5 to pH 9). Nine different particle systems with wide spread apparent pKa values (from pH 5.01 to pH 7.51) have therefore been realized. Imaging in the near infrared is also possible and seems to be a promising tool. However, there are sill some problems to overcome, mainly concerning the stability of the colloids.

The used aza-BODIPY dyes provide enough brightness to enable measurements based on nanoparticles. Although the signal intensities are quite low it could be shown that they are sufficient to receive reliable results with the used equipment and it is possible to measure even in 200 µm deep microfluidic channels.
In general the photophysical properties of the tree different dyes are quite similar. They exhibit approximately the same molar absorption coefficient and during the experiments no real difference in their luminescent properties (lifetime, luminescence intensity, Stocks shift) was noticed. Nevertheless these parameters should be investigated in more detail in the future to be able to compare the different dyes better and optimize their application.
Nonetheless the main difference between the three used dyes is their pKa value. The OHbutoxy-complex with no other electron withdrawing substitutes has hereby the highest value of 8.78. As expected the ClOHbutoxy-complex has the lowest value with 7.42 and the FOHbutoxy-complex is with an pKa of 8.71 between those two. However, it is quite surprising that the difference between the OHbutoxy-complex and the FOHbutoxy-complex is so small. This might be due to a hydrogen bond of the fluorine to the hydrogen in close proximity. It is also noteworthy that the Stocks shift of the FOHbutoxy-complex is slightly larger than that of the other two dyes.

The combination of above mentioned aza-BODIPY dyes with $PtTPTBPF_4$ to get a referenced signal worked in principal. However, the used system is still not ideal since the absorption spectra of the two dyes do not overlap ideally and if excited at 620 nm mainly the reference dye absorbs light. Since $PtTPTBPF_4$ exhibits due to its longer lifetime a better quantum yield it would be favorable to excite at a slightly higher wavelength (650 - 660 nm). This is still not at the maximal absorption of the indicator dye but since the stock shift of the aza-BODPY's is quite small, one would probably get troubles to filter the excitation light from the emission

light, in order to prevent a low background, when excitation would happen at the maximum. However, a higher excitation wavelength would of course lower the signal intensity of the reference dye and it might be necessary to look for a different dye which absorbs at higher wavelength. Since the intensities of the reference dye was not troublesome in any of the conducted experiments, it still might be possible to use $PtTPTBPF_4$ due its excellent brightness.
Another spectral interaction effect which is not ideal should be mentioned at this point. Since the absorption spectrum of the basic form of the indicator dye is shifted to longer wavelength at basic conditions it overlaps with the emission spectrum of the reference dye which leads to a inner-filter effect. Since this should not influence the lifetime of the reference dye (see static quenching section 2.1.2), it is just a minor problem and leads, as long there is enough signal intensity, just to a slight deformation of sigmaoidal calibration curve.

The most stable colloids are **PSPVP particles**. They lower the apparent pKa about 1 to 1.5 pH units, have an average size of 245 nm and do not show a drift. Since the unstained particles are commercially available their quality doesn't change and therefore the manufacturing results are very reproducible. PSPVP beads are stable even at very high concentrations (up to 38 % w/w). However the concentration process (freeze-drying or evaporation of solvent) to get the particle stocks often leads to the formation of aggregates. Those might be the reason why the intensity value is less stable in the drift measurements than for the other particles. Another disadvantage is, that their brightness is just only about a tenth of the one of RL100 or PAcM particles. Further they show a high cross-sensitivity to ionic strength (shift of about 0.5 pH units of the apparent pKa between 15 mM and 160 mM salinity).
RL100 particles lower the apparent pKa about 2.25 to 2.5 pH units. They show an excellent brightness (ten times brighter than PSPVP) and have just a small cross-sensitivity to the ionic strength (shift of about 0.1 pH units of the apparent pKa between 15 mM and 160 mM salinity). They are very small (average size of about 25 nm) and easy to manufacture. However, every batch has to be made separately and it is hard to ensure a constant particle size since the speed of the precipitation has an influence. Another problem with this kind of colloid is the aggregation, especially at higher particle concentrations and in solutions with a higher ionic strength. It has been reported that, if kept diluted (concentrations of less than 0.25 mg/ml), no aggregation occurs under physiological conditions (150 mM).[31] However, a closer investigation of the aggregation behavior of RL100 particles, with respect to the ionic strength and the particle concentration, is necessary and should be done in the future.
PAcM beads do not offer any real advantage over the other two particle types. They generally behave similar to RL100 particles and show good brightness. The only advantage is the exhibit a lower shift of the apparent pKa, which is about 1.5 pH units for PAcM. Their average size is approximately 380 nm and therefore the highest of the used beads. Since the polymer is not commercially available and is made by radical polymerization ensuring a constant quality

is very challenging. Another disadvantage is the strong cross-sensitivity to the ionic strength (shift of about 0.7 pH units of the apparent pKa between 15 mM and 160 mM salinity). PAcM beads also show a slight intensity drift over time at conditions with low ionic strength. This drift is expected to increase with increasing ionic strength since the polymer can be precipitated with salt from aqueous colloids. It is also probable, that high particle concentrations lead to an aggregation like it has been reported for RL100 particles. This has not be studied but might be interesting in the future.
Since PSPVP beads are permeable to oxygen, which leads to a cross-sensitivity and to a shorter life time of the reference dye (therefore the phase angel is smaller and consequently also the resolution gets smaller), **PViCl-PAN** was used as a matrix for the reference particles. They have an average particle size of 250 nm and experiments showed that indeed the cross-sensitivity to oxygen is negligible. Their main problem is, that they seem to aggregate and sediment not only at higher concentrations or higher ionic strength, but also when they are very diluted (particle concentration of 0.007%) with no background electrolyte inside microfluidic devices. Since this might be due to the interaction of the particle matrix with the chip material their stability in other chips (e.g. polymieric chips with no SiO_2-groups) should be tested. Another possible solution for the aggregation problem of the PViCl-PAN particles might be coating of the microfluidic chips or, as mentioned before, the use of surfactants like PEG (polyethylen glycol). Anyhow further work is necessary to enable PViCl-PAN particles to serve as reference in microfluidic systems, especially when experiments are conducted over longer time.

Since aggregation and sedimentation processes seem to play such an important role in microfluidic pH measurements it would be very beneficial to entrap both dyes into one particle. This strategy would improve the DLR referencing since the ratio between the two dyes would be stable and slight sedimentation would be referenced out. The only trouble with the sedimenting particles which would be unchanged, is the photodegradation of the stuck particles due to the high light intensities. This would change the lifetime and therefore the phaseangle.
The realization of such a system would require core-shell particles, where the core would ideally be oxygen impermeable. Another approach might be the substitution of the reference dye with an oxygen insensitive phosphorescent dye with a long lifetime. However, both adaptations are not that easy to realize and the development of the perfect pH sensitive nanoparticles remains challenging.

7 References

[1] Dorota Wencel, Tobias Abel, and Colette McDonagh. “Optical Chemical pH Sensors”. In: *Analytical Chemistry* 86.1 (Jan. 7, 2014), pp. 15–29.

[2] S.C. Terry, J.H. Jerman, and J.B. Angell. “A gas chromatographic air analyzer fabricated on a silicon wafer”. In: *IEEE Transactions on Electron Devices* 26.12 (Dec. 1979), pp. 1880–1886.

[3] A. Manz, N. Graber, and H. M. Widmer. “Miniaturized total chemical analysis systems: A novel concept for chemical sensing”. In: *Sensors and Actuators B: Chemical* 1.1 (Jan. 1990), pp. 244–248.

[4] Bernard Valeur. *Molecular fluorescence: principles and applications*. Weinheim ; New York: Wiley-VCH, 2002. 387 pp.

[5] Bo Tang, Fabiao Yu, Ping Li, Lili Tong, Xia Duan, Ting Xie, and Xu Wang. “A Near-Infrared Neutral pH Fluorescent Probe for Monitoring Minor pH Changes: Imaging in Living HepG2 and HL-7702 Cells”. In: *Journal of the American Chemical Society* 131.8 (Mar. 4, 2009), pp. 3016–3023.

[6] Wenshen Zhang, Bo Tang, Xia Liu, Yuanyuan Liu, Kehua Xu, Jianping Ma, Lili Tong, and Guiwen Yang. “A highly sensitive acidic pH fluorescent probe and its application to HepG2 cells”. In: *Analyst* 134.2 (Feb. 1, 2009), pp. 367–371.

[7] Antony S. Jeevarajan, Sundeep Vani, Thomas D. Taylor, and Melody M. Anderson. “Continuous pH monitoring in a perfused bioreactor system using an optical pH sensor”. In: *Biotechnology and Bioengineering* 78.4 (May 20, 2002), pp. 467–472.

[8] Gernot T. John, Detlef Goelling, Ingo Klimant, Holger Schneider, and Elmar Heinzle. “PH-sensing 96-well microtitre plates for the characterization of acid production by dairy starter cultures”. In: *The Journal of Dairy Research* 70.3 (Aug. 2003), pp. 327–333.

[9] Michael Kühl. “Optical Microsensors for Analysis of Microbial Communities”. In: *Methods in Enzymology*. Ed. by Jared R. Leadbetter. Vol. 397. Environmental Microbiology. Academic Press, 2005, pp. 166–199.

[10] Morten Larsen, Sergey M. Borisov, Björn Grunwald, Ingo Klimant, and Ronnie N. Glud. “A simple and inexpensive high resolution color ratiometric planar optode imaging approach: application to oxygen and pH sensing.” In: *Limnology and Oceanography: Methods* 9.9 (Sept. 1, 2011), pp. 348–360.

[11] Sarina Arain, Gernot T. John, Christian Krause, Jochen Gerlach, Otto S. Wolfbeis, and Ingo Klimant. “Characterization of microtiterplates with integrated optical sensors for oxygen and pH, and their applications to enzyme activity screening, respirometry, and toxicological assays”. In: *Sensors and Actuators B: Chemical* 113.2 (Feb. 2006), pp. 639–648.

[12] Katherine Schouest, Alice Zitova, Charles Spillane, and Dmitri Papkovsky. “Toxicological assessment of chemicals using Caenorhabditis elegans and optical oxygen respirometry”. In: *Environmental toxicology and chemistry / SETAC* 28.4 (Apr. 2009), pp. 791–799.

[13] Andrew Mills. “Oxygen indicators and intelligent inks for packaging food”. In: *Chemical Society Reviews* 34.12 (Dec. 2005), pp. 1003–1011.

[14] Peter Gründler. *Chemische Sensoren: Eine Einführung für Naturwissenschaftler und Ingenieure*. Springer, Mar. 23, 2004. 312 pp.

[15] Todd W. Roy and A. S. Bhagwat. “Kinetic studies of Escherichia coli AlkB using a new fluorescence-based assay for DNA demethylation”. In: *Nucleic Acids Research* 35.21 (Dec. 2007), e147.

[16] Miguel A. Acosta, Patrick Ymele-Leki, Yordan V. Kostov, and Jennie B. Leach. “Fluorescent microparticles for sensing cell microenvironment oxygen levels within 3D scaffolds”. In: *Biomaterials* 30.17 (June 2009), pp. 3068–3074.

[17] Nicholas Hamilton. “Quantification and its Applications in Fluorescent Microscopy Imaging”. In: *Traffic* 10.8 (Aug. 1, 2009), pp. 951–961.

[18] Jiri Janata. “Do optical sensors really measure pH?” In: *Analytical Chemistry* 59.9 (May 1, 1987), pp. 1351–1356.

[19] Bernhard M. Weidgans, Christian Krause, Ingo Klimant, and Otto S. Wolfbeis. “Fluorescent pH sensors with negligible sensitivity to ionic strength”. In: *Analyst* 129.7 (June 22, 2004), pp. 645–650.

[20] Claudia R. Schröder, Bernhard M. Weidgans, and Ingo Klimant. “pH Fluorosensors for use in marine systems”. In: *Analyst* 130.6 (May 23, 2005), pp. 907–916.

[21] Anna S. Vasylevska, Alexander A. Karasyov, Sergey M. Borisov, and Christian Krause. “Novel coumarin-based fluorescent pH indicators, probes and membranes covering a broad pH range”. In: *Analytical and Bioanalytical Chemistry* 387.6 (Mar. 2007), pp. 2131–2141.

[22] Sergey M. Borisov, Karl Gatterer, and Ingo Klimant. “Red light-excitable dual lifetime referenced optical pH sensors with intrinsic temperature compensation”. In: *Analyst* 135.7 (June 21, 2010), pp. 1711–1717.

[23] Ramaier Narayanaswamy and Otto S. Wolfbeis. *Optical Sensors: Industrial Environmental and Diagnostic Applications*. Berlin, Heidelberg: Springer Berlin Heidelberg, 2004.

[24] Sergey M. Borisov, Danielle L. Herrod, and Ingo Klimant. “Fluorescent poly(styrene-block-vinylpyrrolidone) nanobeads for optical sensing of pH”. In: *Sensors and Actuators B: Chemical*. EUROPT(R)ODE IX Proceedings of the 9th European Conference on Optical Chemical Sensors and Biosensors EUROPT(R)ODE IX Proceedings of the 9th European Conference on Optical Chemical Sensors and Biosensors 139.1 (May 20, 2009), pp. 52–58.

[25] Niklas Strömberg, Erik Mattsson, and Aron Hakonen. “An imaging pH optode for cell studies based on covalent attachment of 8-hydroxypyrene-1,3,6-trisulfonate to amino cellulose acetate films”. In: *Analytica Chimica Acta* 636.1 (Mar. 16, 2009), pp. 89–94.

[26] M. Graber, T. Dixon, D. Coachman, and P. Devine. “Acetazolamide inhibits acidification by the turtle bladder independent of cell pH”. In: *American Journal of Physiology - Renal Physiology* 256.5 (May 1, 1989), F923–F931.

[27] E Pastoriza-Munoz, R M Harrington, and M L Graber. “Parathyroid hormone decreases HCO3 reabsorption in the rat proximal tubule by stimulating phosphatidylinositol metabolism and inhibiting base exit.” In: *Journal of Clinical Investigation* 89.5 (May 1992), pp. 1485–1495.

[28] Christian Huber, Ingo Klimant, Christian Krause, and Otto S. Wolfbeis. “Dual Lifetime Referencing as Applied to a Chloride Optical Sensor”. In: *Analytical Chemistry* 73.9 (May 1, 2001), pp. 2097–2103.

[29] Ronnie N. Glud Gerhard Holst. “A microoptode array for fine-scale measurement of oxygen distribution”. In: *Sensors and Actuators B: Chemical* (1997), pp. 122–129.

[30] Sergey M. Borisov and Ingo Klimant. “Optical nanosensors—smart tools in bioanalytics”. In: *Analyst* 133.10 (Sept. 9, 2008), pp. 1302–1307.

[31] Sergey M. Borisov, Torsten Mayr, Günter Mistlberger, Kerstin Waich, Klaus Koren, Pavel Chojnacki, and Ingo Klimant. “Precipitation as a simple and versatile method for preparation of optical nanochemosensors”. In: *Talanta* 79.5 (Oct. 15, 2009), pp. 1322–1330.

[32] Daniel Aigner, Birgit Ungerböck, Torsten Mayr, Robert Saf, Ingo Klimant, and Sergey M. Borisov. “Fluorescent materials for pH sensing and imaging based on novel 1,4-diketopyrrolo-[3,4-c]pyrrole dyes”. In: *Journal of Materials Chemistry C* 1.36 (Aug. 22, 2013), pp. 5685–5693.

[33] B. Korzeniowska, R. Nooney, D. Wencel, and C. McDonagh. “Silica nanoparticles for cell imaging and intracellular sensing”. In: *Nanotechnology* 24.44 (Nov. 8, 2013), p. 442002.

[34] Xu-dong Wang, Robert J. Meier, and Otto S. Wolfbeis. “Fluorescent pH-Sensitive Nanoparticles in an Agarose Matrix for Imaging of Bacterial Growth and Metabolism”. In: *Angewandte Chemie International Edition* 52.1 (Jan. 2, 2013), pp. 406–409.

[35] Yong-Eun Koo Lee and Raoul Kopelman. “Chapter twenty-one - Nanoparticle PEBBLE Sensors in Live Cells”. In: *Methods in Enzymology*. Ed. by P. Michael conn. Vol. 504. Imaging and Spectroscopic Analysis of Living Cells Optical and Spectroscopic Techniques. Academic Press, 2012, pp. 419–470.

[36] Günter Mistlberger and Ingo Klimant. “Luminescent magnetic particles: structures, syntheses, multimodal imaging, and analytical applications”. In: *Bioanalytical Reviews* 2.1 (Dec. 7, 2010), pp. 61–101.

[37] Sergei A. Vinogradov, Leu-Wei Lo, and David F. Wilson. “Dendritic Polyglutamic Porphyrins: Probing Porphyrin Protection by Oxygen-Dependent Quenching of Phosphorescence”. In: *Chemistry – A European Journal* 5.4 (Apr. 1, 1999), pp. 1338–1347.

[38] Sergey M. Borisov, Torsten Mayr, and Ingo Klimant. “Poly(styrene-block-vinylpyrrolidone) Beads as a Versatile Material for Simple Fabrication of Optical Nanosensors”. In: *Analytical Chemistry* 80.3 (Feb. 1, 2008), pp. 573–582.

[39] Josef Ehgartner, Helmar Wiltsche, Sergey M. Borisov, and Torsten Mayr. “Low cost referenced luminescent imaging of oxygen and pH with a 2-CCD colour near infrared camera”. In: *Analyst* 139.19 (Aug. 26, 2014), pp. 4924–4933.

[40] Tijana Jokic, Sergey M. Borisov, Robert Saf, Daniel A. Nielsen, Michael Kühl, and Ingo Klimant. “Highly Photostable Near-Infrared Fluorescent pH Indicators and Sensors Based on BF2-Chelated Tetraarylazadipyrromethene Dyes”. In: *Analytical Chemistry* 84.15 (Aug. 7, 2012), pp. 6723–6730.

[41] Michael J. Hall, Shane O. McDonnell, John Killoran, and Donal F. O’Shea. “A Modular Synthesis of Unsymmetrical Tetraarylazadipyrromethenes”. In: *The Journal of Organic Chemistry* 70.14 (July 1, 2005), pp. 5571–5578.

[42] Aoife Gorman, John Killoran, Caroline O’Shea, Tony Kenna, William M. Gallagher, and Donal F. O’Shea. “In Vitro Demonstration of the Heavy-Atom Effect for Photodynamic Therapy”. In: *Journal of the American Chemical Society* 126.34 (Sept. 1, 2004), pp. 10619–10631.

[43] Aurore Loudet, Rakeshwar Bandichhor, Liangxing Wu, and Kevin Burgess. “Functionalized BF2 Chelated Azadipyrromethene Dyes”. In: *Tetrahedron* 64.17 (Apr. 21, 2008), pp. 3642–3654.

[44] Hua Lu, John Mack, Yongchao Yang, and Zhen Shen. “Structural modification strategies for the rational design of red/NIR region BODIPYs”. In: *Chemical Society Reviews* 43.13 (June 9, 2014), pp. 4778–4823.

[45] Toomas H. Allik, Robert E. Hermes, Govindarao Sathyamoorthi, and Joseph H. Boyer. "Spectroscopy and laser performance of new BF2-complex dyes in solution". In: vol. 2115. 1994, pp. 240–248.

[46] S. M. Borisov, G. Nuss, W. Haas, R. Saf, M. Schmuck, and I. Klimant. "New NIR-emitting complexes of platinum(II) and palladium(II) with fluorinated benzoporphyrins". In: *Journal of Photochemistry and Photobiology A: Chemistry* 201.2 (Jan. 25, 2009), pp. 128–135.

8 List of Figures

9 List of Tables

10 Appendix

10.1 NMR Spectra

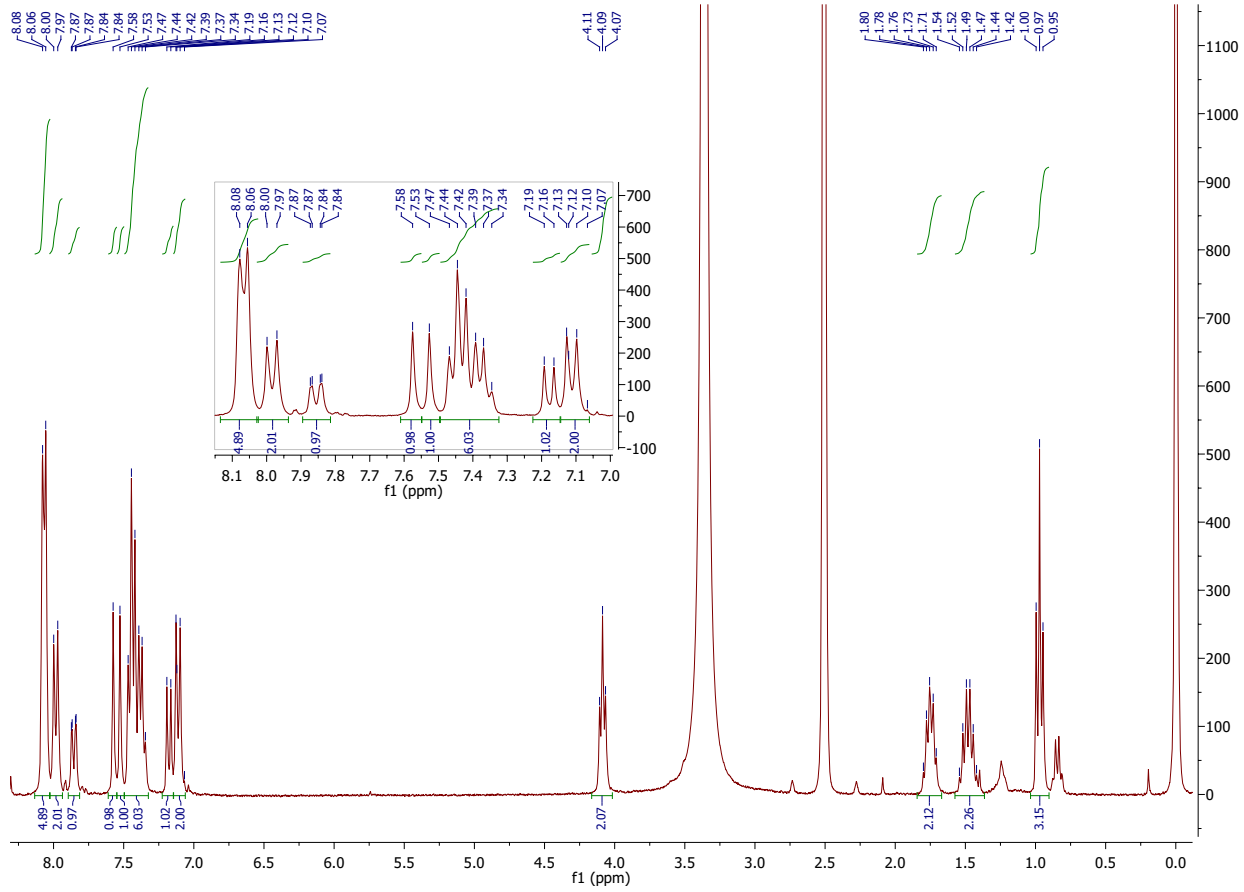

Figure 10.1: NMR spectrum of the ClOHbutoxy-ligand.

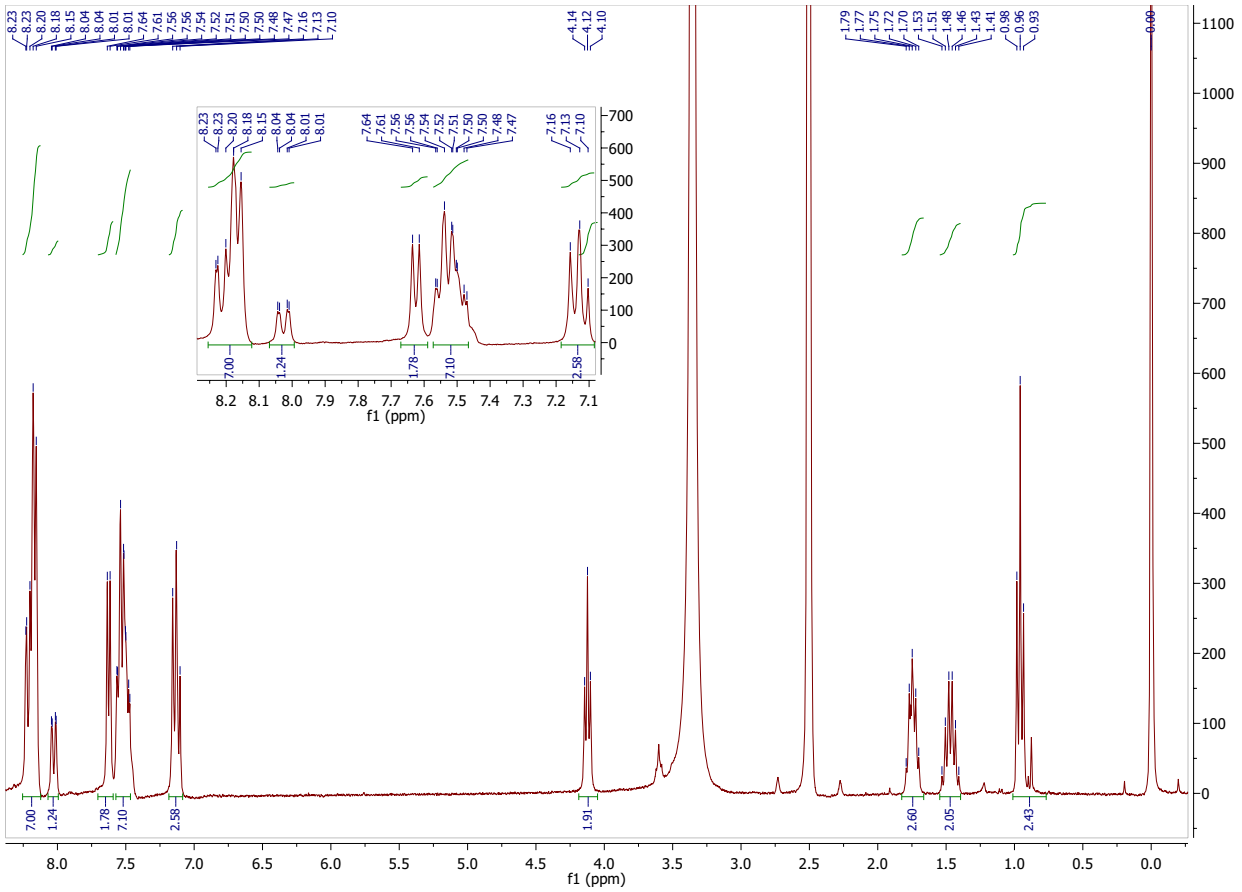

Figure 10.2: NMR spectrum of the ClOHbutoxy-complex.

10.2 Emission Spectra of the ClOHbutoxy-complex

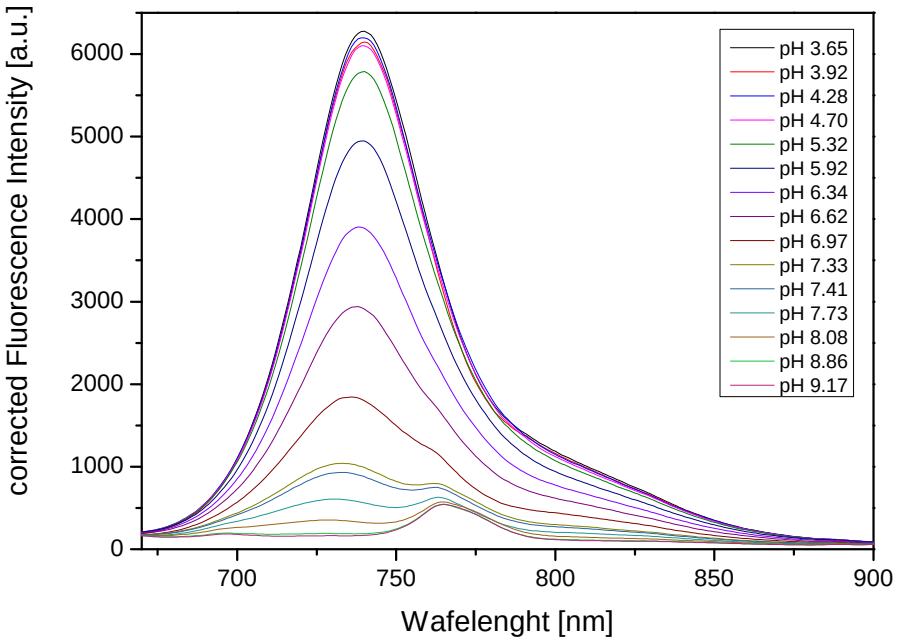

Figure 10.3: Emission spectra of the ClOHbutoxy-complex in D4.

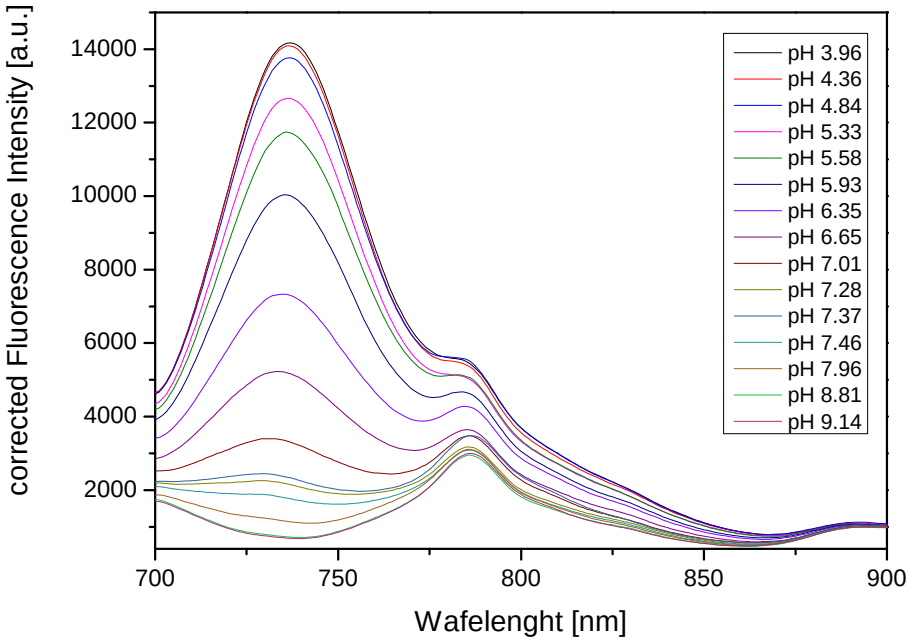

Figure 10.4: Emission spectra of the ClOHbutoxy-complex in PSPVP.

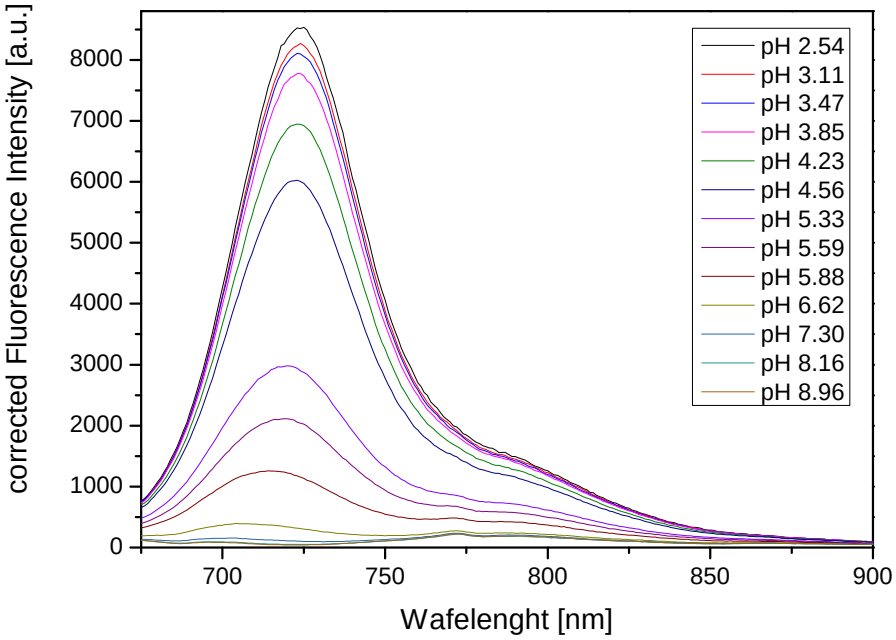

Figure 10.5: Emission spectra of the ClOHbutoxy-complex in RL100.

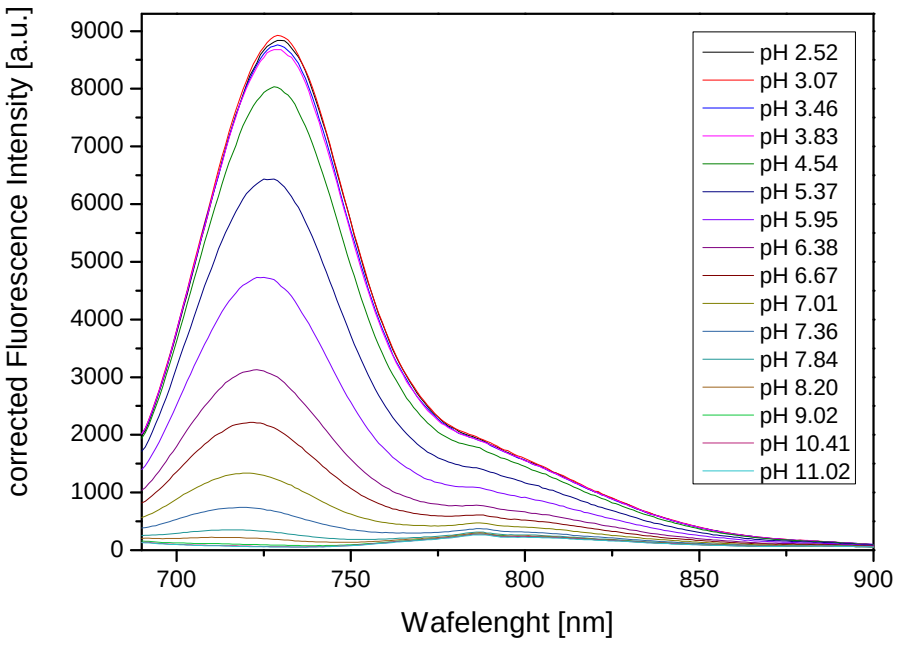

Figure 10.6: Emission spectra of the ClOHbutoxy-complex in PAcM.

10.3 Emission Spectra of the FOHbutoxy-complex

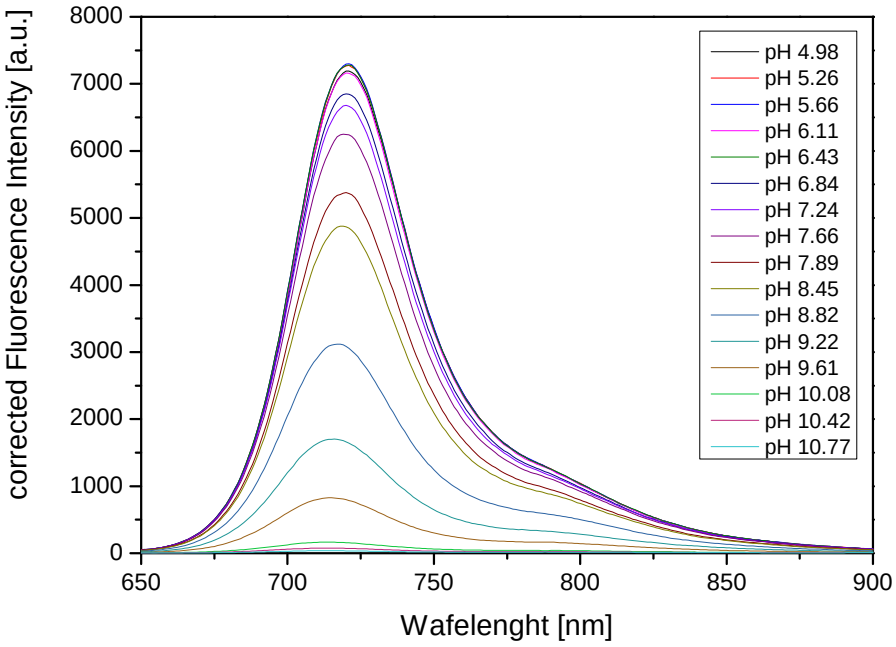

Figure 10.7: Emission spectra of the FOHbutoxy-complex in EtOH/H_2O.

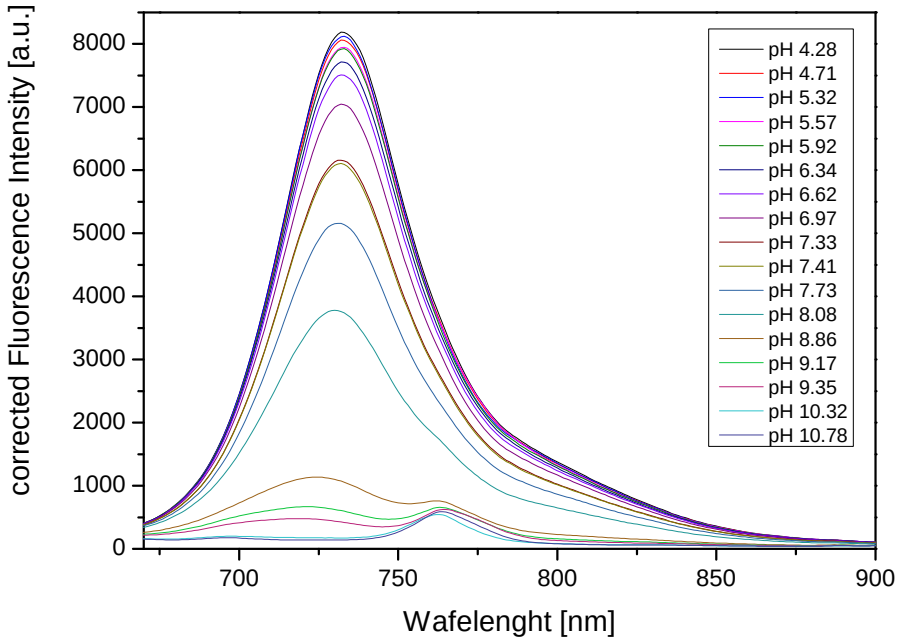

Figure 10.8: Emission spectra of the FOHbutoxy-complex in D4.

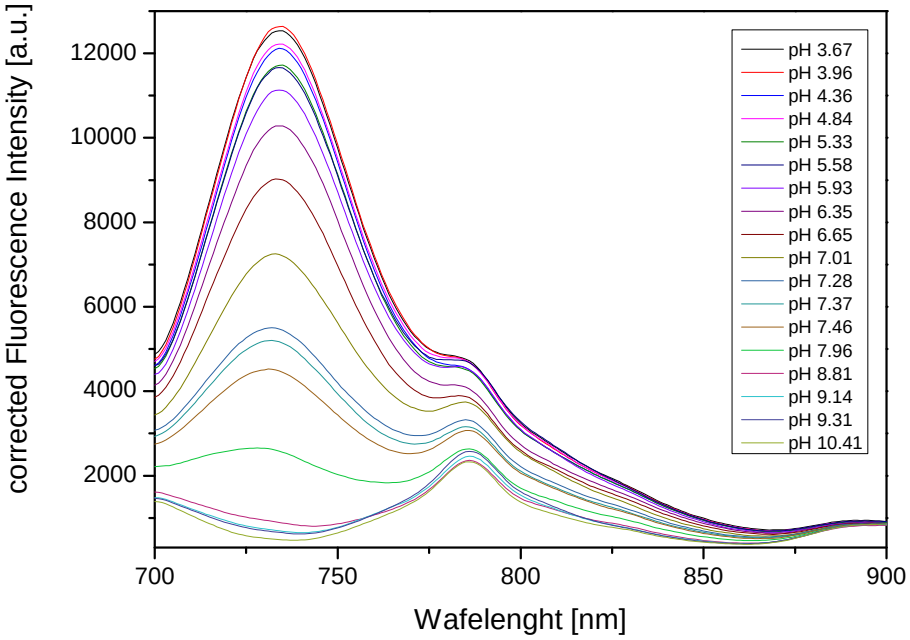

Figure 10.9: Emission spectra of the FOHbutoxy-complex in PSPVP.

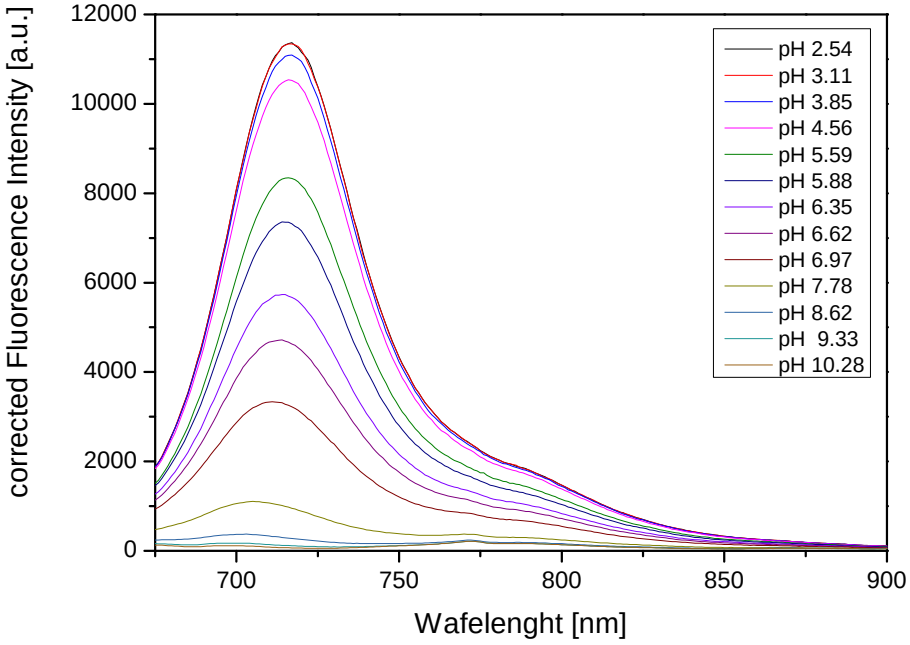

Figure 10.10: Emission spectra of the FOHbutoxy-complex in RL100.

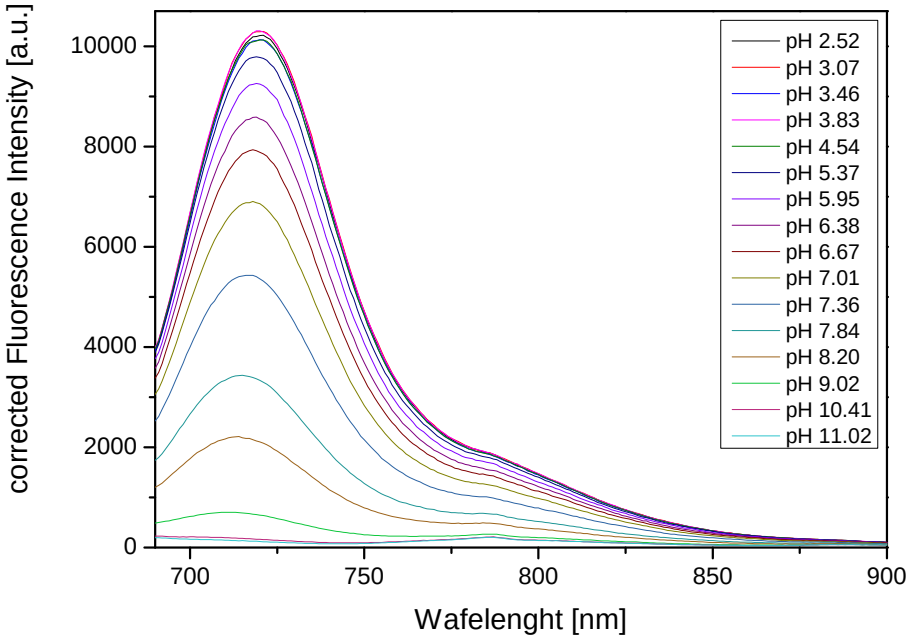

Figure 10.11: Emission spectra of the FOHbutoxy-complex in PAcM.

10.4 Emission Spectra of the OHbutoxy-complex

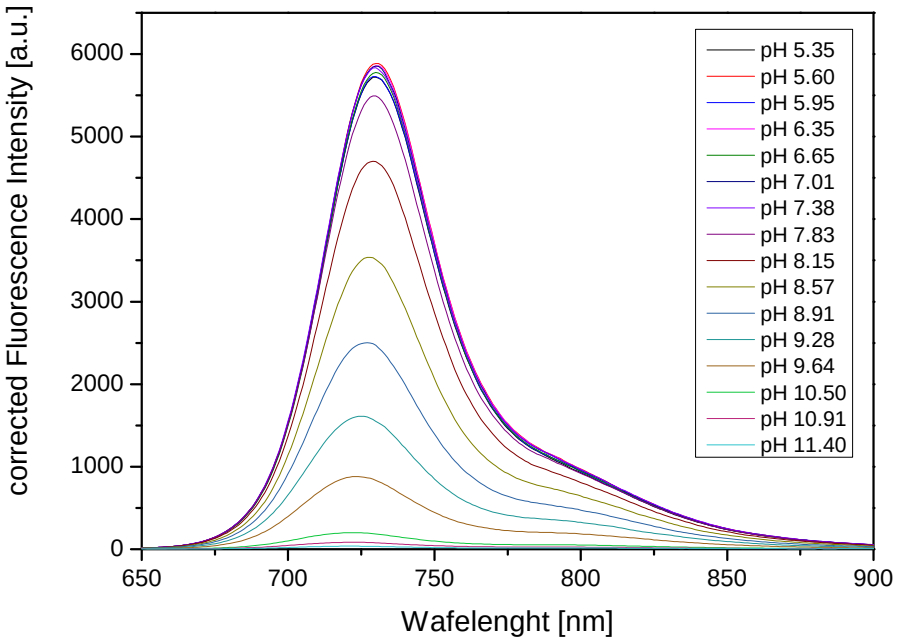

Figure 10.12: Emission spectra of the OHbutoxy-complex in EtOH/H_2O.

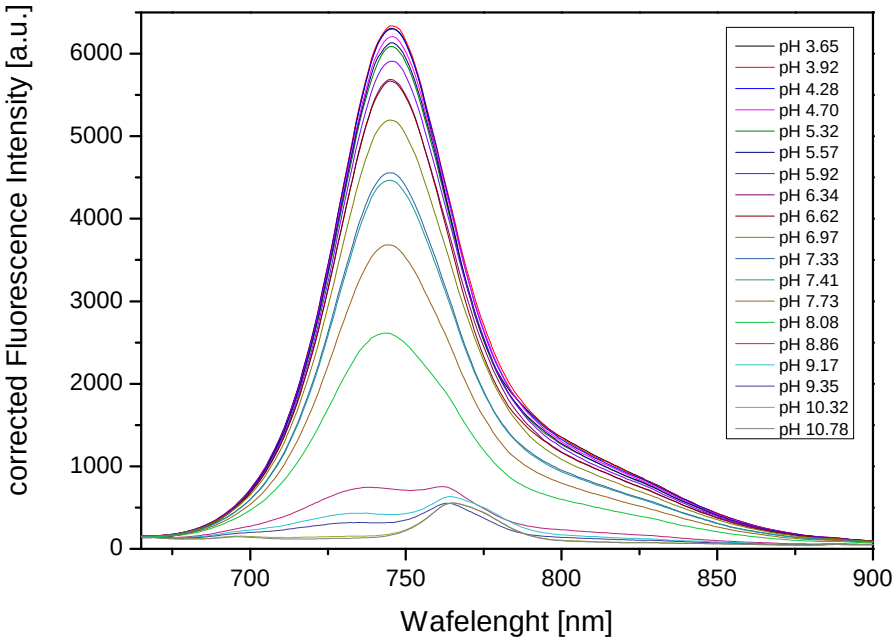

Figure 10.13: Emission spectra of the OHbutoxy-complex in D4.

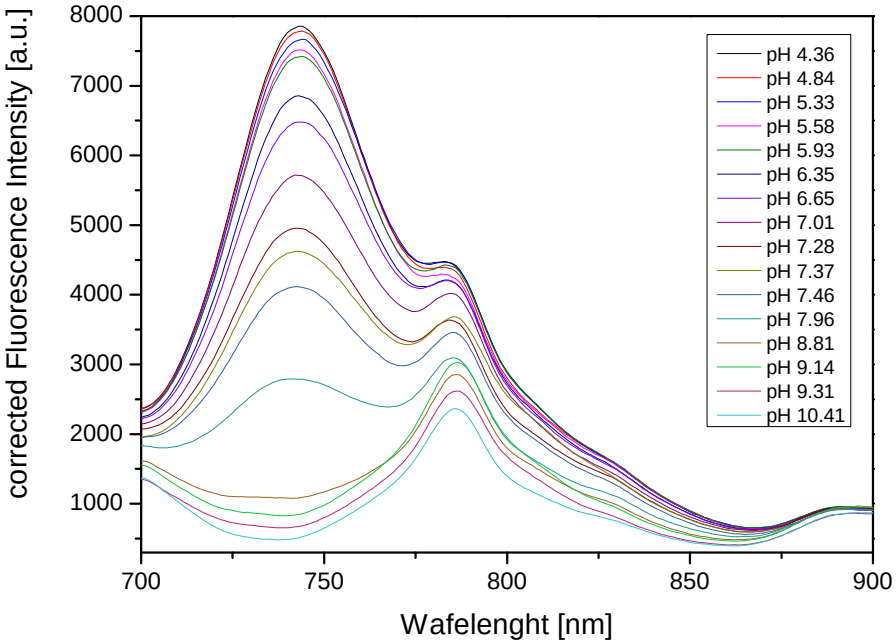

Figure 10.14: Emission spectra of the OHbutoxy-complex in PSPVP.

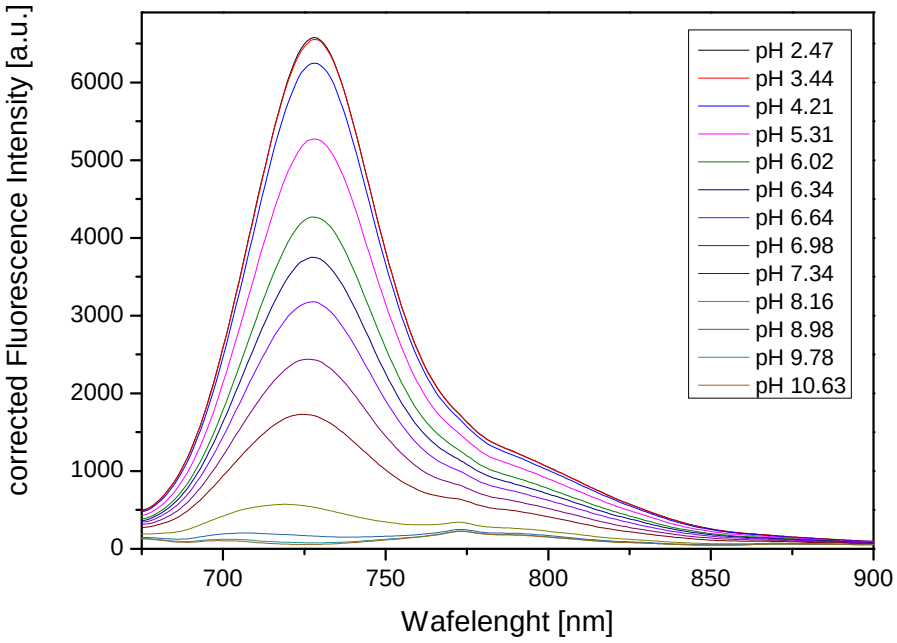

Figure 10.15: Emission spectra of the OHbutoxy-complex in RL100.

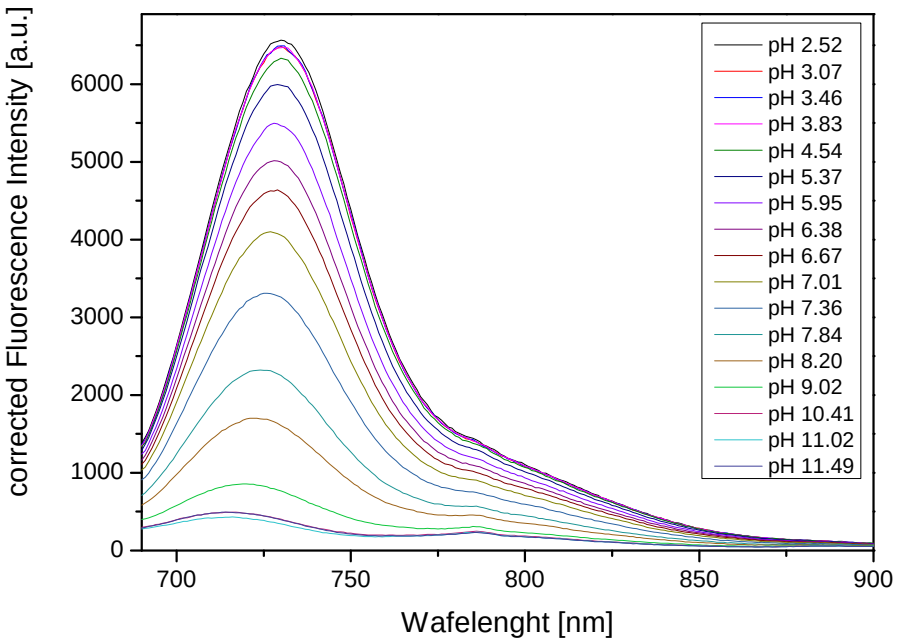

Figure 10.16: Emission spectra of the OHbutoxy-complex in PAcM.

10.5 Calibration Curves of the Ionic Strength Measurements

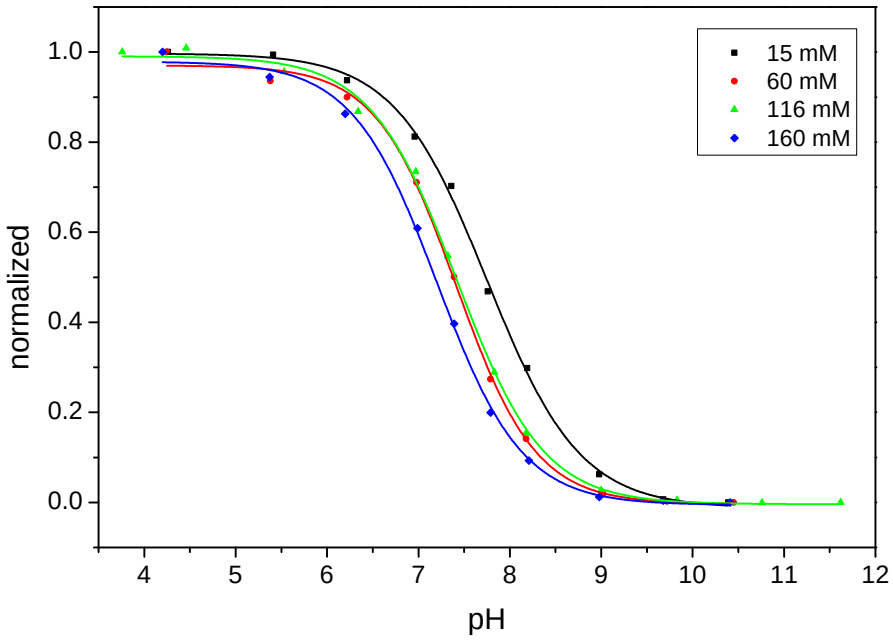

Figure 10.17: Calibration curves of the OHbutoxy-complex entrapped in PSPVP particles at different ionic strength.

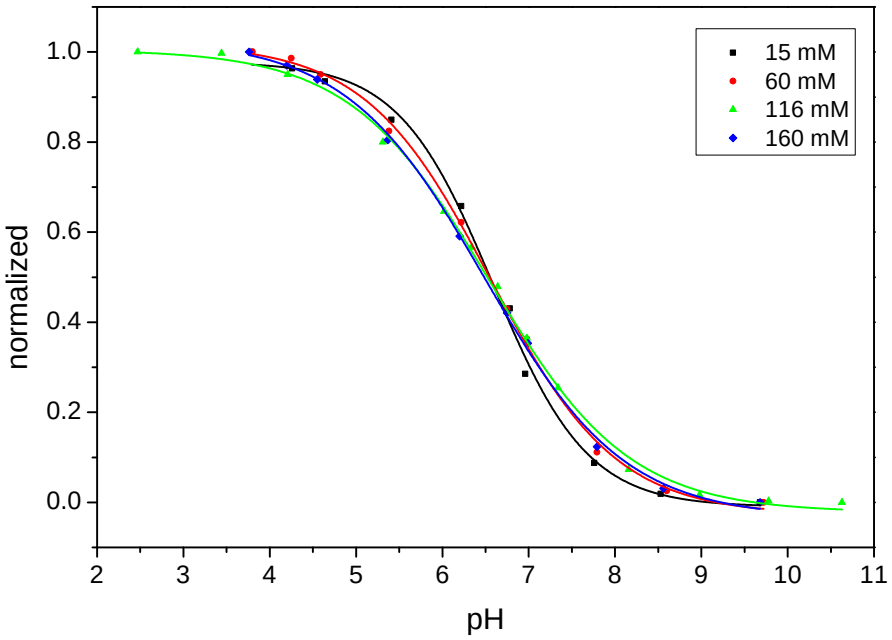

Figure 10.18: Calibration curves of the OHbutoxy-complex entrapped in RL100 particles at different ionic strength.

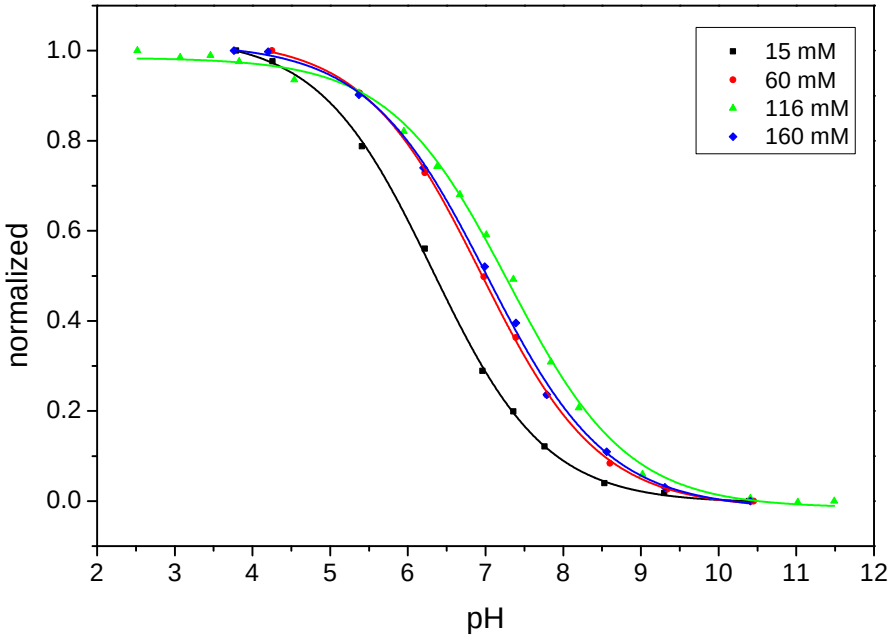

Figure 10.19: Calibration curves of the OHbutoxy-complex entrapped in PAcM particles at different ionic strength.

10.6 Calibration Curves of the DLR Measurements

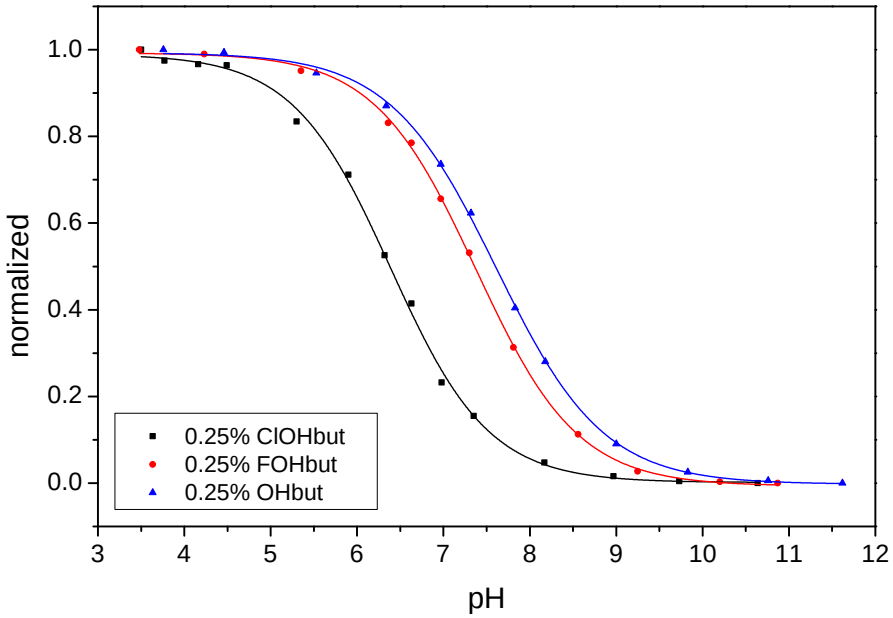

Figure 10.20: Calibration curves of the indicator dyes entrapped in PSPVP beads.

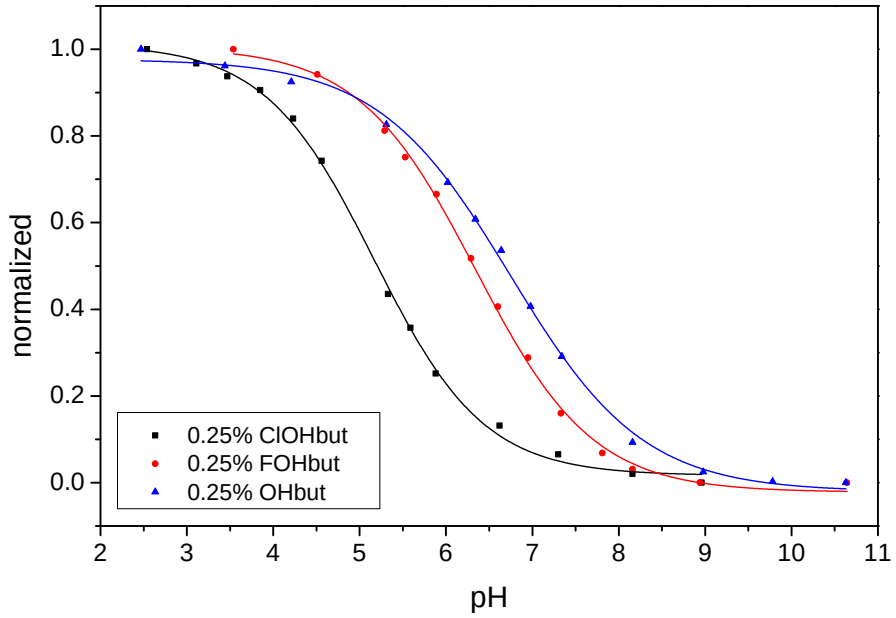

Figure 10.21: Calibration curves of the indicator dyes entrapped in RL100 beads.

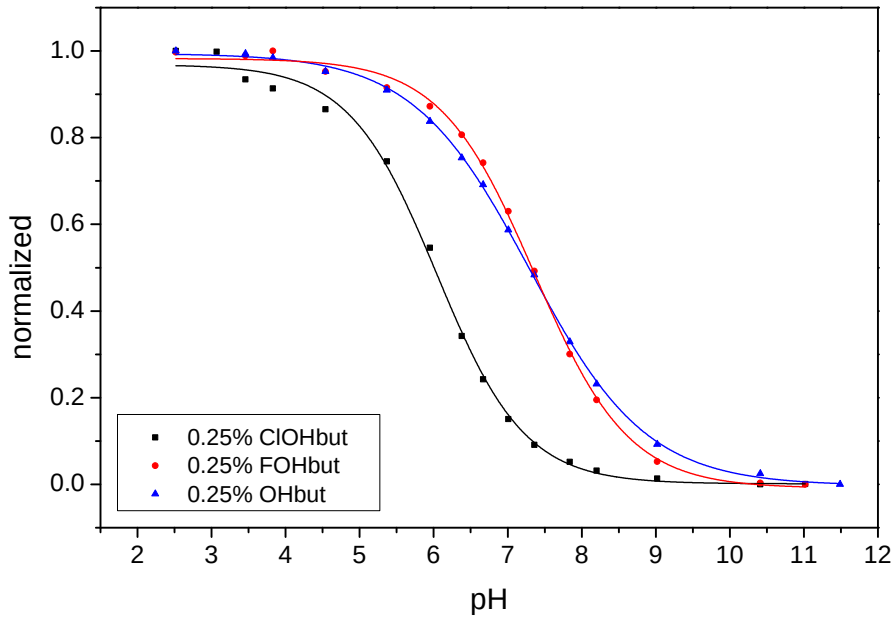

Figure 10.22: Calibration curves of the indicator dyes entrapped in PAcM beads.